Paper del canal de clorur CIC-2 en les patologies de la mielina

Tanit Arnedo Llena

Paper del canal de clorur ClC-2 en les patologies de la mielina.

Tesi doctoral: Tanit Arnedo Llena

Departament de Ciències Fisiològiques II,

Unitat de Fisiologia

Universitat de Barcelona 2015

Director: Raúl Estévez Povedano

Departament de Ciències Fisiològiques II, UB

ANNEX

ARTÍCLES PUBLICATS DURANT LA REALITZACIÓ D'AQUESTA TESI

GlialCAM, a Protein Defective in a Leukodystrophy, Serves as a ClC-2 Cl^- Channel Auxiliary Subunit.

Article publicat el març del 2012 a la revista Neuron.

Neuron
Article

GlialCAM, a Protein Defective in a Leukodystrophy, Serves as a ClC-2 Cl^- Channel Auxiliary Subunit

Elena Jeworutzki,[1,11] Tania López-Hernández,[2,11] Xavier Capdevila-Nortes,[2] Sònia Sirisi,[2,5] Luiza Bengtsson,[4] Marisol Montolio,[2,6] Giovanni Zifarelli,[1] Tanit Arnedo,[2] Catrin S. Müller,[8] Uwe Schulte,[8] Virginia Nunes,[3,5,7] Albert Martínez,[9] Thomas J. Jentsch,[4] Xavier Gasull,[10] Michael Pusch,[1,11] and Raúl Estévez[2,6,11,*]
[1]Istituto di Biofisica, Consiglio Nazionale delle Ricerche, 16149 Genoa, Italy
[2]Physiology section
[3]Genetic section
Department Physiological Sciences II, School of Medicine, University of Barcelona, 08907 Barcelona, Spain
[4]Leibniz-Institut für Molekulare Pharmakologie (FMP) and Max-Delbrück-Centrum für Molekulare Medizin (MDC), D-13125 Berlin, Germany
[5]Laboratorio de Genética Molecular-IDIBELL
[6]U-750, Centro de Investigación en Red de Enfermedades Raras (CIBERER), ISCIII
[7]U-730, Centro de Investigación en Red de Enfermedades Raras (CIBERER), ISCIII
[8]Logopharm GmbH, D-79232 March-Buchheim, Germany
[9]Department of Cell Biology, Faculty of Biology, University of Barcelona, 08028 Barcelona, Spain
[10]Laboratory Neurophysiology, Department Physiological Sciences I, School of Medicine, University of Barcelona-IDIBAPS, 08007, Spain
[11]These authors contributed equally to this work
*Correspondence: restevez@ub.edu
DOI 10.1016/j.neuron.2011.12.039

SUMMARY

Ion fluxes mediated by glial cells are required for several physiological processes such as fluid homeostasis or the maintenance of low extracellular potassium during high neuronal activity. In mice, the disruption of the Cl^- channel ClC-2 causes fluid accumulation leading to myelin vacuolation. A similar vacuolation phenotype is detected in humans affected with megalencephalic leukoencephalopathy with subcortical cysts (MLC), a leukodystrophy which is caused by mutations in *MLC1* or *GLIALCAM*. We here identify GlialCAM as a ClC-2 binding partner. GlialCAM and ClC-2 colocalize in Bergmann glia, in astrocyte-astrocyte junctions at astrocytic endfeet around blood vessels, and in myelinated fiber tracts. GlialCAM targets ClC-2 to cell junctions, increases ClC-2 mediated currents, and changes its functional properties. Disease-causing *GLIALCAM* mutations abolish the targeting of the channel to cell junctions. This work describes the first auxiliary subunit of ClC-2 and suggests that ClC-2 may play a role in the pathology of MLC disease.

INTRODUCTION

Megalencephalic leukoencephalopathy with subcortical cysts (MLC) is a rare type of leukodystrophy (van der Knaap et al., 1995a) characterized by macrocephaly that appears in the first years of life. MRI of patients shows swelling of the cerebral white matter and the presence of subcortical cysts, mainly in the anterior temporal regions. In MLC patients, diffusion studies indicate increased water content of the brain (van der Knaap et al., 1995b). A brain biopsy from an MLC patient revealed myelin (van der Knaap et al., 1996) and astrocyte vacuolation (Duarri et al., 2011). It was suggested that MLC may be caused by impaired ion transport across cellular membranes, thereby leading to an osmotic imbalance and disturbed fluid homeostasis (Brignone et al., 2011; Duarri et al., 2011). Indeed, *MLC1*, the first disease gene discovered to underlie MLC in most patients (Leegwater et al., 2001), encodes an integral membrane protein with 8 putative transmembrane domains with low and questionable homology to ion channels (Teijido et al., 2004). Recently, MLC1 has been proposed to be related to the activation of the volume-regulated anion channel (Ridder et al., 2011). However, the precise role of MLC1 in volume-regulated chloride transport is not clear (Ridder et al., 2011).

Among the ion channels that are expressed in glia, the hyperpolarization-activated and osmosensitive ClC-2 Cl^- channel (Gründer et al., 1992; Thiemann et al., 1992) has been proposed to be an important player in extracellular ion homeostasis (Blanz et al., 2007; Fava et al., 2001; Makara et al., 2003). Mice lacking ClC-2 (*Clcn2*$^{-/-}$ mice) exhibit vacuolation of the white matter that resembles the pathology of MLC patients (Blanz et al., 2007). *MLC1* mutations account for only 75% of patients with MLC, but none of the patients without mutations in *MLC1* carried bona fide disease-causing mutations in *CLCN2* (Blanz et al., 2007; Scheper et al., 2010). Tests for a crosstalk between ClC-2 and MLC1 also gave negative results. The proteins could not be coprecipitated, and reduction of MLC1 levels by RNA interference did not change ClC-2 protein levels (Duarri et al., 2011). Hence, no role of ClC-2 in human MLC could be established.

GLIALCAM was recently identified as a second MLC gene (López-Hernández et al., 2011a). GlialCAM is an Ig-like cell-adhesion molecule of poorly characterized function (Favre-Kontula

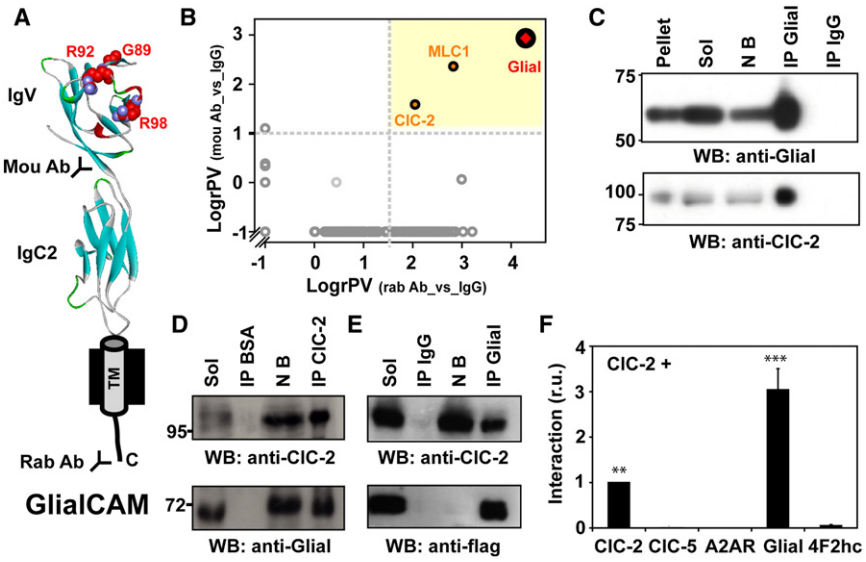

Figure 1. Identification of ClC-2 as a GlialCAM-Interacting Protein

(A) Scheme of the GlialCAM molecule. Mutated residues studied in this work are depicted. Antibodies used for purification (mou: mouse; rab: rabbit) are shown.

(B) Evaluation of GlialCAM affinity purification from mouse brain. The scheme shows a 2D plot of relative protein enrichment in affinity purifications versus IgG controls. Proteins specifically copurified are shown in the yellow area; dashed lines indicate the specificity thresholds as suggested by the distribution of all protein ratios (gray circles).

(C), Immunoblot analysis of a sample of the affinity purification with the anti-GlialCAM rabbit polyclonal antibody stained with the same antibody (upper) and with anti-ClC-2 C1 antibody (lower); lanes resolve aliquots of pellet after solubilization, solubilizate (Sol), not bound (NB), or eluates from the purification (IP Glial). IP IgG: eluate from an IgG control.

(D) Copurification of GlialCAM with anti-ClC-2 C2 antibody. Lanes were labeled as before.

(E) Coimmunoprecipitation from HeLa cells transiently transfected with ClC-2 and Flag-tagged GlialCAM. Lanes were labeled as before.

(F) Quantification of interaction using the split-TEV assay. ClC-2 was tested for interaction with the proteins indicated below the graph. $^{**}p < 0.01$; $^{***}p < 0.001$ versus 4F2hc.

See also Figure S1.

et al., 2008). A role of GlialCAM in MLC was first suggested by biochemical assays that demonstrated that both proteins bind each other and colocalize in astrocyte-astrocyte junctions at astrocytic endfeet (López-Hernández et al., 2011a). GlialCAM targets MLC1 to cell-cell junctions (López-Hernández et al., 2011b) and *GLIALCAM* mutations identified in MLC patients impair the correct trafficking of GlialCAM and MLC1 to astrocyte-astrocyte junctions (López-Hernández et al., 2011a, 2011b).

Unlike MLC1, GlialCAM is also detected in myelin (López-Hernández et al., 2011a), mainly in oligodendroglial extensions (Favre-Kontula et al., 2008). In the present work, we show that GlialCAM interacts with ClC-2 in several glial cell types including oligodendrocytes, targeting it to cell junctions and dramatically increasing its conductance. We thus identified GlialCAM as an auxiliary subunit of ClC-2, potentially implicating the channel in the pathogenesis of MLC.

RESULTS

Identification of ClC-2 as GlialCAM Binding Partner

We used two different antibodies directed against GlialCAM (Figure 1A) to identify proteins from solubilized mouse brain membranes that copurify with GlialCAM. In addition to peptides from GlialCAM and MLC1, quantitative mass spectroscopy identified peptides corresponding to the ClC-2 chloride channel (Figure 1B and see Figure S1 available online) as the only other consistently and specifically copurified protein in the eluate. Western blot analysis confirmed that ClC-2 was copurified with at least a fraction of GlialCAM (Figure 1C), which may result from a partial dissociation of the complex or may indicate that not all GlialCAM is associated with ClC-2. Coimmunoprecipitation experiments using an antibody against ClC-2 confirmed the interaction between GlialCAM and ClC-2 (Figure 1D). Similar experiments using extracts from cells transfected with ClC-2 and C terminally tagged GlialCAM (Figure 1E), as well as split-TEV interaction experiments (Figure 1F), suggested that ClC-2 and GlialCAM directly interact. The interaction appeared specific since no association was observed between ClC-2 and the related $2Cl^-/H^+$ antiporter ClC-5, the unrelated polytopic adenosine 2A receptor (A2AR), or the unrelated single transmembrane span protein 4F2hc (Figure 1F).

Colocalization of ClC-2 and GlialCAM in Tissue

For the interaction of GlialCAM and ClC-2 to be physiologically relevant, both proteins must colocalize in native tissue. GlialCAM is found exclusively in brain, where it localizes to astrocyte-astrocyte junctions at endfeet, Bergmann glia, some pyramidal neurons and to myelin (López-Hernández et al., 2011a). In addition to neurons, ClC-2 is expressed on astrocytes and oligodendrocytes and was found in myelin-enriched fractions (Blanz et al., 2007; Fava et al., 2001; Földy et al., 2010; Makara et al., 2003; Rinke et al., 2010; Sík et al., 2000). GlialCAM colocalized in mouse brain with ClC-2 in cerebellar Bergmann glia which was counterstained for GFAP (Figure 2A). Both proteins were present at astrocytic endfeet surrounding blood vessels (Figure 2B; Blanz et al., 2007; López-Hernández et al., 2011a; Sík et al., 2000) in the cortex and in the cerebellum. In human cerebellum, immunogold electron microscopy detected ClC-2 at astrocyte-astrocyte contacts in the endfeet (Figures 2C and 2D), a location where also GlialCAM and MLC1 are present (López-Hernández et al., 2011a). GlialCAM and ClC-2 were also found to colocalize in myelinated fiber tracts along the circumference of oligodendrocytic cell bodies in mouse cerebellum (Figure 2E), where GlialCAM, ClC-2, and the oligodendrocyte-expressed gap junction protein Cx47 were present in the same cell membrane (Figure 2F; Blanz et al., 2007). In vitro cell culture

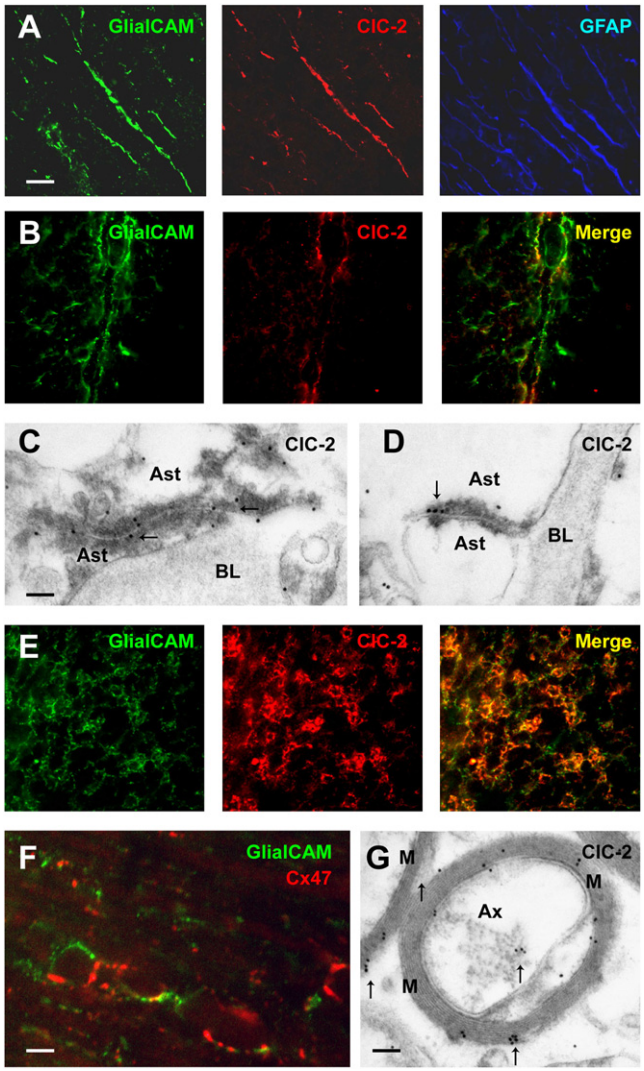

Figure 2. Localization of ClC-2 and GlialCAM in the Brain

Mouse brain sections labeled with antibodies against GlialCAM, ClC-2, or GFAP antibodies. (A) cerebellar Bergmann glia; (B) astrocytic endfeet surrounding blood vessels in cortex; (C and D) EM immunolabeling of human cerebellum shows localization of ClC-2 (arrows) in astrocyte-astrocyte junctions near basal lamina; (E) oligodendrocytic cell bodies in myelinated fibers of cerebellar white matter tracts.

(F) Coexpression of GlialCAM and the oligodendrocyte marker Cx47 in membranes of oligodendrocytic bodies in the cerebellum.

(G) EM immunolabeling detects ClC-2 in myelin (arrows).

Scale bars for (A), (B), and (E) 20 μm; (F) 5 μm; for panels (C) and (D) 200 nm; (G) 500 nm. M: myelin; Ax: axon; Ast: astrocyte; BL: basal lamina. ClC-2 antibodies used: C1 (A); C2 (B–F). See also Figure S2.

studies have shown that GlialCAM is expressed in different stages of oligodendrocytic differentiation, including the bipotential O2-A progenitor NG2 positive cells (OPC cells) (Favre-Kontula et al., 2008). Immunogold EM confirmed the presence of ClC-2 in human myelin (Figure 2G).

Localization and expression of GlialCAM is independent of MLC1 (López-Hernández et al., 2011b). We similarly asked whether the expression of GlialCAM or MLC1 depends on ClC-2. Western blots revealed that the total amount of GlialCAM and MLC1 proteins were unchanged in the brain of *Clcn2*$^{-/-}$ mice (Figure S2A). Likewise, there was no change in the subcellular localization of GlialCAM and MLC1 in Bergmann glia, nor in the astrocytic endfeet around blood vessels in *Clcn2*$^{-/-}$ mice (Figures S2B and S2C).

GlialCAM Changes the Subcellular Distribution of ClC-2

We then studied whether GlialCAM changes the abundance or localization of ClC-2 in heterologous expression systems. We could not detect that GlialCAM changes ClC-2 protein levels (data not shown) and ClC-2 surface expression after transfection of HeLa cells or transduction of primary astrocytes, as ascertained in a chemiluminescence assay (Figure S3).

Since GlialCAM has been described to target MLC1 to cell-cell junctions (López-Hernández et al., 2011b), we assayed if GlialCAM could also modify ClC-2 localization in the same manner. In HeLa cells, ClC-2 transfected alone was detected at the plasma membrane and intracellularly (Figure 3A). Coexpression with GlialCAM directed the ClC-2 channel to cell-cell contacts (Figures 3B–3D), where both proteins colocalized (data not shown). Localization of ClC-2 together with GlialCAM was observed in long (Figure 3B) or short (Figure 3C) cell-cell contact processes and in extensive contact areas between opposite cells (Figure 3D). Such a clustering was never observed in contacting cells expressing only ClC-2 (Figure 3A). Similar results were observed in HEK293 cells (data not shown). We performed analogous experiments in primary cultures of astrocytes, where both proteins are endogenously expressed. In these cultures, adenoviral-mediated expression of ClC-2 with or without GlialCAM showed that the latter protein was necessary to target ClC-2 to astrocyte-astrocyte processes (compare Figures 3E and 3F). In these junctions, ClC-2 and GlialCAM displayed colocalization (Figures 3F–3H).

GlialCAM Modifies ClC-2 Currents

We next asked whether GlialCAM could modify ClC-2 function. Coexpression of GlialCAM and ClC-2 in *Xenopus* oocytes dramatically increased ClC-2-mediated currents and changed their characteristics (Figure 4A). Initial currents measured at +60 mV were more than 15-fold larger in cells coexpressing ClC-2 and GlialCAM compared to ClC-2 alone. Whereas ClC-2 currents are strongly inwardly rectifying and activate slowly upon hyperpolarization, ClC-2/GlialCAM currents were almost ohmic and displayed time-independent, instantaneously active currents (Figure 4B). Of note, the apparent inactivation observed sometimes at very negative voltages is an artifact caused by chloride depletion inside the oocytes.

Similar effects of GlialCAM on ClC-2 currents were seen in transfected HEK293 cells, although a residual time-dependent component was present (Figure 4C). Importantly, GlialCAM alone does not induce any significant current in HEK cells or *Xenopus* oocytes (Figure S4). Similarly, in transfected cells, ClC-2 steady state currents at +60 mV were dramatically increased by GlialCAM (Figure 4D). Specificity of the currents was demonstrated by the characteristic block by extracellular

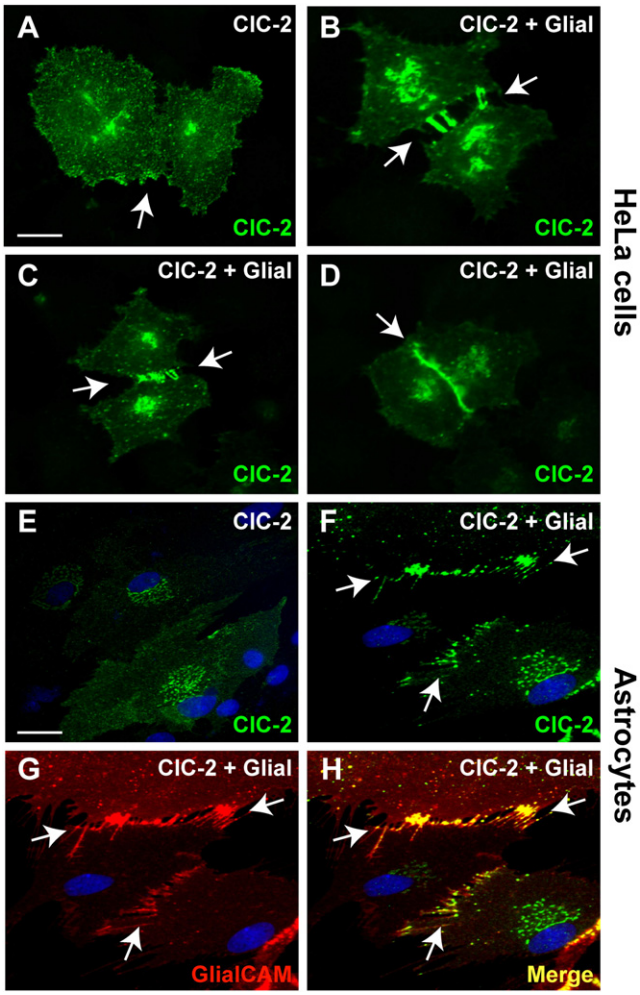

Figure 3. GlialCAM Changes the Subcellular Distribution of ClC-2 in HeLa Cells and in Primary Cultures of Astrocytes

(A–D) GlialCAM changed the subcellular distribution of ClC-2 in transiently transfected HeLa cells from being at the plasma membrane when transfected alone (A) versus being at long cell-cell contact processes (B), at short cell-cell contact processes (C), or in extensive contact regions (D) when cotransfected with GlialCAM (arrows label cell-cell contacts). Scale bar: 10 μm.

(E–H) Astrocytes were transduced with adenoviruses expressing ClC-2 alone or together with C terminally tagged GlialCAM at MOI 3. GlialCAM similarly brought ClC-2 to cell-cell contacts. Arrows point to astrocyte-astrocyte contacts. Immunofluorescence used a flag monoclonal antibody detecting GlialCAM protein (red) or a rabbit polyclonal antibody (C1) detecting ClC-2 (green). Colocalization between the red and the green fluorescence results in a yellow coloring (Merge). Nuclei of astrocytes were stained using DAPI (blue). Scale bar: 20 μm.

See also Figure S3.

iodide (Gründer et al., 1992; Thiemann et al., 1992; Figure 4B) and cadmium (Clark et al., 1998) (data not shown).

To test if GlialCAM may alter native ClC-2 currents we performed whole-cell patch-clamp experiments in differentiated rat astrocytes. These cells exhibit typical hyperpolarization-activated ClC-2-like currents that were blocked by iodide (Ferroni et al., 1997; Makara et al., 2003; Figure 4E). After GlialCAM overexpression, currents were increased and showed a large instantaneous component and less rectification (Figure 4F), qualitatively similar to the effect on ClC-2 in the heterologous systems. These currents were also blocked by iodide to similar degree (Figure 4E).

Even if GlialCAM and connexins do not overlap significantly (Figures 2F and S4D), it may be hypothesized that GlialCAM expression increases ionic currents by stimulating currents through gap junction proteins. However, overexpression of GlialCAM did not modify expression and localization of connexin 43, the major connexin of astrocytes (Figures S4C and S4E). Furthermore, blocking gap junctions with glycyrrhetinic acid did not influence GlialCAM-induced currents in coupled astrocytes (Figure S4F), which were, however, blocked by iodide which is known to block ClC-2 (Gründer et al., 1992; Thiemann et al., 1992; Figure 4F).

We next addressed whether the effect of GlialCAM was specific to ClC-2. GlialCAM did not change currents of ClC-5 at positive or negative voltages (Figure 5A). We studied if human GlialCAM could interact with the ClC-2 ortholog from *Drosophila melanogaster* (DmClC-2) (Flores et al., 2006), whose genome lacks a GlialCAM ortholog. GlialCAM interacted biochemically and increased currents of DmClC-2 (Figures 5B and 5C), suggesting that GlialCAM evolved to interact with the channel at an interface that is evolutionary conserved among ClC-2 like channels. Additionally, we addressed interaction with the closest homolog of GlialCAM named HepaCAM2. No biochemical and functional interaction was observed between HepaCAM2 and ClC-2 (Figures 5D and 5E). Finally, we asked whether wild-type MLC1 or MLC1 containing MLC-causing mutations could influence ClC-2 or ClC-2/GlialCAM induced current in *Xenopus* oocytes. We did not find any effect on ClC-2 mediated currents (Figure 5F).

Insights into the Molecular Mechanism of ClC-2 Activation by GlialCAM

Currents of *Xenopus* oocytes expressing GlialCAM/ClC-2 resemble those of an N-terminal deletion of ClC-2 (ΔN), in which the osmosensitivity and the voltage-dependence is drastically altered (Gründer et al., 1992). This might suggest that GlialCAM activates ClC-2 by interacting with its N terminus. However, we found that GlialCAM still interacted biochemically with (Figure S5A) and targeted the ΔN mutant to cell-cell contacts (Figure S5B) just like wild-type ClC-2. Moreover, GlialCAM potentiated ΔN currents in transfected HEK293 cells (Figure S5C).

We then compared the functional properties of ClC-2, ΔN and GlialCAM/ClC-2. Hypo-osmolarity increased currents of GlialCAM/ClC-2 and ClC-2, but had no effect on ΔN (Gründer et al., 1992; Figure 6A). All of them have the same anion permeability sequence (Figure 6B), strongly suggesting that GlialCAM has no effect on the open-pore properties of the channel. We also addressed whether GlialCAM could increase the single channel conductance of the channel by performing nonstationary noise analysis of currents induced by ClC-2 or by ClC-2/GlialCAM at −100 mV in transfected HEK cells. The conductance of ClC-2 was estimated at 2.9 ± 0.4 pS (n = 8), a value very similar to what has been previously reported (Weinreich and Jentsch,

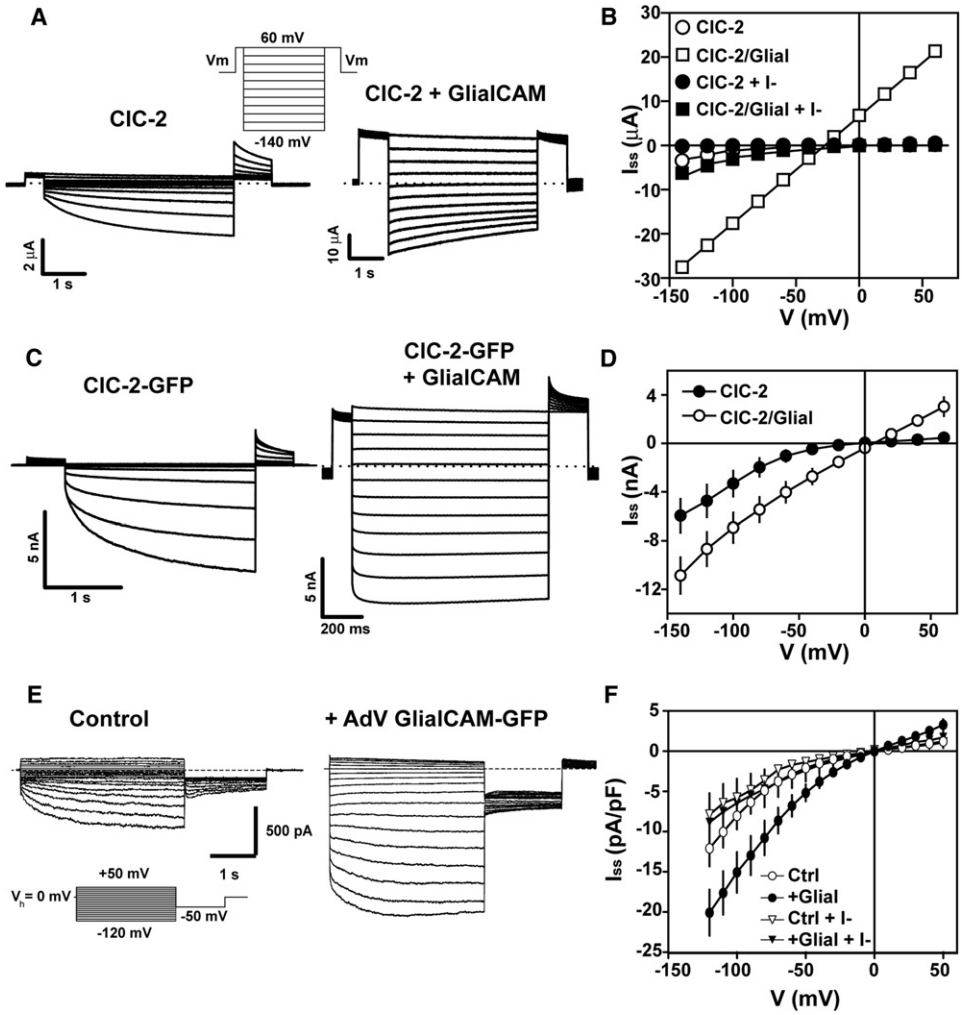

Figure 4. GlialCAM Modifies ClC-2 Currents in *Xenopus* Oocytes, HEK Cells, and Primary Rat Astrocytes

(A) Currents mediated by ClC-2 (left) expressed in oocytes and after coexpression of ClC-2 with GlialCAM (right).

(B) Representative steady-state current-voltage relationship of ClC-2 (circles) and ClC-2 coexpressed with GlialCAM (squares) in chloride (open symbols) or iodide (filled symbols). Average initial currents measured at +60 mV were 0.96 ± 0.17 μA (n = 14) for ClC-2 and 17.2 ± 2.2 μA (n = 10) for ClC-2/GlialCAM.

(C) Typical whole-cell currents from transfected HEK293 cells with ClC-2-GFP alone (left) or together with GlialCAM (right). The GFP tag does not affect ClC-2 current properties.

(D) Average steady-state current voltage from ClC-2-GFP (filled circles) or ClC-2-GFP/GlialCAM (circles) transfected HEK293 cells.

(E) Left: representative trace of whole-cell inwardly rectifying chloride currents in dbcAMP-treated cultured neocortical rat astrocytes. These currents, as described (Ferroni et al., 1997), were blocked when chloride was replaced by iodide (F) and were not blocked by tamoxifen (data not shown). Right: representative trace of chloride currents of dbcAMP-treated astrocytes transduced with adenoviruses expressing GlialCAM fused to GFP. The inset shows the voltage protocol used.

(F) Average steady-state current-voltage relationship of dbcAMP-treated astrocytes (circles, n = 14) or transduced with adenoviruses expressing GlialCAM-GFP (filled circles, n = 14) in chloride medium. Recordings were performed in symmetrical chloride concentrations. In some recordings chloride was exchanged by iodide (triangles or filled triangles). At hyperpolarizing voltages iodide block was by 32.7% ± 3.2% for control astrocytes (n = 6) and by 56.8% ± 2.9% for astrocytes transduced with adenoviruses expressing GlialCAM-GFP (n = 8).

See also Figure S4.

2001). For ClC-2/GlialCAM we obtained a value of 2.6 ± 0.2 pS (n = 8), not statistically significantly different from the value for ClC-2 alone ($p > 0.5$). We conclude that GlialCAM does not modify single-channel properties of ClC-2. Interestingly, GlialCAM similarly diminished the inhibition by acidic pH of both ClC-2 and ΔN (Figure 6C). This result suggested that GlialCAM may activate ClC-2 by opening the common gate that acts on both pores of the homodimeric channel, as this gate is sensitive to acidic pH (Niemeyer et al., 2009).

GlialCAM displays a long cytoplasmatic C terminus comprising about 30% of the protein (Favre-Kontula et al., 2008). However, consistent with its poor sequence conservation between species, the deletion of the entire C terminus did not abolish the interaction with ClC-2, its targeting to cell junctions, and the

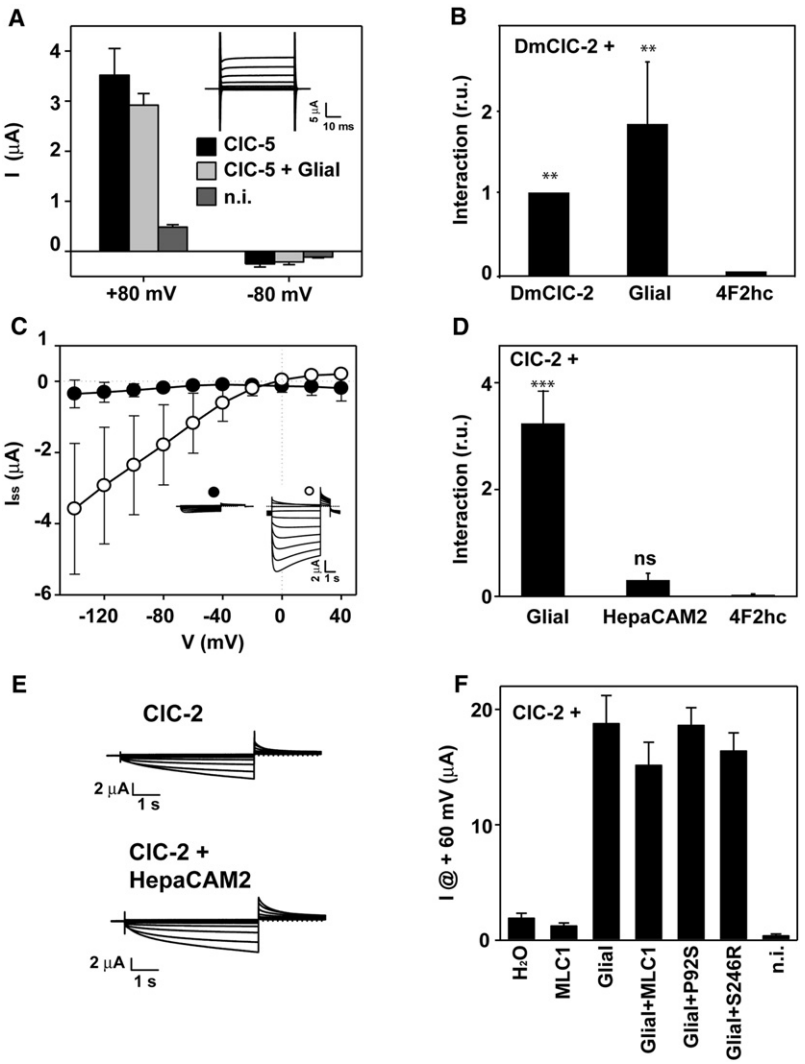

Figure 5. Specificity of the ClC-2 GlialCAM Interaction

(A) Human ClC-5 was expressed in oocytes with and without GlialCAM. Currents were quantified at positive (+80 mV) and negative (−80 mV) voltages 3 days after injection. The inset shows representative ClC-5 + GlialCAM traces using a voltage-clamp protocol with pulses ranging from +120 mV to −120 mV in 20 mV steps.

(B) Interaction between DmClC-2 and DmClC-2 or GlialCAM was monitored using split-TEV assays. 4F2hc was used as a negative control. The result is an average of 5 independent experiments. **$p < 0.01$ versus 4F2hc.

(C) DmClC-2 was expressed in *Xenopus* oocytes by itself or together with GlialCAM. Two days after injection in oocytes DmClC-2 ± GlialCAM currents were determined. Steady state currents are plotted against voltage (n = 5 ± SEM). The inset shows representative current traces of DmClC-2 (filled circle) and DmClC-2 / GlialCAM (open circle).

(D) Interaction between ClC-2 and GlialCAM or HepaCAM2 by split-TEV assays. 4F2hc was used as a negative control. The result is an average of 13 independent experiments. ***$p < 0.001$; "ns" indicates no significant difference versus 4F2hc.

(E) Typical ClC-2 currents in *Xenopus* oocytes expressed by itself (left) or coexpressed with HepaCAM2 (right). HepaCAM2 positive protein expression was assessed by Western blot (data not shown).

(F) Currents measured in *Xenopus* oocytes at + 60 mV after the expression of ClC-2 alone (3 ng), ClC-2 (3 ng) + GlialCAM (5 ng), or ClC-2 (3 ng) + GlialCAM (5 ng) + wild-type MLC1 (3 ng) or containing the MLC-causing mutations P92S and S246R (3 ng). The result is a representative experiment of two experiments with at least 5 oocytes measured for each condition.

activation of ClC-2 currents in transfected cells (Figures S5D–S5F). Hence the interaction between both proteins may depend on the transmembrane and/or the N-terminal part of GlialCAM. Deletion of the N-terminal part of GlialCAM, while keeping the cleavable signal peptide, resulted in a lack of surface expression (data not shown), precluding proper biochemical studies.

Impact of MLC-Related Mutations Identified in *GLIALCAM* on ClC-2

Several *GLIALCAM* mutations found in patients with MLC truncate the protein before the transmembrane domain or result in amino-acid changes in the N-terminal, extracellular part of GlialCAM (López-Hernández et al., 2011a). We studied four of these missense mutations located within the IgV domain (Figure 1A). All GlialCAM proteins containing MLC-causing missense mutations retained their physical interaction with ClC-2 (Figures 7A and S6A) and increased ClC-2 activity similar to wild-type GlialCAM in *Xenopus* oocytes (Figures 7B and S6B) and in transfected cells (data not shown). In contrast, all of them abolished the targeting of ClC-2 to cell junctions in HeLa or HEK293 cells (Figures 7C and 7D).

We also analyzed the effect of the MLC-causing mutations in GlialCAM on the localization of ClC-2 in primary cultures of rat astrocytes through adenoviral-mediated transduction (Figure 8). Coexpression of ClC-2 with GlialCAM mutant variants resulted in intracellular and cell membrane staining of ClC-2 (Figures 8B–8E), but not the typical wild-type GlialCAM induced localization in cell junctions (Figure 8A).

DISCUSSION

In this work, we have identified GlialCAM as an interaction partner of the ClC-2 chloride channel. As ClC-2 is functional in the absence of GlialCAM, albeit displays different biophysical properties, and since GlialCAM shows a much more restricted expression pattern than ClC-2 (Thiemann et al., 1992), it is clear that GlialCAM is not an obligate β-subunit of ClC-2, but an auxiliary subunit that associates with ClC-2 only in some cell types. MLC1 wild-type or containing MLC-causing mutations, by contrast, does not modify ClC-2 currents neither in the presence nor in the absence of GlialCAM, and biochemical studies indicate that ClC-2 and MLC1 do not interact directly (Duarri

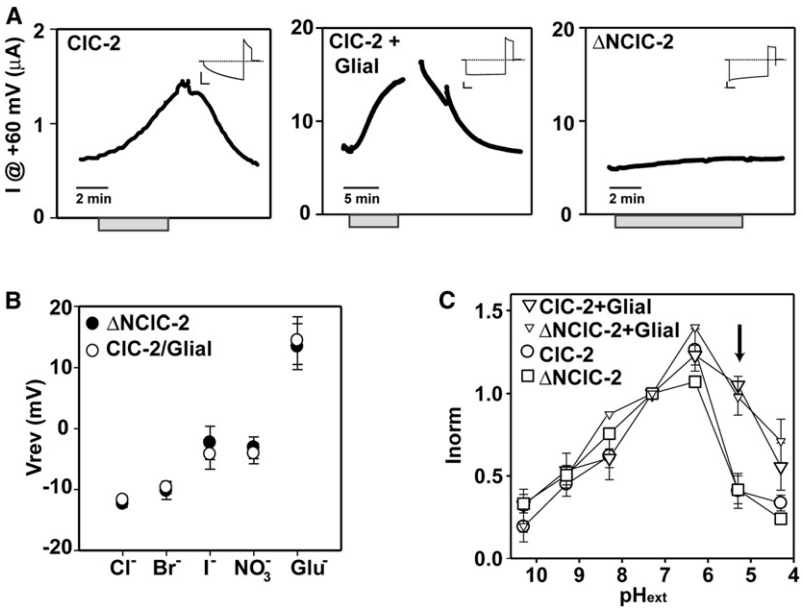

Figure 6. Electrophysiological Characterization of the GlialCAM/ClC-2 Complex

(A) Dependence on the extracellular osmolarity of ClC-2, ClC-2 + GlialCAM, or ΔNClC-2 currents. Gray bars indicate application of the hypotonic solution. Insets show typical responses of the same oocytes to a pulse to −140 mV before swelling.

(B) Reversal potential of ΔNClC-2 (n = 5 ± SEM) and ClC-2/GlialCAM (n = 5 ± SEM) currents under different anionic conditions.

(C) pH dependence of ClC-2 and ΔNClC-2, each without and with GlialCAM. Currents were normalized to the value at pH 7.3. Arrow points to the pH value with the largest difference between the groups that express or not GlialCAM.

See also Figure S5.

et al., 2011). Furthermore, MLC1 expression and localization is unaltered in *Clcn2*$^{-/-}$ mice. These data suggest that GlialCAM/MLC1 and GlialCAM/ClC-2 may form distinct complexes. Recently, the lack of MLC1 has been correlated with a variable impairment in cell volume regulation that may be mediated by the volume regulated anion channel (VRAC) (Ridder et al., 2011). However, VRAC is distinct from ClC-2 as evident from very different biophysical characteristics (Jordt and Jentsch, 1997). Furthermore, the mechanism of modulation of VRAC by MLC1 is unclear. As MLC1 and ClC-2 share GlialCAM as a subunit, we cannot exclude that MLC1 could regulate ClC-2 function in an indirect/unknown manner. Therefore, an interesting hypothesis that should be tested in the next future is whether ClC-2 function is altered in cells lacking MLC1.

GlialCAM by itself localizes to cell-cell junctions (López-Hernández et al., 2011b), probably being retained there by homophilic or heterophilic interactions with membrane proteins of the apposing cell. In other GlialCAM homolog proteins such as the members of the SLAM family (Engel et al., 2003), localization at the immunological synapse of SLAM proteins is achieved by trans-homophilic interactions between the IgV domains of opposite molecules. Furthermore, GlialCAM is also able to localize ClC-2 and MLC1 (López-Hernández et al., 2011b) to cell-cell junctions in heterologous expression systems and in primary cultures of astrocytes. The role of GlialCAM as a ClC-2 subunit appears to be specific within its protein family, as its closest homolog, HepaCAM2, did not interact with ClC-2. GlialCAM carrying MLC-related mutations (López-Hernández et al., 2011a) fails to arrive at cell-cell junctions (López-Hernández et al., 2011b). As a consequence, also their associated subunits, MLC1 and ClC-2, are not properly targeted to cell-cell junctions. Thus, GlialCAM function may be needed to cluster ClC-2 and MLC1 in particular to astrocyte-astrocyte junctions at astrocytic endfeet. Here, the ClC-2 chloride channel may be needed to support a transcellular chloride flux or to compensate large electrochemical ion gradients that may occur at these junctions during ion-driven changes in osmolarity. However, the chloride flux mediated by ClC-2/GlialCAM in cell junctions most likely fulfills a different role compared to the one mediated by gap junctions as these proteins do not colocalize completely. Our experiments also exclude that GlialCAM activates astrocyte gap junctions, since their blockade did not influence currents induced by GlialCAM overexpression, and GlialCAM overexpression had no influence on connexin 43 protein levels or its subcellular localization.

Recent reports indicated that the ClC-2 channel in neurons constitutes a part of the background conductance regulating input resistance and providing an efflux pathway for chloride (Földy et al., 2010; Rinke et al., 2010), which may be a safeguard mechanism to prevent chloride accumulation in active GABAergic synapses. In contrast, the role of ClC-2 in glial cells is unknown. Recordings from mouse slices demonstrated that ClC-2-mediated current was reduced in reactive astrocytes within a lesion (Makara et al., 2003). Strong evidence in favor of an important physiological role of ClC-2 in glial cells is provided by the phenotype of *Clcn2*$^{-/-}$ mice, which display an MLC-like vacuolization in the brain (Blanz et al., 2007). Vacuolization in the brain has been also observed in mice disrupted for the potassium channel Kir4.1 (Neusch et al., 2001) or double-disrupted for connexins 32 *and* 47 (Menichella et al., 2006). These proteins are thought to be crucial for potassium siphoning by glial cells, a process that is needed to avoid neuronal depolarization by extracellular K^+ during repetitive action potential firing (Rash, 2010). In agreement with this role in ion siphoning, in Kir4.1 knockout mice there was no vacuolation in the optic nerve after blocking action potential generation with tetrodotoxin (Neusch et al., 2001). It was neither observed in the *Clcn2*$^{-/-}$ mice possibly because they are blind due to retinal degeneration (Blanz et al., 2007). Hence degeneration in both mouse models depend on nerve activity, in accord with the siphoning process that is required after neuronal repolarization. It has been suggested that ClC-2 may play a role in charge compensation during potassium influx or efflux in glial cells (Blanz et al., 2007).

ClC-2-mediated currents were increased upon GlialCAM expression and showed less inward rectification. However,

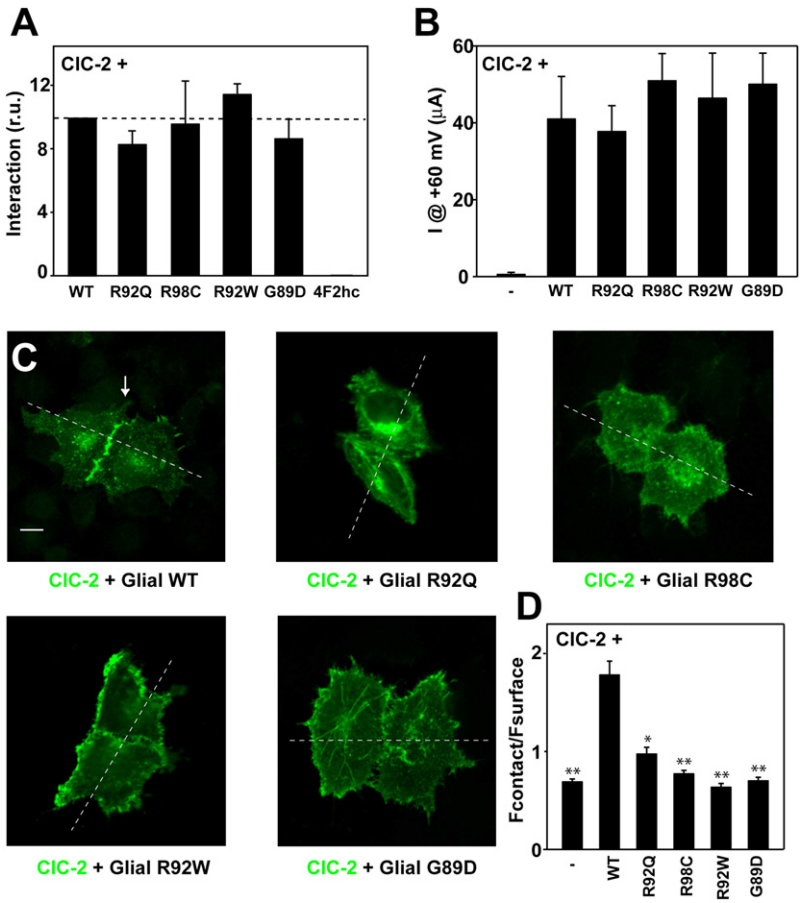

Figure 7. Biochemical and Functional Consequences of *GLIALCAM* Mutations on ClC-2

(A) Interaction between ClC-2 and GlialCAM or GlialCAM containing MLC-related mutations revealed by split-TEV interaction assays (n = 5).

(B) Average instantaneous currents at +60 mV from ClC-2 expressing oocytes coinjected with saturating concentrations of GlialCAM or the indicated GlialCAM variants. The result is an average of n = 5 in each experiment from three independent experiments.

(C) Immunofluorescence of HeLa cells expressing ClC-2 plus wild-type GlialCAM or GlialCAM containing the MLC-related mutations R92Q, R98C, R92W, and G89D. Scale bar: 10 μm. Expression at contact sites and non-contact surface membrane was determined by the analysis of the intensity profile along the dashed line.

(D) Relative fluorescence intensity at cell contacts. Intensity profile analysis revealed that ClC-2 alone had a ratio R of fluorescence $F_{contact}/F_{surface}$ (see Experimental Procedures) of 0.7 ± 0.03 (n = 58), ClC-2 + GlialCAM a value of 1.8 ± 0.14 (n = 55), and the GlialCAM variants studied (with at least 24 pair of cells analyzed) had R values less than 1 (see Experimental Procedures), indicating that the variants containing MLC-related mutations were not able to cluster ClC-2 to cell junctions. *p < 0.05, **p < 0.01 versus wild-type GlialCAM plus ClC-2. Similar results were observed in HEK cells (not shown).

See also Figure S6.

ClC-2 activity recorded in cultured astrocytes (Ferroni et al., 1997) or in astrocytes in brain slices (Makara et al., 2003) resembles that of ClC-2 alone. This may be due to different recording conditions, or, alternatively, it may be that GlialCAM interacts with ClC-2 only under special circumstances, such as those occurring during high neuronal activity.

A polarized distribution of the Kir4.1 channel in astrocyte membranes in contact with endothelial cells, mediated by interaction with proteins of the DGC (dystrophin-glycoprotein complex) (Nagelhus et al., 2004), is required for potassium siphoning. In an analogous way, the polarized localization of ClC-2 mediated by GlialCAM in astrocyte-astrocyte or oligodendrocyte-astrocyte contacts may be also needed to support a directional flux of potassium from neurons to blood vessels. As a cell-adhesion molecule, GlialCAM could influence the expression of other molecules expressed in cell junctions such as connexins. Similar to DGC proteins, the localization in cell-cell contacts of GlialCAM itself and of associated molecules may be achieved by transmediated interactions or by interactions with intracellular scaffolds in each cell. It seems possible that GlialCAM may organize a more extensive cluster of proteins at the astrocytic junctions in the endfeet.

We propose that the lack of the stimulatory effect of GlialCAM on ClC-2 currents, or a mislocalization of this Cl^- channel, or both, will impair glial chloride transport. This may impair not only chloride homeostasis, but also potassium siphoning and cell volume regulation that is particularly important during neuronal activity. This in turn may entail accumulation of osmotically driven water, lead to the vacuolization observed in MLC patients with mutations in *GLIALCAM* or in *Clcn2*$^{-/-}$ mice. Vacuolization observed in MLC patients with *GLIALCAM* mutations could also be due to defects in GlialCAM by itself, or to a mislocalization of MLC1, an established causal player in MLC. Additionally, the adhesive properties of GlialCAM, and their importance for the anatomy of the brain and the pathogenesis of MLC remain to be studied.

The fact that so far no disease-causing *CLCN2* mutation has been found in patients with MLC (Blanz et al., 2007; Scheper et al., 2010) might be explained by the presence of additional symptoms (e.g., blindness, male infertility, as expected from the phenotype of *Clcn2*$^{-/-}$ mice [Bösl et al., 2001]) that could result in improper disease classification. The male infertility could also lead to an underrepresentation of *CLCN2* mutations in the human population. Thus, proof of the involvement of ClC-2 in MLC disease will require, for example, immunolocalization studies in brain biopsies of MLC patients with *GLIALCAM* mutations.

In summary, the discovery of GlialCAM as the first auxiliary subunit of ClC-2 increases the complexity of regulation of the CLC chloride transporter/channel family for which so far only two β-subunits have been described (Estévez et al., 2001; Lange et al., 2006). Our work provides new clues to uncover the physiological role of the ClC-2 channel in glial cells, and suggests that

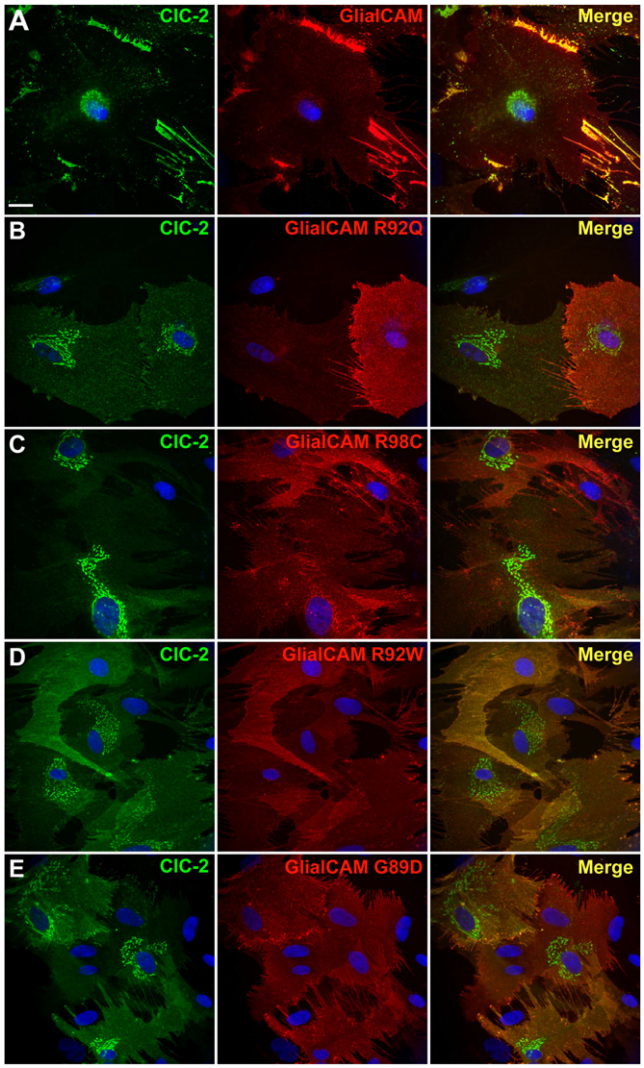

Figure 8. ClC-2 and GlialCAM Subcellular Localization Changes Caused by *GLIALCAM* Mutations in Primary Cultures of Astrocytes

(A–E) Astrocytes were cotransduced with adenoviruses expressing ClC-2 together with wild-type GlialCAM (A) or containing the MLC-related mutations R92Q (B), R98C (C), R92W (D), and G89D (E). Cells were fixed, permeabilized, and then immunofluorescence was performed with a rabbit polyclonal antibody against ClC-2 (green) and a monoclonal antibody detecting GlialCAM protein (red). Nuclei were stained with DAPI (blue). Colocalization between the green and the red channel is shown in yellow. Images correspond to representative cells from three independent experiments. Scale bar: 20 μm.

the ClC-2 channel may be involved in the physiopathology of MLC disease.

EXPERIMENTAL PROCEDURES

Biochemistry

Proteomic analysis: for solubilization, membrane vesicles (1 mg) were resuspended in ComplexioLyte buffer 47a (at 0.8 mg protein/ml, LOGOPHARM GmbH, Germany; with protease inhibitors), incubated for 30 min at 4°C and cleared by ultracentrifugation (10 min at 150,000 × g). 0.8 ml solubilizates were incubated for 2 hr at 4°C with 10 μg of immobilized anti-rabbit GlialCAM (López-Hernández et al., 2011a), anti-mouse GlialCAM (Vitro, Spain) and control IgG (Upstate, USA), respectively. After brief washing (2 × 5 min) with ComplexioLyte 47a, bound proteins were eluted with Laemmli buffer (DTT added after elution). Eluates were shortly run on SDS-PAGE gels and silver-stained prior to tryptic digestion for MS analysis. LC-MS/MS analysis was performed as described (López-Hernández et al., 2011a). Immunoprecipitation and western blot studies of HeLa cells transiently transfected or solubilized rat brain to confirm protein-protein interactions with ClC-2 and GlialCAM antibodies was performed as described (López-Hernández et al., 2011a). Relative MS sequence coverage of ClC-2 protein (Figure S1) was calculated as $SC = N_i/(N_i + N_{an})$, where N_i is the number of amino acid residues of the identified peptides (with Mascot score $\geq$ 20) and N_{an} is the number of MS-accessible but not identified amino acids (peptides with mass of 740–3,000 u) of the respective Swiss-Prot sequence.

Molecular Biology

Rat ClC-2 and the N-terminal deletion (Δ16–61) mutant ΔN (Gründer et al., 1992) constructs for expression in oocytes were in the pTLN vector (Lorenz et al., 1996). For localization studies in HEK293 or HeLa cells, rClC-2 and ΔN were C-terminally fused to GFP or to flag. DmClC-2 and ClC-2 with an HA extracellular tag was provided by LP Cid (Centro de Estudios Científicos, Chile). GlialCAM-ΔC was constructed eliminating residues from 289 until the stop codon.

Voltage-Clamp Experiments

Xenopus oocytes were injected and maintained as described (Estévez et al., 2003). For ClC-2, 5 ng cRNA and for ΔN 0.25 ng cRNA/oocyte were injected. When coexpressing, 1.25 ng cRNA of GlialCAM were coinjected with ClC-2. Oocytes were perfused with (in mM): 100 NaCl, 5 $MgSO_4$, and 10 HEPES/NaOH (pH 7.3). To estimate the specific ClC-2-mediated chloride currents, iodide (100 mM NaI replacing the NaCl), which blocks ClC-2-mediated outward currents (Gründer et al., 1992; Thiemann et al., 1992), was applied in every experiment. Oocytes which did not exhibit a significant block were discarded. For selectivity experiments (Figure 6B), 100 mM Cl^- was exchanged by 100 mM of the tested anion. For pH experiments, 10 mM buffer was used (pH 10–9: CAPS [*N*-cyclohexyl-3-aminopropanesulfonic acid]; pH 8–7: HEPES; pH 6–5: MES; and pH 4: Glutamic acid). Hypotonicity effects were studied as described (Gründer et al., 1992). For ClC-2, an initial 1 s voltage pulse at +60 mV was applied, followed by 5 s voltage steps from −140 mV to +60 mV in 20 mV increments and a tail pulse of 1 s to 60 mV. To quantify expression levels, the initial tail current (at +60 mV) after the −140 mV test pulse was estimated by back extrapolation of a single exponential fit to the decaying tail current. To estimate the number of constitutively active channels, instantaneous currents were measured during a short test pulse to +60 mV without prior activation by hyperpolarization.

Patch-Clamp Experiments

Fluorescent HEK293 cells, expressing CLC-2-GFP or ΔN-GFP with or without GlialCAM, were measured with an extracellular solution containing (in mM): 140 NaCl, 2 $MgSO_4$, 2 $CaCl_2$, and 10 HEPES/NaOH (pH 7.3) using standard patch-clamp technique. Intracellular solution was (in mM) 130 NaCl, 2 $MgSO_4$, 2 EGTA, and 10 HEPES/NaOH (pH 7.3). Only cells for which currents were reversibly blocked by iodide were used for analysis. Patch-clamp of astrocytes was performed as described (Ferroni et al., 1997).

Surface Expression by Chemiluminescence

Surface expression in transfected mammalian cells or astrocytes was performed similarly as previously described (Duarri et al., 2008; Teijido et al., 2004). Briefly, 48 hr after transfection, cells were cleaned with PBS and fixed with 3% paraformaldehyde. After PBS washing, cells were blocked with 1% BSA in PBS for 30 min, and incubated with 1 ml of 3F10 anti-HA antibody at 0.2 μg/ml in blocking solution for 1 hr at RT. Cells were washed six times with blocking solution, and incubated for 20 min with 1 ml of a 1:1,000 dilution horseradish peroxidase-coupled secondary antibody (donkey anti-rat IgG, Jackson, Suffolk, UK) in blocking solution. Cells were washed four times with blocking solution and eight times with PBS. Luminescence was measured

of one dish at a time with 500 μl of Power Signal ELISA solution (Pierce) in a Turner TD-20/20 luminometer (Turner Biosystems, Madison, WI, USA).

Immunological Procedures

Two immune sera against ClC-2 were generated against overlapping sequences of the C terminus. In the first antibody (C1 Ab), the peptide used for immunization was (C)HGLPREGTPSDSDDKSQ. The native protein sequence contains a cysteine residue instead of the highlighted serine in order to avoid coupling this residue to the carrier protein. In the second antibody (C2 Ab), the peptide used for immunization was (C)RSRHGLPREGTPSDSDD. (C) is the cysteine that was used for coupling. Affinity purification of the antibodies was used as described (López-Hernández et al., 2011a). Mostly, the C1 antibody was used in western blot studies, and the C2 antibody was used in immunoprecipitation, immunocytochemistry, and EM immunogold. Both antibodies gave no staining in the *Clcn2*$^{-/-}$ mice.

Primary Culture and Adenoviral Transduction

Rat primary quiescent astrocyte cultures were prepared as described previously (Duarri et al., 2008). Dibutyryl-cAMP differentiated rat astrocytes were obtained as described (Ferroni et al., 1997). Adenoviruses expressing three copies of the flag epitope fused to human GlialCAM, either wild-type or containing mutations have been described (López-Hernández et al., 2011a). Adenoviruses expressing GlialCAM fused to EmGFP or ClC-2 fused to three copies of the Flag epitope or containing an extracellular HA epitope were constructed in a similar manner. Transduction of astrocytes was performed as already described (López-Hernández et al., 2011a).

Immunofluorescence and Electron Microscopic Studies

Tissue immunohistochemistry and immunofluorescence were performed as previously described (Blanz et al., 2007; Teijido et al., 2004). For electron microscopic studies, human cerebellum samples were processed as previously described (López-Hernández et al., 2011a).

Quantification of Localization in Cell Contacts

Image J (http://rsbweb.nih.gov/ij/) was used to quantify fluorescence at cell contacts and in the plasma membrane at cell contact free sites by performing intensity profile experiments. We defined a ratio (R) considering the fluorescence signal at the plasma membrane of two cells (cell 1 and cell 2) and the signal in junctions. [$R = F_{junction}/(F_{membrane1}+F_{membrane2})$]. Thus, if the R value is > 1, the signal will be concentrated at junctions.

Split-TEV Method

Split-TEV (Tobacco etch virus protease) assays were performed as described (López-Hernández et al., 2011b). We used a mutant form of the TEV protease (S219V) which prevents its self-digestion but does not affect its catalytic efficiency. The oligopeptide substrate used as the TEV protease-recognition site was ENLYFQS, and the chimeric transcription factor used was GV (obtained from the pM3-VP16 vector) (Clontech, Nucliber, Madrid, Spain), which contains the yeast Gal4DNA binding domain and the herpes simples VP16 transactivaction domain. After TEV protease cleavage, GV translocates into the nucleus and induces the reporter Gaussia Luciferase gene expression (pNEBr-X1Gluc) (New England BioLabs, IZASA, Barcelona, Spain), which is secreted into the cell culture medium.

TEV protease was divided in two fragments: the TEV-N (residues 1–118) and the TEV-C (residues 119–242). We fused the TEV-N fragment, the TEV protease recognition site and the chimeric transcription factor GV to the C-terminal of ClC-2, the mutant ΔNClC-2, or DmClC-2 in a pCDNA3 vector containing a CMV promoter. In addition, we fused the TEV-C fragment to the C-terminal of ClC-2, ClC-5, ΔNClC-2, GlialCAM wild-type, HepaCAM2, GlialCAMΔC, GlialCAM containing the mutations R92Q, R98C, R92W, and G89D, and the adenosine 2A receptor. The fusion of the TEV-C fragment to 4F2hc was done N-terminal. All the proteins with the TEV-C fragments were cloned in a pCDNA6.2/V5-pL Dest, containing the herpes simplex virus thymidine kinase (HSV-TK) promoter, to provide low to moderate levels of expression.

All the expression plasmids were constructed by PCR using a polymerase with proofreading (KOD Hot Start polymerase, Calbiochem, Darnstadt, Germany), adding the attB1, attB2, attB5R, or attB5 recombination sites compatible with the Multisite Gateway System (Invitrogen, Carlsbad, CA, USA). All protocols were performed according to the manufacturer's instructions (Invitrogen).

HeLa cells were transiently transfected with the corresponding cDNA constructs. The total DNA transfected was 2 μg, with the following ratios: 0.75 μg of each protein containing the TEV-N and the TEV-C fragments, 0.3 μg of the reporter gene pNEBr-X1GLuc, and 0.2 μg of the pCMV-βGal vector, which was used to monitor the transfection efficiency. After 48 hr, 20 μl were removed from the supernatant of the cells and Gaussia luciferase activity was measured in a TD-20/20 luminometer (Turner BioSystems, Madison, USA), after the addition of 20 μM of native colenterazine. To normalize the data, cells were solubilized and 30 μl of the cell lysates were used to measure the β-Galactosidase enzyme activity using the Luminiscent β-Galactosidase Detection Kit II (Clontech) in the same luminometer.

Statistical Analyses

For determination of the statistical significance between groups, either the Student's t test or the Bonferroni's comparison test were used. p values are annotated in each figure. Values depicted are means ± SEM.

SUPPLEMENTAL INFORMATION

Supplemental Information includes six figures and can be found with this article online at doi:10.1016/j.neuron.2011.12.039.

ACKNOWLEDGMENTS

We thank Pablo Cid for the gift of DmClC-2 and human ClC-2 with an HA extracellular tag, Muriel Auberson for the generation of the ClC-2 C1 antibody and Soledad Alcántara for the NG2 antibody. We thank Alejandro Barrallo and Manuel Palacín for comments on the manuscript. This study was supported in part by SAF 2009-07014 (R.E.), PS09/02672-ERARE to R.E., ELA Foundation 2009-017C4 project (R.E. and V.N.), 2009 SGR 719 to R.E., SAF 2009-12606-C02-02 (V.N.), 2009 SGR01490 to V.N., FIS08/0014 (X.G.), FIS PI11/01601 (X.G.), and 2009 SGR869 (X.G.). R.E. is a recipient of an ICREA Academia prize. M.P. and E.J. are supported by the Compagnia San Paolo (Torino, Italy), Telethon Italy (GGP08064), and the Italian Institute of Technology (progetto SEED). This work is dedicated to the memory of Günter Jeworutzki.

Accepted: December 23, 2011
Published: March 7, 2012

REFERENCES

Blanz, J., Schweizer, M., Auberson, M., Maier, H., Muenscher, A., Hübner, C.A., and Jentsch, T.J. (2007). Leukoencephalopathy upon disruption of the chloride channel ClC-2. J. Neurosci. *27*, 6581–6589.

Bösl, M.R., Stein, V., Hübner, C., Zdebik, A.A., Jordt, S.E., Mukhopadhyay, A.K., Davidoff, M.S., Holstein, A.F., and Jentsch, T.J. (2001). Male germ cells and photoreceptors, both dependent on close cell-cell interactions, degenerate upon ClC-2 Cl^- channel disruption. EMBO J. *20*, 1289–1299.

Brignone, M.S., Lanciotti, A., Macioce, P., Macchia, G., Gaetani, M., Aloisi, F., Petrucci, T.C., and Ambrosini, E. (2011). The beta1 subunit of the Na,K-ATPase pump interacts with megalencephalic leucoencephalopathy with subcortical cysts protein 1 (MLC1) in brain astrocytes: new insights into MLC pathogenesis. Hum. Mol. Genet. *20*, 90–103.

Clark, S., Jordt, S.E., Jentsch, T.J., and Mathie, A. (1998). Characterization of the hyperpolarization-activated chloride current in dissociated rat sympathetic neurons. J. Physiol. *506*, 665–678.

Duarri, A., Teijido, O., López-Hernández, T., Scheper, G.C., Barriere, H., Boor, I., Aguado, F., Zorzano, A., Palacín, M., Martínez, A., et al. (2008). Molecular pathogenesis of megalencephalic leukoencephalopathy with subcortical cysts: mutations in MLC1 cause folding defects. Hum. Mol. Genet. *17*, 3728–3739.

Duarri, A., Lopez de Heredia, M., Capdevila-Nortes, X., Ridder, M.C., Montolio, M., López-Hernández, T., Boor, I., Lien, C.F., Hagemann, T., Messing, A., et al. (2011). Knockdown of MLC1 in primary astrocytes causes cell vacuolation: a MLC disease cell model. Neurobiol. Dis. *43*, 228–238.

Engel, P., Eck, M.J., and Terhorst, C. (2003). The SAP and SLAM families in immune responses and X-linked lymphoproliferative disease. Nat. Rev. Immunol. *3*, 813–821.

Estévez, R., Boettger, T., Stein, V., Birkenhäger, R., Otto, E., Hildebrandt, F., and Jentsch, T.J. (2001). Barttin is a Cl^- channel beta-subunit crucial for renal Cl^- reabsorption and inner ear K^+ secretion. Nature *414*, 558–561.

Estévez, R., Schroeder, B.C., Accardi, A., Jentsch, T.J., and Pusch, M. (2003). Conservation of chloride channel structure revealed by an inhibitor binding site in ClC-1. Neuron *38*, 47–59.

Fava, M., Ferroni, S., and Nobile, M. (2001). Osmosensitivity of an inwardly rectifying chloride current revealed by whole-cell and perforated-patch recordings in cultured rat cortical astrocytes. FEBS Lett. *492*, 78–83.

Favre-Kontula, L., Rolland, A., Bernasconi, L., Karmirantzou, M., Power, C., Antonsson, B., and Boschert, U. (2008). GlialCAM, an immunoglobulin-like cell adhesion molecule is expressed in glial cells of the central nervous system. Glia *56*, 633–645.

Ferroni, S., Marchini, C., Nobile, M., and Rapisarda, C. (1997). Characterization of an inwardly rectifying chloride conductance expressed by cultured rat cortical astrocytes. Glia *21*, 217–227.

Flores, C.A., Niemeyer, M.I., Sepúlveda, F.V., and Cid, L.P. (2006). Two splice variants derived from a Drosophila melanogaster candidate ClC gene generate ClC-2-type Cl^- channels. Mol. Membr. Biol. *23*, 149–156.

Földy, C., Lee, S.H., Morgan, R.J., and Soltesz, I. (2010). Regulation of fast-spiking basket cell synapses by the chloride channel ClC-2. Nat. Neurosci. *13*, 1047–1049.

Gründer, S., Thiemann, A., Pusch, M., and Jentsch, T.J. (1992). Regions involved in the opening of CIC-2 chloride channel by voltage and cell volume. Nature *360*, 759–762.

Jordt, S.E., and Jentsch, T.J. (1997). Molecular dissection of gating in the ClC-2 chloride channel. EMBO J. *16*, 1582–1592.

Lange, P.F., Wartosch, L., Jentsch, T.J., and Fuhrmann, J.C. (2006). ClC-7 requires Ostm1 as a beta-subunit to support bone resorption and lysosomal function. Nature *440*, 220–223.

Leegwater, P.A., Yuan, B.Q., van der Steen, J., Mulders, J., Könst, A.A., Boor, P.K., Mejaski-Bosnjak, V., van der Maarel, S.M., Frants, R.R., Oudejans, C.B., et al. (2001). Mutations of MLC1 (KIAA0027), encoding a putative membrane protein, cause megalencephalic leukoencephalopathy with subcortical cysts. Am. J. Hum. Genet. *68*, 831–838.

López-Hernández, T., Ridder, M.C., Montolio, M., Capdevila-Nortes, X., Polder, E., Sirisi, S., Duarri, A., Schulte, U., Fakler, B., Nunes, V., et al. (2011a). Mutant GlialCAM causes megalencephalic leukoencephalopathy with subcortical cysts, benign familial macrocephaly, and macrocephaly with retardation and autism. Am. J. Hum. Genet. *88*, 422–432.

López-Hernández, T., Sirisi, S., Capdevila-Nortes, X., Montolio, M., Fernández-Dueñas, V., Scheper, G.C., van der Knaap, M.S., Casquero, P., Ciruela, F., Ferrer, I., et al. (2011b). Molecular mechanisms of MLC1 and GLIALCAM mutations in megalencephalic leukoencephalopathy with subcortical cysts. Hum. Mol. Genet. *20*, 3266–3277.

Lorenz, C., Pusch, M., and Jentsch, T.J. (1996). Heteromultimeric CLC chloride channels with novel properties. Proc. Natl. Acad. Sci. USA *93*, 13362–13366.

Makara, J.K., Rappert, A., Matthias, K., Steinhäuser, C., Spät, A., and Kettenmann, H. (2003). Astrocytes from mouse brain slices express ClC-2-mediated Cl^- currents regulated during development and after injury. Mol. Cell. Neurosci. *23*, 521–530.

Menichella, D.M., Majdan, M., Awatramani, R., Goodenough, D.A., Sirkowski, E., Scherer, S.S., and Paul, D.L. (2006). Genetic and physiological evidence that oligodendrocyte gap junctions contribute to spatial buffering of potassium released during neuronal activity. J. Neurosci. *26*, 10984–10991.

Nagelhus, E.A., Mathiisen, T.M., and Ottersen, O.P. (2004). Aquaporin-4 in the central nervous system: cellular and subcellular distribution and coexpression with KIR4.1. Neuroscience *129*, 905–913.

Neusch, C., Rozengurt, N., Jacobs, R.E., Lester, H.A., and Kofuji, P. (2001). Kir4.1 potassium channel subunit is crucial for oligodendrocyte development and in vivo myelination. J. Neurosci. *21*, 5429–5438.

Niemeyer, M.I., Cid, L.P., Yusef, Y.R., Briones, R., and Sepúlveda, F.V. (2009). Voltage-dependent and -independent titration of specific residues accounts for complex gating of a ClC chloride channel by extracellular protons. J. Physiol. *587*, 1387–1400.

Rash, J.E. (2010). Molecular disruptions of the panglial syncytium block potassium siphoning and axonal saltatory conduction: pertinence to neuromyelitis optica and other demyelinating diseases of the central nervous system. Neuroscience *168*, 982–1008.

Ridder, M.C., Boor, I., Lodder, J.C., Postma, N.L., Capdevila-Nortes, X., Duarri, A., Brussaard, A.B., Estevez, R., Scheper, G.C., Mansvelder, H.D., and van der Knaap, M.S. (2011). Megalencephalic leucoencephalopathy with cysts: defect in chloride currents and cell volume regulation. Brain *134*, 3342–3354.

Rinke, I., Artmann, J., and Stein, V. (2010). ClC-2 voltage-gated channels constitute part of the background conductance and assist chloride extrusion. J. Neurosci. *30*, 4776–4786.

Scheper, G.C., van Berkel, C.G., Leisle, L., de Groot, K.E., Errami, A., Jentsch, T.J., and Van der Knaap, M.S. (2010). Analysis of *CLCN2* as candidate gene for megalencephalic leukoencephalopathy with subcortical cysts. Genet. Test. Mol. Biomarkers *14*, 255–257.

Sík, A., Smith, R.L., and Freund, T.F. (2000). Distribution of chloride channel-2-immunoreactive neuronal and astrocytic processes in the hippocampus. Neuroscience *101*, 51–65.

Teijido, O., Martínez, A., Pusch, M., Zorzano, A., Soriano, E., Del Río, J.A., Palacín, M., and Estévez, R. (2004). Localization and functional analyses of the MLC1 protein involved in megalencephalic leukoencephalopathy with subcortical cysts. Hum. Mol. Genet. *13*, 2581–2594.

Thiemann, A., Gründer, S., Pusch, M., and Jentsch, T.J. (1992). A chloride channel widely expressed in epithelial and non-epithelial cells. Nature *356*, 57–60.

van der Knaap, M.S., Barth, P.G., Stroink, H., van Nieuwenhuizen, O., Arts, W.F., Hoogenraad, F., and Valk, J. (1995a). Leukoencephalopathy with swelling and a discrepantly mild clinical course in eight children. Ann. Neurol. *37*, 324–334.

van der Knaap, M.S., Valk, J., Barth, P.G., Smit, L.M., van Engelen, B.G., and Tortori Donati, P. (1995b). Leukoencephalopathy with swelling in children and adolescents: MRI patterns and differential diagnosis. Neuroradiology *37*, 679–686.

van der Knaap, M.S., Barth, P.G., Vrensen, G.F., and Valk, J. (1996). Histopathology of an infantile-onset spongiform leukoencephalopathy with a discrepantly mild clinical course. Acta Neuropathol. *92*, 206–212.

Weinreich, F., and Jentsch, T.J. (2001). Pores formed by single subunits in mixed dimers of different CLC chloride channels. J. Biol. Chem. *276*, 2347–2353.

Insights into MLC pathogenesis: GlialCAM is an MLC1 chaperone required for proper activation of volume-regulated anion currents.

Article publicat el juny del 2013 a la revista Human Molecular Genetics.

Human Molecular Genetics, 2013, Vol. 22, No. 21 **4405–4416**
doi:10.1093/hmg/ddt290
Advance Access published on June 20, 2013

Insights into MLC pathogenesis: GlialCAM is an MLC1 chaperone required for proper activation of volume-regulated anion currents

Xavier Capdevila-Nortes[1], Tania López-Hernández[1,7], Pirjo M. Apaja[3,4], Miguel López de Heredia[5,6], Sònia Sirisi[1,5], Gerard Callejo[8,9], Tanit Arnedo[1,7], Virginia Nunes[2,5,6], Gergely L. Lukacs[3,4], Xavier Gasull[8,9] and Raúl Estévez[1,7,*]

[1]Sección de Fisiología, Departamento de Ciencias Fisiológicas II and [2]Sección de Genética, Departamento de Ciencias Fisiológicas II, University of Barcelona, Barcelona, Spain, [3]Department of Physiology and [4]Research Group Focused on Protein Structure, McGill University, Montréal, Quebec, Canada H3E 1Y6, [5]Laboratorio de Genética Molecular, IDIBELL, Barcelona, Spain, [6]U-730 and [7]U-750, Centro de Investigación en red de enfermedades raras (CIBERER), ISCIII, Barcelona, Spain, [8]Neurophysiology Lab, Department Physiological Sciences I, Medical School, University of Barcelona, Barcelona, Spain and [9]Institut d'Investigacions Biomèdiques August Pi i Sunyer (IDIBAPS), Barcelona, Spain

Received May 11, 2013; Revised and Accepted June 18, 2013

Megalencephalic leukoencephalopathy with subcortical cysts (MLC) is a rare type of leukodystrophy caused by mutations in either *MLC1* or *GLIALCAM* genes and is associated with myelin and astrocyte vacuolation. It has been suggested that MLC is caused by impaired cell volume regulation as a result of defective activation of astrocytic volume-regulated anion currents (VRAC). GlialCAM brings MLC1 and the ClC-2 Cl^- channel to cell–cell junctions, even though the role of ClC-2 in MLC disease remains incompletely understood. To gain insights into the biological role of GlialCAM in the pathogenesis of MLC disease, here we analyzed the gain- and loss-of-function phenotypes of GlialCAM in Hela cells and primary astrocytes, focusing on its interaction with the MLC1 protein. Unexpectedly, GlialCAM ablation provoked intracellular accumulation and reduced expression of MLC1 at the plasma membrane. Conversely, over-expression of GlialCAM increased the cellular stability of mutant MLC1 variants. Reduction in GlialCAM expression resulted in defective activation of VRAC and augmented vacuolation, phenocopying MLC1 mutations. Importantly, over-expression of GlialCAM together with MLC1 containing MLC-related mutations was able to reactivate VRAC currents and to reverse the vacuolation caused in the presence of mutant MLC1. These results indicate a previously unrecognized role of GlialCAM in facilitating the biosynthetic maturation and cell surface expression of MLC1, and suggest that pharmacological strategies aimed to increase surface expression of MLC1 and/or VRAC activity may be beneficial for MLC patients.

INTRODUCTION

Megalencephalic leukoencephalopathy with subcortical cysts (MLC) is a rare type of leukodystrophy (genetic alteration of the white matter) that affects brain chloride and fluid homeostasis (1). MRI of patients shows diffuse signal abnormality, swelling of the cerebral white matter and the presence of subcortical cysts, mainly in the anterior temporal regions (2,3). Studies from an MLC patient brain biopsy revealed that the major phenotype of the disease was myelin vacuolation (4). These results, together with proton magnetic spectroscopic resonance data (5,6), suggested that MLC is caused by disturbed fluid homeostasis.

MLC1 was the first gene to be identified in MLC patients (7) and accounts for MLC in most patients. In mouse and human tissue, high MLC1 levels were present in astroglial–astroglial junctions and ependymal cells in blood–brain and CSF–brain barriers, apart from astrocytic junctions of Bergmann glia in the cerebellum (8–11). Thus, it has been proposed that MLC

*To whom correspondence should be addressed at: Facultat de Medicina, Departament de Ciències Fisiològiques II, Universitat de Barcelona, C/Feixa Llarga s/n 08907 L'Hospitalet de Llobregat, Barcelona, Spain. Tel: +34 934039781; Fax: +34 934024268; Email: restevez@ub.edu

has an astrocytic origin (12), based on the fact that MLC1 is mostly expressed in astrocytes. In agreement with this hypothesis, depletion of MLC1 in astrocytes causes vacuolation, a phenotype that was also observed after re-examination of a MLC patient's brain biopsy (13), which showed previously only myelin vacuoles. Interestingly, reduction in MLC1 in astrocytes and in lymphoblast cell lines from MLC patients was found to be associated with a reduced activity of volume-regulated anion currents (VRAC) by an unknown mechanism (14). In parallel, the rate of regulatory volume decrease after cell swelling was reduced in MLC1-depleted cells (14). It has also been suggested that MLC1 could interact functionally with the β-subunit of the Na^+/K^+ ATPase (15) and with the TRPV4 ion channel (16). However, the role of MLC1 is still completely unknown, and whether these interactions are related to the effects of MLC1 depletion on VRAC activity is unknown.

GLIALCAM was recently identified as a second gene mutated in MLC (17). It was demonstrated that GlialCAM functions as an escort molecule necessary to target MLC1 to cell–cell junctions (18). Moreover, the changed localization of the MLC1/GlialCAM complexes seems to play an important role in the development of the disease, as most *GLIALCAM* mutations impair the correct trafficking of GlialCAM and MLC1 to astrocyte–astrocyte junctions (17,18).

Histological studies in tissue indicated that GlialCAM is mostly localized in astrocyte–astrocyte junctions where it co-localizes with MLC1 (17), but also in oligodendrocyte processes (19,20). Proteomic studies searching for additional GlialCAM protein partners revealed that GlialCAM also acts as an auxiliary subunit of the ClC-2 chloride channel, targeting it to astrocytic cell junctions and modifying its functional properties (20). Similar to its effect on MLC1 targeting, *GLIALCAM* MLC-related mutations also impair the trafficking of ClC-2 to cell junctions. Strikingly, *Clcn2* KO mice also displayed similar vacuolation to what is seen in MLC patients (21), suggesting its involvement in the pathogenesis of MLC. However, no *CLCN2* mutations were detected in MLC patients (22) and no direct protein interaction was found between MLC1 and ClC-2 (13,20). Thus, the involvement of ClC-2 in MLC disease is unclear. However, very recently, it has been shown that CLCN2 mutations may cause certain forms of a human leukodystrophy characterized by white matter oedema (23).

Dominant mutations in *GLIALCAM* cause other type of disease called MLC2B characterized by transient features of MLC (24). Similar to the recessive *GLIALCAM* mutations, also dominant mutations cause MLC1 and ClC-2 trafficking defects (17,18,20). It is still unknown why dominant mutations and not recessive mutations show a trafficking dominant behavior. Furthermore, dominant mutations are also associated with different clinical phenotypes than MLC1 mutations, while the clinical and MRI phenotypes related to recessive *MLC1* and *GLIALCAM* mutations are the same.

In the present work, we have analyzed biochemically and functionally what the consequences of a reduced GlialCAM expression are, and compared them with the effects of a reduced MLC1 expression. The effect of *GLIALCAM* and *MLC1* mutations was also addressed. The results obtained indicate that GlialCAM is necessary for MLC1 protein expression, and its reduction affects the activity of VRAC, which may cause astrocyte vacuolation. Thus, this work extends the role of GlialCAM as a chaperone of MLC1 needed for proper VRAC activation. In addition, based on functional data obtained, we suggest that a therapeutic strategy aimed to recover the surface expression of MLC1 and/or the activation of VRAC currents can be envisaged as beneficial for all MLC patients.

RESULTS

Experimental approach to create an astrocyte cell model with reduced GlialCAM expression

To study the cellular effects of GlialCAM ablation, adenoviral vectors expressing two distinct shRNA (1 or 2) against rat GlialCAM with the fluorescent protein EmGFP, allowing visualization of transduced cells, were produced. An adenoviral vector expressing non-targeted or scrambled shRNA (SCR) was used as a control. RT-qPCR experiments performed 7 days after GlialCAM shRNA infection of astrocytes demonstrated that endogenous GlialCAM mRNA levels were profoundly depleted (Fig. 1A). Accordingly, western blot (WB) analysis indicated that the GlialCAM protein level was reduced by 80% when compared with the control SCR (Fig. 1B and Supplementary Material, Fig. S1). Immunofluorescence experiments confirmed no detectable GlialCAM protein in shRNA-treated cells (Fig. 1C). Both types of experiments (WB and immunofluorescence) also demonstrated the specificity of the GlialCAM antibodies used (17). As an additional control, to exclude side effects of shRNAs, we also complemented with an adenovector expressing human C-terminally flag-tagged GlialCAM, which was resistant to the rat-specific GlialCAM shRNAs (Fig. 1B and C).

Reduction in GlialCAM expression led to intracellular retention and reduced expression of MLC1 in rat astrocytes

We studied the consequences of reduced GlialCAM expression at the mRNA, protein and subcellular localization of MLC1 (Fig. 2). As a specificity control, we monitored the expression and subcellular localization of a subset of proteins associated with tight, adherent and gap junctions. Knockdown of GlialCAM led to a reduction (about 30%) of the *MLC1* mRNA levels (not significant) (Fig. 2A). However, the MLC1 protein abundance was reduced to 60% of wild-type values (Fig. 2B and Supplementary Material, Fig. S1), which cannot be explained by the reduction in the mRNA levels. Protein levels of some junction proteins were not altered, excluding non-specific effects (Fig. 2B and data not shown).

Importantly, while MLC1 was predominantly confined to an intracellular perinuclear compartment (Fig. 2D, arrowheads) in astrocyted depleted of GlialCAM, MLC1 remained associated with cell–cell junctions in astrocytes transduced with control shRNA (Fig. 2C). Furthermore, the junctional localization of MLC1 was recovered after complementation of the astrocytes with flag-tagged human GlialCAM cDNA (Fig. 2E), which was resistant to this shRNA (Fig. 1 and Supplementary Material, Fig. S1). Therefore, altered processing and decreased stability of the MLC1 may account for the cellular phenotype of MLC1 rather than non-specific effects of the shRNA. Additional control experiments also showed that localization of some junction proteins was not changed in GlialCAM-depleted astrocytes (Supplementary Material, Fig. S2 and data not shown).

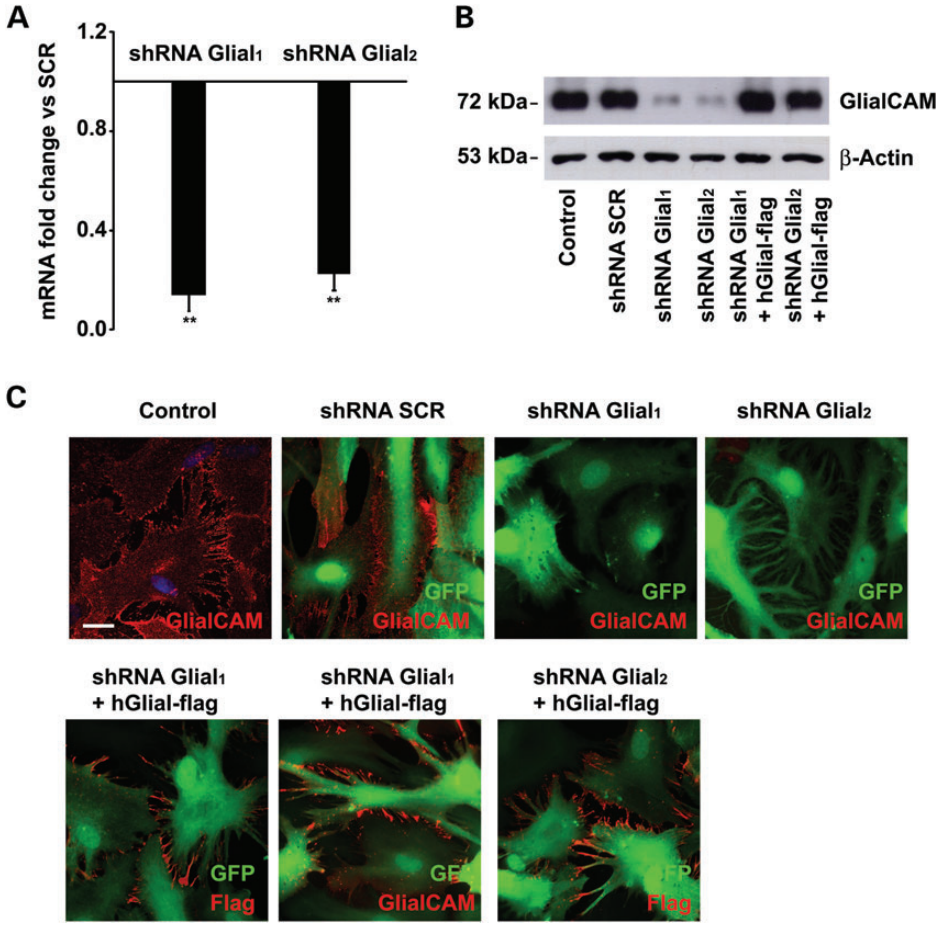

Figure 1. Adenovector-mediated knockdown of GlialCAM in primary astrocytes. (**A**) RT-qPCR experiments using specific primers to detect rat *GLIALCAM* mRNA. Data represent the ratio of mRNA fold change versus the SCR control (mean ± SEM) of at least four different astrocyte preparations either treated at MOI 10 with SCR (scrambled) or with 2 different shRNAs against *GLIALCAM*. Both shRNA Glial1 and Glial2 (see Materials and Methods) caused almost complete inhibition of mRNA expression. $^{**}P < 0.01$ (**B**) Astrocytes (untreated or transduced at MOI 10 with the shRNA indicated during 7 days, or complemented with adenovirus expressing flag-tagged human GlialCAM at MOI 2 during 2 days) were analyzed by WB using antibodies against GlialCAM. The GlialCAM antibodies used were able to detect the rat and human GlialCAM proteins. β-Actin was used as a loading control. Other different experiments gave similar results ($n = 5$). (**C**) Control or astrocytes transduced with the adenovirus indicated were fixed and processed for immunofluorescence using antibodies against GlialCAM. Transduced cells were visualized by the positive GFP signal. GlialCAM signal in astrocyte–astrocyte processes was detected in control cells and in cells transduced with the SCR shRNA but not in cells transduced with the shRNA1 against GlialCAM. In the panels below, cells were co-transduced with an shRNA against GlialCAM and flag-tagged human GlialCAM (resistant to shRNA) and immunofluorescence was performed using antibodies against the flag epitope or GlialCAM. Scale bar: 20 μm.

GlialCAM improves the protein stability and surface expression of MLC1 variants containing MLC-related mutations

The above results suggest that GlialCAM may function as a chaperone needed for correct MLC1 folding and expression. If this is the case, GlialCAM over-expression may correct the localization of MLC1 variants containing MLC-related mutations, which primarily affect MLC1 protein folding (25). To test this hypothesis, we constructed adenoviruses expressing a HA-tagged human MLC1 variant containing the MLC-related mutations Pro92Ser (P92S) or Ser246Arg (S246R), and they were used to transduce rat astrocytes with or without GlialCAM. The immunostaining of the mutant MLC1-P92S showed a perinuclear intracellular distribution in astrocytes (Fig. 3A), similar to the endoplasmatic reticulum (ER) (25). However, co-expression with GlialCAM led to a re-distribution of the P92S variant to astrocyte–astrocyte junctions (Fig. 3B left, arrowheads), co-localizing with GlialCAM (Fig. 3B, right, arrowheads). Similar results were obtained with the MLC1-S246R mutant (Supplementary Material, Fig. S3A). We next asked whether MLC1 intracellular retention could be attenuated in HeLa cells expressed heterologously. GlialCAM was indeed able to rescue the intracellular accumulation of all MLC1 mutants studied (G59E, C85W, L311Ins and N141K) and re-locate them to the cell junction [Supplementary Material, Fig. S3B–E and (18)].

Using a chemiluminescence-based cell surface ELISA assay, the MLC1 cell surface density was determined as a function of GlialCAM expression, taking advantage of the extracellular HA epitope. The MLC1-P92S has an 80% reduced cell surface expression relative to its wild-type counterpart (Fig. 3C). GlialCAM over-expression increased the relative surface-expression levels of the MLC1-P92S in rat astrocytes (Fig. 3D). The

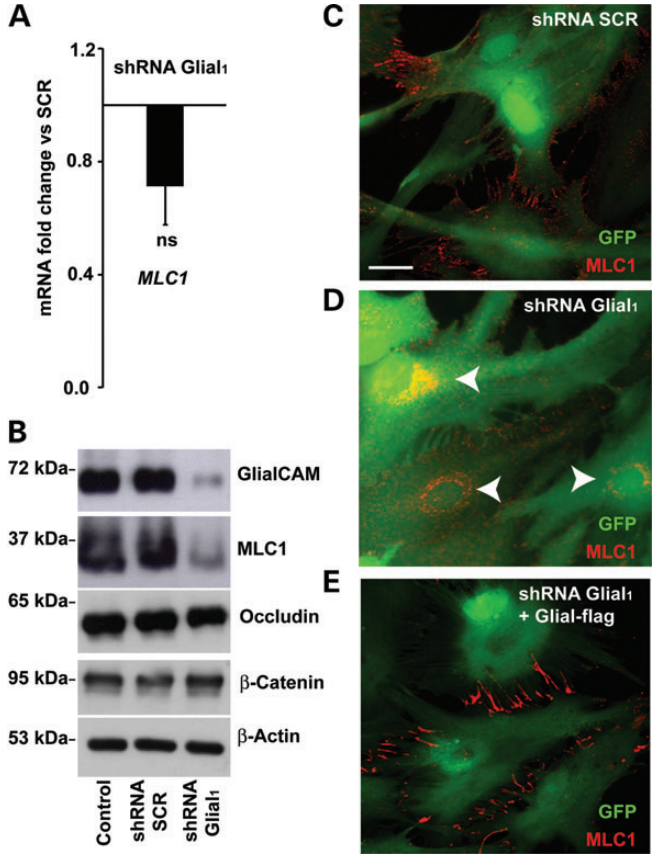

Figure 2. Expression of MLC1 in GlialCAM-depleted astrocytes. (**A**) RT-qPCR experiments using specific primers to detect rat *MLC1* mRNA. Data represent the mean ± SEM of four different astrocyte preparations either treated at MOI 10 with SCR (scrambled) or with a shRNAs against GlialCAM. Both shRNA Glial1 and Glial2 gave similar results. Ns, not significative; $^{*}P < 0.01$. (**B**) Astrocytes (untreated or transduced at MOI 10 with the shRNA indicated during 7 days) were analyzed by WB using antibodies against the indicated proteins. β-Actin was used as a loading control. Different experiments gave similar results ($n = 3–5$). (**C**) Localization of MLC1 in astrocyte–astrocyte junction in cells transduced with the adenovirus expressing a control shRNA, which were visualized by the positive GFP signal. (**D**) Localization of MLC1 in astrocytes with reduced expression of GlialCAM was detected mostly intracellular around the nucleus (arrowheads). (**E**) Astrocytes were co-transduced with a shRNA against GlialCAM and flag-tagged human GlialCAM (resistant to shRNA) and processed by immunofluorescence. Localization of endogenous MLC1 was detected in astrocyte–astrocyte junctions. Scale bar: 20 μm.

increase in surface levels detected by this method was moderate but significant. It may be that the surface levels of MLC1 quantified by this assay in astrocytes were underestimated, due to a possible masking of the extracellular HA epitope present in MLC1 by GlialCAM in astrocyte–astrocyte junctions, as happened in other membrane proteins with accessory subunits (26).

To assess whether GlialCAM can influence MLC1 stability, the disappearance kinetics of the cellular pool was monitored by WB during a cycloheximide chase (CHX). The MLC1-P92S variant showed significantly reduced stability as demonstrated by the accelerated removal of the mutant upon translation termination with CHX (Fig. 3E and F). Co-expression with GlialCAM considerably improved the protein stability of the mutated P92S variant and also of the wild-type MLC1 protein.

Knockdown of GlialCAM affects MLC1 protein expression also in HeLa cells

The above results indicate that GlialCAM has two important functions. On the one hand, as reported previously, it is necessary to target MLC1 to cell–cell junctions (18,20). On the other hand, GlialCAM is necessary to stabilize MLC1 and this stabilization is important for translocation to the plasma membrane. This second role was unexpected, as MLC1 localization at the plasma membrane was detected without GlialCAM expression in HeLa cells. To explain this controversy, we hypothesized that GlialCAM is endogenously expressed in HeLa cells at low levels. Importantly, GlialCAM protein could be detected at the plasma membrane, using a monoclonal antibody directed against extracellular GlialCAM by a chemiluminescence-based ELISA assay (Fig. 4A). Transfection of two independent shRNAs against GlialCAM reduced the antibody signal, confirming that the plasma membrane signal detected by the antibody was due to GlialCAM (Fig. 4A).

To address whether the stabilization effect of GlialCAM in MLC1 could be also observed in HeLa cells, we transfected HeLa cells with wild-type MLC1 or MLC-related mutant variants P92S (PS) or C326R (CR) together with and unrelated shRNA as a control or shRNAs against GlialCAM, and assayed the cellular and surface MLC1 expression by immunoblotting and cell surface ELISA, respectively. Knockdown of GlialCAM reduced total (Fig. 4B) and cell surface (Fig. 4C) expression of all MLC1 variants, including the wild-type MLC1, as observed in rat astrocytes. Considering that GlialCAM and MLC1 physically interact [revealed by split-TEV or FRET studies (18)], these data strongly suggest that GlialCAM exerts a stabilizing effect on MLC1, which is independent of the cell system studied.

Effect of GlialCAM MLC-related variants on MLC1 expression

GlialCAM variants containing MLC-related mutations affect GlialCAM and MLC1 trafficking to cell junctions, without substantially interfering with GlialCAM expression or the biochemical interaction between GlialCAM/MLC1 (17,18,20). We thus addressed whether *GLIALCAM* mutations can compromise MLC1 stabilization in astrocytes. To this aim, we first depleted endogenous GlialCAM in astrocytes by adenovirus-mediated RNA interference, and then complemented with wild-type GlialCAM wild-type or two mutant variants, Arg92Gln (R92Q), found in MLC2A patients, or Arg92Trp (R92W), found in MLC2B patients. As a control for protein expression, we complemented with MLC1. Astrocytes were analyzed by WB or immunofluorescence (Fig. 5 and Supplementary Material, Fig. S1). Knockdown of GlialCAM reduced both GlialCAM and MLC1 expression (Fig. 5A and Supplementary Material, Fig. S1), and led to a mislocalization of MLC1 to an intracellular compartment (Fig. 5B). After knockdown of endogenous GlialCAM, complementation with human GlialCAM rescued MLC1 protein expression (Fig. 5A and Supplementary Material, Fig. S1) and junctional localization (Fig. 5C).

Complementation with GlialCAM variants containing the mutations R92Q or R92W also rescued MLC1 protein expression (Fig. 5A and Supplementary Material, Fig. S1). However,

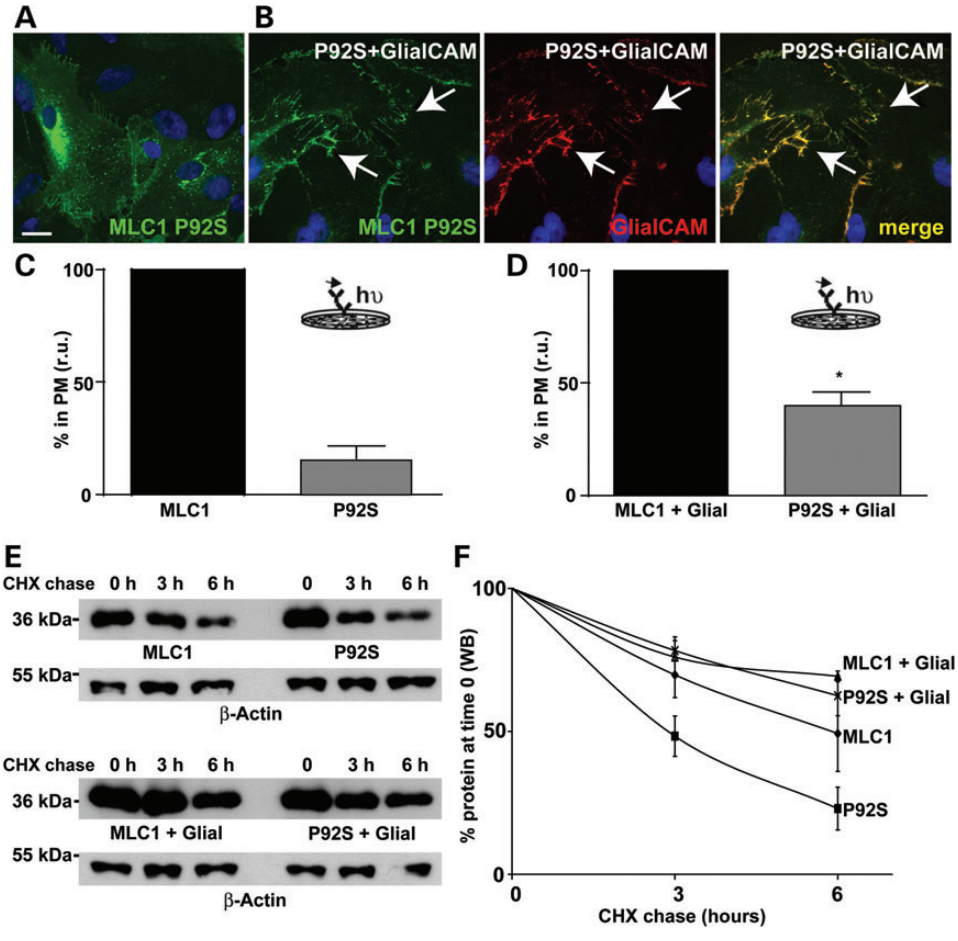

Figure 3. GlialCAM increases surface expression and protein stability of MLC1 containing MLC-related mutations in primary astrocytes. (**A** and **B**) Astrocytes were transduced with adenoviruses expressing *HA*-tagged MLC1 containing the MLC-related mutation P92S alone (A) or in combination with GlialCAM (B). After 48 h, cells were fixed and processed by immunofluorescence using antibodies against HA tag (3F10) or GlialCAM. The yellow merge channel indicates co-localization. Arrowheads point to contacts between astrocytes, where MLC1 P92S and GlialCAM co-localized. Scale bar: 20 μm. (**C** and **D**) Astrocytes were transduced with adenoviruses expressing MLC1 wild-type or MLC1 containing the MLC-related mutation P92S alone (C) or in combination with GlialCAM (D). MLC1 constructs have an extracellular *HA* epitope. Plasma membrane levels were measured using a luminescence-based method, as described in Materials and Methods, and they were normalized to the level of the wild-type MLC1 in each condition. The inset shows an overview of the method. Data correspond to the average of three independent experiments. $^{*}P < 0.05$, comparing the levels of the mutant at the plasma membrane with or without GlialCAM. (**E** and **F**) Astrocytes were transduced with adenoviruses expressing MLC1 wild-type or MLC1 containing the MLC-related mutation P92S alone or in combination with GlialCAM. 48 h after transduction, cells were treated or not with cycloheximide (CHX, 100 μg/ml) at the times indicated. Cells extracts were obtained, and the remaining protein was analyzed by western-blot against the *HA* epitope. β-Actin detection was used as a loading control. The result is a representative experiment of four with similar results. In (F), a summary of the quantification of all experiments using ImageJ software is shown. To quantify signals by WB, we performed at least three expositions of all WBs, to ensure linearity. The signal is normalized to the value at time 0 for each of the experimental groups. The stability of the mutant P92S increased significantly when co-expressed with GlialCAM ($P < 0.01$).

the junctional localization of endogenous MLC1 was not corrected by the different mutated variants (Fig. 5D for R92Q and Fig. 5E for R92W).

Volume-regulated chloride currents are affected in MLC1- and GlialCAM-depleted astrocytes

Lack of MLC1 in rat astrocytes or in lymphoblast cell lines obtained from MLC patients have been related with a defective activation of VRAC (14), whose molecular identity is still unknown (27). We next addressed whether lack of GlialCAM may also affect VRAC currents.

Previous electrophysiological studies addressing VRAC currents were performed in mild trypsin-treated astrocytes (14). As this assays needed an enzymatic treatment to round astrocytes potentially leading to other effects related with the trypsin treatment (28), we switched to dB-cAMP-treated astrocytes that are already rounded due to the elongation of processes (29). We focused only in changes in VRAC activity, taking advantage of the fact that not all astrocytes express ClC-2 mRNA in isotonic conditions (30), but most express VRAC currents in hypotonic conditions. In both cases, reduction in MLC1 or GlialCAM led to a dramatic decrease of VRAC activity of 80%, although it was still detectable (Fig. 6).

Lack of GlialCAM and MLC1 causes astrocyte vacuolation

Lack of MLC1 in astrocytes and in MLC patients caused the appearance of vacuoles in the cytoplasm of astrocytes [(13) and compare Fig. 7A with Fig. 7B]. Similarly, knockdown of

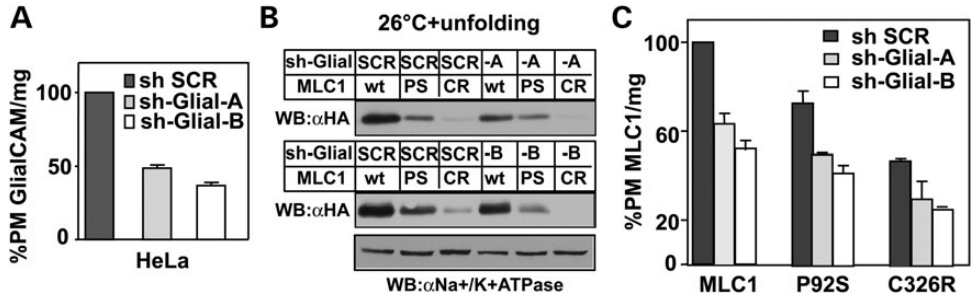

Figure 4. Effect of GlialCAM expression levels on MLC1 expression levels and trafficking in HeLa cells. Hela cells transduced with two lentivirus expressing shRNAs against GlialCAM (sh-Glial-A, sh-Glial-B) or shRNA Scrambled (sh SCR) were analyzed with anti-HepaCAM antibody for GlialCAM cell surface expression using ELISA as described in Materials and Methods. (**B**) The shGlialCAM cells (A or B) were transfected with indicated MLC1 cDNAs (wt, wild-type; PS, P92S; CR, C326R). Cells were seeded on 24-well plates 20 h after transfection and incubated at 37°C for 24 h. Cells were temperature rescued at 26°C for 24 h, and unfolding was performed at 37°C for 1 h prior of experiment. They were analyzed by immunoblotting against the *HA* epitope present in MLC1. Na^+–K^+-ATPase was used as a loading control. (**C**) Cell surface density of MLC1 in shGlialCAM cells was done as in (A), but using anti-HA antibody. The expression was normalized for MLC1 wt expression in shSCR cells.

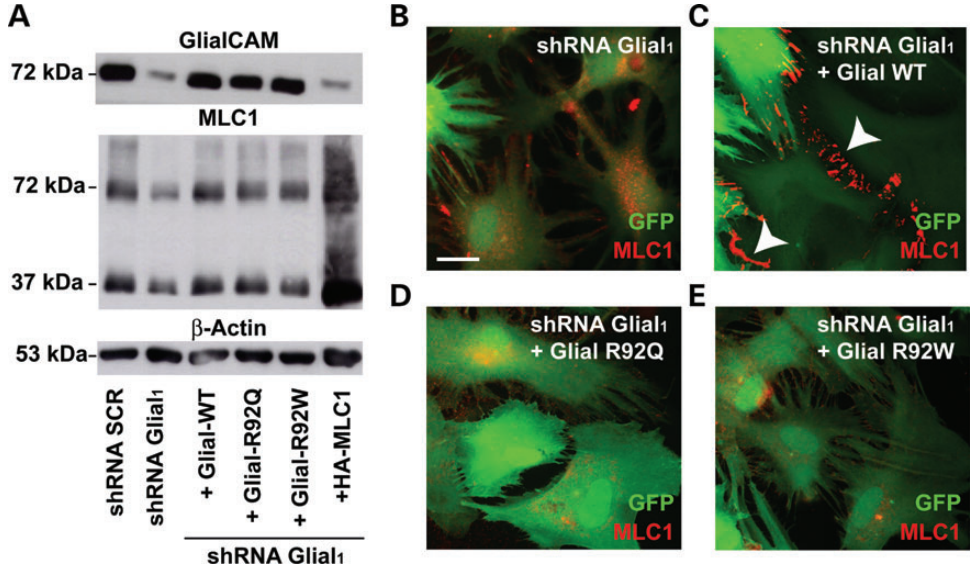

Figure 5. GlialCAM with MLC-related mutations increase MLC1 expression but show a trafficking defect. (**A**) Astrocytes transduced with the shRNA indicated during 7 days and complemented or not with the indicated constructs were analyzed by WB using antibodies against the indicated proteins GlialCAM and MLC1. β-Actin was used as a loading control. Four different experiments gave similar results. A quantification of several experiments is shown in Supplementary Material, Figure S1. (**B**–**E**) Similarly, for the different experimental groups showed here, astrocytes were fixed and processed by immunofluorescence using antibodies against MLC1. Green signal indicates the GFP which is co-expressed with the shRNA. Arrows label contacts between astrocytes. Scale bar: 20 μm.

GlialCAM also led to astrocyte vacuolation (Fig. 7C). Vacuoles appearing in MLC1 or GlialCAM-depleted astrocytes were also of endosomal origin, as revealed by staining with the endodomal protein marker EEA1 (early-endosomal antigen 1) (Fig. 7B and C).

We next aimed to correlate if vacuolation was directly linked to an increase in intracellular water. Treatment of astrocytes for 24 h with a hypoosmotic medium induced the appearance of water vacuoles of endosomal origin [(15) and Fig. 7D]. To test if a defective VRAC activity causally can contribute to the vacuolation phenotype, we inhibited VRAC activity, indirectly by attenuating the chloride gradient or directly. This was accomplished by incubating astrocytes with Bumetanide (Fig. 7E), which blocks sodium/potassium/chloride co-transporters (31–34), or by DCPIB (Fig. 7F), the most specific VRAC inhibitor known (35). Both treatments led to the appearance of vacuoles of endosomal origin. In order to correlate the biochemical and electrophysiological data with the vacuolation phenotype, we quantified the number of cells containing vacuoles for all experimental groups (see Materials and Methods). Quantification of the vacuolation phenotype in cells treated with Bumetanide or DCPIB revealed a similar degree of defect as cells treated with the shRNAs against MLC1 or GlialCAM (Fig. 8 and Supplementary Material, Fig. S4) [Bumetanide, $15.4 \pm 2.3\%$ (4 independent exp, 1033 cells); DCPIB, $18.8 \pm 2.9\%$ (4 independent exp, 1226 cells)].

Recovery of MLC1 in junctions rescued the vacuolation defect and VRAC activation

The astrocyte vacuolation caused by the lack of GlialCAM was rescued with complementation with human GlialCAM (Fig. 8A and Supplementary Material, Fig. S4). However,

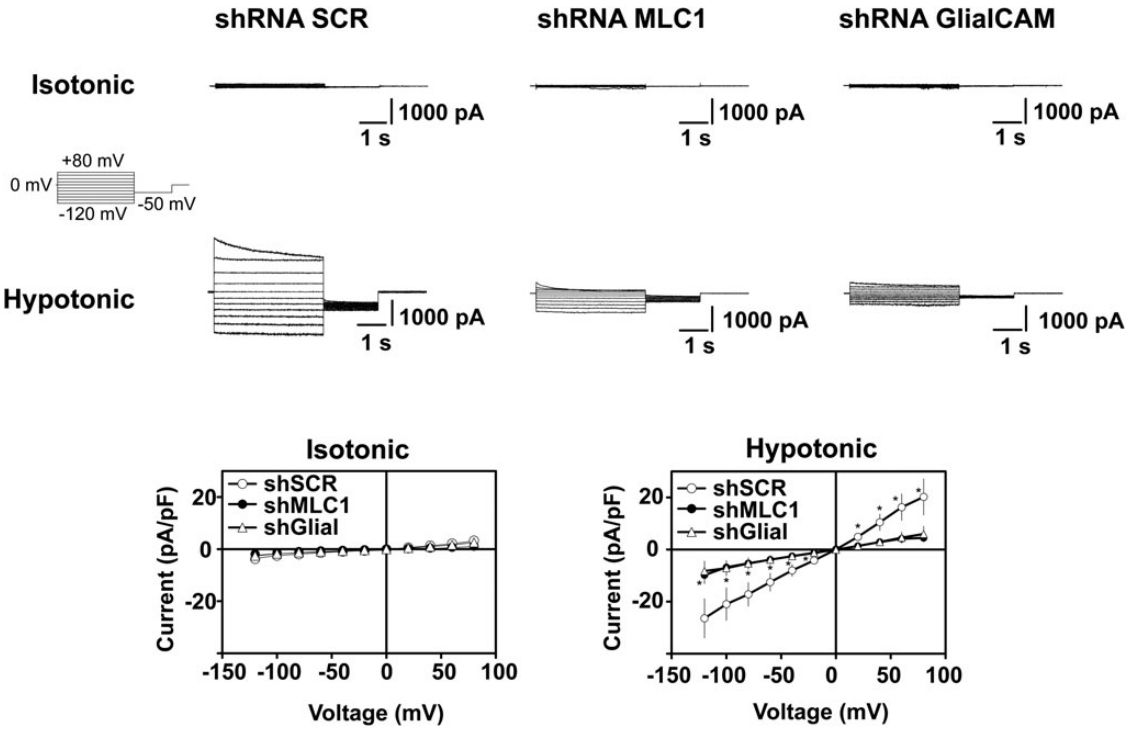

Figure 6. VRAC activity is reduced in astrocytes with reduced expression of MLC1 and GlialCAM. Representative family of whole-cell chloride currents in dbcAMP-treated cultured neocortical astrocytes transduced with shRNA scrambled or shRNA against MLC1 or GlialCAM, elicited by the pulse protocol shown in the inset. Astrocytes that did not show ClC-2-like currents in isotonic conditions were selected. They correspond to about 60% of recorded cells. In about 85% of these cells do not having ClC-2 current in isotonic conditions, application of a hypotonic solution activated VRAC current. As expected, these currents were blocked by DCPIB, but not with iodide replacement (data not shown). The plot shows average steady-state current–voltage relationship of dbcAMP-treated astrocytes transduced with shRNA SCR (circles), shRNA MLC1 (filled circles) or shRNA GlialCAM (triangles) in isotonic and hypotonic conditions. Results corresponds to $n = 15$ for shRNA SCR, $n = 14$ for shRNA MLC1 and $n = 14$ for shRNA GlialCAM. $^{*}P < 0.05$ *t*-test versus scramble for both MLC1 and GlialCAM groups.

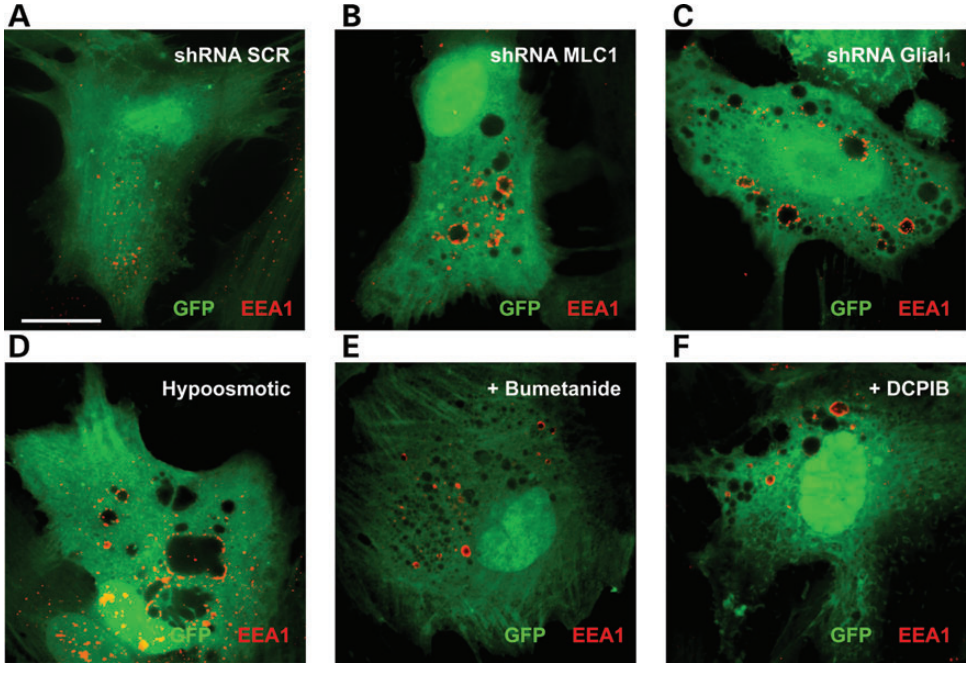

Figure 7. Similarities between the vacuolation induced by the lack of GlialCAM and the inhibition of VRAC activity. (**A**–**C**) Primary cultures of astrocytes were transduced with adenovectors expressing shRNA SCR, shRNA against MLC1 or shRNA against GlialCAM. After 7 days, cells were fixed and immunostained using antibodies against early-endosomal antigen 1 (EEA1). In (**D**–**F**), cells were transduced with adenovector expressing shRNA SCR and incubated with 50 μM bumetanide during 7 days (D) or 10 μM DCPIB during 7 days (E) or with a hypo-osmotic medium during 24 h (F). Cells were then fixed and immunostained using antibodies against EEA1. Green signal corresponds to GFP which is expressed together with the shRNA. Scale bar: 20 μm.

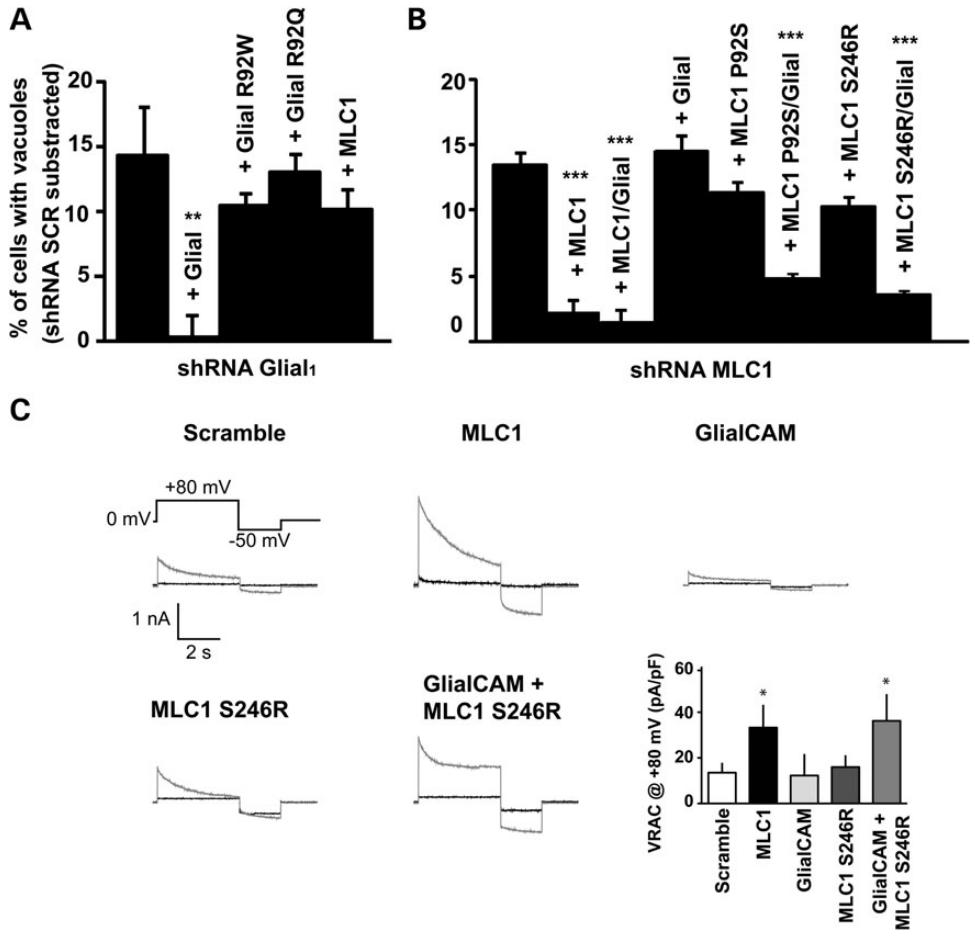

Figure 8. Correlation between VRAC activity and the vacuolation phenotype of astrocytes. (**A** and **B**) Quantification of the number of cells showing vacuolation after transduction with the shRNA-indicated and complemented or not with adenoviruses expressing the indicated constructs. In (A), data correspond to four to five independent experiments with the number of cells analyzed for each group as follows: shRNA SCR ($n = 1483$), shRNA Glial1 ($n = 1646$), shRNA Glial1 + Glial ($n = 1502$), shRNA Glial1 + Glial R92W ($n = 1776$), shRNA Glial1 + Glial R92Q ($n = 1917$), i shRNA Glial1 + MLC1 ($n = 1606$). $^{**}P < 0.01$ compared with shRNA Glial1. The background of cells with vacuoles of shRNA SCR (MOI 10) is 13.81 ± 1.98%. In (B), data correspond to four to five independent experiments with the number of cells analyzed for each group as follows: shRNA SCR ($n = 1009$), shRNA MLC1 ($n = 1064$), shRNA MLC1 + MLC1 ($n = 1094$), shRNA MLC1 + Glial ($n = 1164$), shRNA MLC1 + MLC1 P92S ($n = 1585$), shRNA MLC1 + MLC1 P92S + Glial ($n = 1379$), shRNA MLC1 + MLC1 S246R ($n = 1248$), shRNA MLC1 + MLC1 S246R + Glial ($n = 1203$). $^{***}P < 0.001$ compared with shRNA MLC1. The background of cells with vacuoles of shRNA SCR (MOI 5) is 5.38 ± 1.23%. (**C**) Representative traces at +80 mV of whole-cell chloride currents in isotonic (black) or hypotonic conditions (grey) elicited by the pulse protocol showed in the inset, in dbcAMP-treated cultured neocortical astrocytes transduced with shRNA scrambled or adenoviruses over-expressing MLC1, GlialCAM, MLC1 S246R or GlialCAM + MLC1 S246R. Astrocytes that did not show ClC-2 currents in isotonic conditions were selected. The plot shows average conductance values at +80 mV in hypotonic conditions. Results correspond to $n = 9$ for shRNA SCR, $n = 8$ for MLC1, $n = 5$ for GlialCAM, $n = 9$ for MLC1 S246R and $n = 9$ for GlialCAM + MLC1 S246R. $^{*}P < 0.05$ *t*-test versus. Scramble for all groups. Differences in the kinetics of inactivation were observed between groups in an unrelated manner, even in the same experimental group, and probably are related with differences in ionic strength between cells.

complementation with GlialCAM containing the MLC-related mutations R92Q or R92W, or further expression of MLC1 did not rescue the vacuolation defect (Fig. 8A). In agreement with these cellular defects, localization of over-expressed human MLC1 in GlialCAM-depleted astrocytes was detected mostly intracellularly (Supplementary Material, Fig. S5).

Similarly, vacuolation caused by the lack of MLC1 was rescued by expressing MLC1 or GlialCAM together with MLC1 (Fig. 8B). However, further expression of GlialCAM did not rescue the vacuolation phenotype. Rescue of MLC1 expression by MLC1 containing MLC-related mutations also failed to counteract the vacuolation phenotype (Fig. 8B), probably due to its intracellular localization (Fig. 3). However, restoring the localization of these proteins in junctions (Fig. 3) after co-expressing with GlialCAM successfully suppressed the vacuolation (Fig. 8B).

We next addressed whether the vacuolation could be correlated with changes in VRAC activity. Over-expression of MLC1 in dB-cAMP-treated astrocytes increased VRAC activity [Fig. 8C and (14)]. However, over-expression of GlialCAM alone or MLC1 containing the MLC-related mutation S246R did not increase VRAC activity [Fig. 8C and (14)]. In agreement with the rescue of the vacuolation defect, over-expression of MLC1 S246R together with GlialCAM also increased VRAC activity (Fig. 8C). Therefore, we suggest that defective VRAC activity may be directly linked to astrocyte vacuolation.

DISCUSSION

In this work, we have studied the effects of reducing GlialCAM expression in astrocytes, a recently identified MLC1 and ClC-2 subunit (18,20). Taking into account these new results presented here, we conclude that whereas GlialCAM is necessary for the targeting to astrocyte–astrocyte junctions of both MLC1 and ClC-2 (18,20), it has an additional role as an MLC1-chaperone. Based on the fact that the stabilization is observed in HeLa cells, that GlialCAM interacts directly with MLC1 (18) and that GlialCAM stabilizes also ER retained folding mutant variants of MLC1 (18), we propose that GlialCAM may protect MLC1 from ER-associated degradation. We hypothesize that this ER-protective effect of GlialCAM was not previously recognized due to the presence of endogenous GlialCAM expression in all the cell lines studied. Thus, it can be seen how expression of MLC1 in astrocytes without GlialCAM resulted in no plasma membrane staining of MLC1. As expression of MLC1 in astrocytes alone is able to arrive to the plasma membrane, it suggests that astrocytes should have an excess of endogenous GlialCAM compared with MLC1.

It has been shown that MLC-related mutations in GlialCAM do not substantially affect the interaction with MLC1 (18). Here, we also show that MLC-related GlialCAM variants are able to stabilize MLC1 protein, although they are not able to direct MLC1 to astrocyte junctions.

Reduction in both GlialCAM and MLC1 led to astrocyte vacuolation and a decreased VRAC activity (14). The function of VRAC currents which are heterogeneous is related with the efflux of water during the regulatory volume response (36). A decreased VRAC activity may cause an increase of intracellular water. We suggest that astrocyte vacuolation could be a consequence of increased water content, as blocking VRAC or the presence of a hypoosmotic medium (15) led to a similar type of vacuolation of endosomal origin. However, it is not clear how increased water content causes the appearance of vacuoles. It could be that astrocytes, which are cells evolutionary adapted to live in changing osmotic conditions, have gained the ability to keep the excess of intracellular water in the form of a vacuole, as happens in other organisms that form contractive vacuoles, and then they can survive in extracellular changing conditions (37–41).

How MLC1 and GlialCAM are related to VRAC activity? At this moment, it is very difficult to provide a clear answer to this question, as the function of MLC1 is unknown and the protein(s) responsible for VRAC activity still have to be discovered (27). Identification of the VRAC channel is a major and difficult task, as revealed by the reports of many potential candidates that later turned out to be wrong, such as ICln, p-Glycoprotein or the ClC-3 transporter (27,36). GlialCAM may affect VRAC activity due to the lack of MLC1, as GlialCAM over-expression by itself cannot compensate the vacuolation caused by the lack of MLC1. However, we believe that it is unlikely that MLC1 is directly responsible of VRAC, as VRAC activity is present in all the cells of the body (36), whereas MLC1 is mostly restricted to the brain and no other MLC1-homologous genes exists in mammals (7). In addition, VRAC activity is still present in astrocytes depleted of MLC1. MLC1 may affect VRAC activity indirectly, for instance, by modifying the adhesion strength of astrocytes or by affecting water or chloride handling in the brain. In this sense, aquaporin 4 depletion has also been shown to affect VRAC activity (42). It is worth to mention that MLC1 protein has also been found surrounding the endosomal membranes of astrocytes treated with a hypoosmotic solution (15) or with blockers such as DCPIB or Bumetanide (this work, data not shown). In these endosomal vesicles, MLC1 could contribute to the formation of water vacuoles by regulating water and/or chloride fluxes.

Interestingly, although GlialCAM proteins containing MLC-related mutations re-establish MLC1 protein expression, they do not direct MLC1 to junctions and are not able to rescue the vacuolation defect caused by the lack of MLC1. Therefore, we suggest that the correct localization of MLC1 is critical to perform its physiological function. In relation with putative roles suggested for MLC1 in ion transport or adhesion (10,14), its localization in junctions may be needed to allow transcellular fluxes of solutes or to detect easily changes in adhesion strength.

No treatment exists yet for MLC disease (1). Although the role of MLC1 is unknown, over-expression of GlialCAM rescues the vacuolation and the VRAC activity defect caused by some MLC1 mutants. Thus, the present data suggest that therapeutic strategies aimed at improving the surface expression of MLC1 or increasing the activity of VRAC may be envisaged as beneficial for MLC patients. This could be done by isolating pharmacological chaperones based on increased MLC1 plasma membrane expression (43) or molecules aimed to increase VRAC activity, as has been done for other chloride channels (44).

MATERIALS AND METHODS

Primary culture, adenoviral transduction and vacuolation analysis

Rat primary quiescent astrocyte cultures were prepared as described previously from P0–P2 pups (13). Dibutyryl-cAMP differentiated rat astrocytes, which were used for electrophysiological measurements, were obtained as described (29). Adenoviruses expressing three copies of the flag epitope fused to human GlialCAM, either wild-type or containing the MLC-related mutations R92Q or R92W have been described (17). Similarly, adenoviruses expressing HA-tagged wild-type MLC1 or containing the MLC-related mutations S246R or P92S were also constructed. Transduction of astrocytes was performed as already described (25).

To study the vacuolation of astrocytes, we counted the cells with showed clear vacuoles. A cell was positive for vacuolation if have at least three vacuoles of a size bigger than 0.5 μm. The minor vacuolation observed in astrocytes transduced with the corresponding group expressing SCR shRNA instead of the specific shRNA was subtracted from all the experimental groups. This was done to compare directly MLC1 and GlialCAM depleted astrocytes, as the multiplicity of infection was different between both groups (MOI 5 for shRNA MLC1 and MOI 10 for shRNA GlialCAM) and the day of processing after the infection (5 days for shRNA MLC1 and 7 days for shRNA GlialCAM).

RNA interference and RT-qPCR

RNAi entry-clone (Gateway, Invitrogen) vectors were prepared using the Block-it PolII miR RNAi EmGFP expression vector kit following manufacturer's instructions. Entry clones were

recombinated using LR clonase into the vector pAdVD EST-CMV/V5. Adenoviruses were produced and titrated using fluorescence microscopy detecting EmGFP which is expressed together with the shRNA. The adenoviruses expressing a negative control shRNA (shRNA SCR, scrambled) or expressing an shRNA directed against rat MLC1 (shRNA 905) were described previously (13). The sequence of the oligos used to knockdown rat GlialCAM expression was: shRNA Glial1 (shRNA 1392): 5′aagatcagcgctccacccattgttttggccactgactgacaatgggtggcgctgatctt3′ and shRNA Glial2 (shRNA 908): 5′tatagagcgccattggattctgtttt ggccactgactgacagaatccaggcgctctata3′.

Total RNA was prepared from a 10 cm culture plate using NucleoSpin RNA/Prot (Macherey–Nagel) as indicated by the manufacturer. RNA concentration was determined in a Nanodrop spectrophotometer. All samples had an A260/A280 ratio >1.8. RNA was stored at −80°C until further use. Eight hundred to 1000 ng of total RNA were reverse-transcribed with Transcriptor First Strand cDNA synthesis kit (Roche) following manufacturer's instructions at 25°C for 10 min followed by 50°C for 60 min, using random hexamers as primers. cDNA was stored at −80°C. qPCR was performed with Lightcycler 480 probes master kit (Roche) following manufacturer's instructions in a final volume of 10 μl, with cDNA at 1:10 dilution. The primers and UPL probes used were designed with the ProbeFinder version 2.45 (Roche) by the on-line application (https://www.roche-applied-science.com/sis/rtpcr/upl/index.jsp?Id=UP030000) considering exon spanning and covering all splicing species and have been previously indicated (13). qPCR was run in a LightCycler 480 II on 384 well plates with the settings previously indicated. Efficiency curves were used for each of the analyzed genes and relative gene expression for each sample was calculated using ACTB (actin) as reference after testing its suitability for the experimental setup. All amplifications were inside the linear range. Data came from six different astrocyte preparations. Means of triplicates were used for each analysis. The standard deviation of the triplicates was 0.2 or lower. Data analysis was made with LightCycler 480 SW 1.5 software (Roche) and MS-Excel and MS-Access 2007. Significance was calculated using a Bootstrap method (45), BootstRatio (http://regstattools.net/br), using the 'with control sample' condition and following tool instructions. Scrambled was used as a control sample.

For HeLa cells knockdown, constitutive (pGIPZ) lentivirus vectors, encoding shRNAmir-adapted short hairpin RNA specific for GlialCAM (GIPZ, V2LMM_69402 and V3LHS_413353), non-targeted variant (NT, ATCTCGCTTGGGCGAGAGTAAG), were obtained from Thermo Scientific, OpenBiosystems (USA). Lentivirus was produced and HeLa cells were transduced as described (46).

Immunofluorescence, western and surface expression studies in cells

For immunofluorescence staining, cells were fixed and processed as previously described (25). Antibodies used were the following: anti-GlialCAM [1:100, (17)], anti-MLC1 [1:100, (10)], anti-Occludin (1:100, Zymed), anti-β-Catenin (1:250, BD Transduction Lab), anti-Connexin 43 (1:100, Zymed) and anti-EEA1 (early endosomal antigen 1) (1:100, AbCAM). For WB studies, astrocyte lysates were prepared and processed as previously described (25). β-Actin protein levels were used as a loading control. To quantify signals by WB, we performed at least three expositions of all WBs, to ensure linearity. Scanned images were quantified using Multigauge software (Fujifilm) or the freely available Image J program (http://rsbweb.nih.gov/ij/) with similar results. Surface expression in transfected mammalian cells or astrocytes was performed as previously described (25).

In HeLa cells, the PM density of MLC1 and GlialCAM knockdown efficiency were determined by ELISA-based assay. HeLa cells expressing shGlialCAM or shSCR were trasfected with MLC1 cDNA constructs with Lipofectamine 2000 (Invitrogen, USA) 72 h prior to analysis. Cells were seeded on 24 well plates 20 h after transfection and incubated at 37°C for 24 h. Cells were temperature rescued at 26°C for 24 h, and unfolding was performed at 37°C for 1 h prior of experiment. Primary and secondary Abs were bound on ice in DMEM containing 5% bovine serum (Gibco, USA). The extracellular epitope was detected with mouse anti-human HepaCAM (1:1000, R&D Systems, USA) and mouse anti-HA (1:1000 cl11, Covance, Canada) antibodies. Excess antibody was washed away and specific binding was determined by HRP-conjugated secondary Ab (Amersham Biosciences, Canada) with Amplex® Red (Invitrogen) as a substrate. The fluorescence intensity was measured from quadruplicate samples using a Infinite 1000 m PRO (Tecan Group Ltd, USA) fluorescence plate-reader at 544 nm excitation and 590 nm emission wavelengths. Total Ab binding was corrected with non-specific Ab binding, determined in mock transfected cells.

For immunoblotting, the cells were lysed in RIPA buffer containing 10 μM MG132, 10 μg/ml pepstatin + leupeptin, 1 mM phenylmethylsulfonyl fluoride and 5 mM *N*-ethylmaleimide. Polypeptides were separated by SDS–PAGE and probed by immunoblotting using Supersignal Western Pico (Pierce, USA). Na^+–K^+-Atpase (1:500, Santa Cruz, USA) was used as a loading control.

Patch-clamp experiments of astrocytes

Three days before the experiment, dB-cAMP differentiated astrocytes were trypsinized and replated at a density of 1- to 3×10^4 onto 24-well plates containing a glass cover slip with DMEM supplemented medium and 250 μM dB-cAMP. For electrophysiological recordings, the glass cover slip was mounted on the stage of an inverted microscopy equipped with phase-contrast optics and fluorescence illumination. Patch pipettes were pulled from borosilicate glass capillaries (Clark Electromedical, UK) and used after fire polishing (Narishige, Japan). Electrophysiological recordings were performed with a patch-clamp amplifier (Axopatch 200B, Molecular Devices, Union City, CA, USA) Patch electrodes were fabricated in a Flaming/Brown micropipettepuller P-97 (Sutter instruments). Electrodes had a resistance between 4 and 5 MΩ when filled with intracellular solution (in mM): 144 NMDG-Cl, 2 $MgCl_2$, 5 EGTA, 5 HEPES at pH 7.3 and 308 ± 2 mOsm/kg. Extracellular solution contained (in mM): 144 NMDG-Cl, 2 $CaCl_2$, 2 $MgCl_2$, 5 HEPES, 5 glucose at pH 7.4 and 310 ± 3 mOsm/kg. Hypotonic extracellular solution (−25%) was prepared by decreasing NMDG-Cl concentration to 105 mM (229 ± 2 mOsm/kg). All solution osmolarities were adjusted with sorbitol. An Ag/AgCl ground electrode

mounted in a 3 M KCl agar bridge was used. Membrane currents were recorded in the whole-cell patch clamp configuration, filtered at 2 kHz, digitized at 10 kHz and acquired with pClamp 9 software (Molecular Devices). Data were analyzed with Clampfit 9 (Molecular Devices) and Prism 4 (GraphPad Software, Inc., La Jolla, CA, USA). Whole-cell capacitance and series resistance were compensated with the amplifier circuitry. Series resistance was always kept below 10 MΩ and compensated at 70–80%. All recordings were performed at room temperature (22–23°C). Currents were evoked with 4 s pulses from +80 to −120 mV from a holding potential of 0 mV.

SUPPLEMENTARY MATERIAL

Supplementary Material is available at *HMG* online.

ACKNOWLEDGEMENTS

We thank Michael Pusch, Thomas Jentsch and Herbert Schwarz for helpful comments about the manuscript.

Conflict of Interest statement. None declared.

FUNDING

This study was supported in part by SAF 2009-07014 (R.E.) and SAF2012-31486 (R.E.), PS09/02672-ERARE to R.E., ELA Foundation 2009-017C4 project (R.E. and V.N.), 2009 SGR 719 (R.E.), FISPI11/01601 (X.G.), 2009 SGR869 (X.G.), RD12/0034/0003 (X.G.), SAF 2009-12606-C02-02 (V.N.), 2009 SGR01490 (V.N.) and Canadian Institute of Health Research and Canada Foundation of Innovation (G.L.L.). G.L.L. is a Canada Research Chair and RE is a recipient of an ICREA Academia prize.

REFERENCES

1. van der Knaap, M.S., Boor, I. and Estevez, R. (2012) Megalencephalic leukoencephalopathy with subcortical cysts: chronic white matter oedema due to a defect in brain ion and water homoeostasis. *Lancet Neurol.*, **11**, 973–985.
2. van der Knaap, M.S., Barth, P.G., Stroink, H., van Nieuwenhuizen, O., Arts, W.F., Hoogenraad, F. and Valk, J. (1995) Leukoencephalopathy with swelling and a discrepantly mild clinical course in eight children. *Ann. Neurol.*, **37**, 324–334.
3. van der Knaap, M.S., Valk, J., Barth, P.G., Smit, L.M., van Engelen, B.G. and Tortori Donati, P. (1995) Leukoencephalopathy with swelling in children and adolescents: MRI patterns and differential diagnosis. *Neuroradiology*, **37**, 679–686.
4. van der Knaap, M.S., Barth, P.G., Vrensen, G.F. and Valk, J. (1996) Histopathology of an infantile-onset spongiform leukoencephalopathy with a discrepantly mild clinical course. *Acta Neuropathol.*, **92**, 206–212.
5. Gelal, F., Calli, C., Apaydin, M. and Erdem, G. (2002) Van der knaap's leukoencephalopathy: report of five new cases with emphasis on diffusion-weighted MRI findings. *Neuroradiology*, **44**, 625–630.
6. De Stefano, N., Balestri, P., Dotti, M.T., Grosso, S., Mortilla, M., Morgese, G. and Federico, A. (2001) Severe metabolic abnormalities in the white matter of patients with vacuolating megalencephalic leukoencephalopathy with subcortical cysts. A proton MR spectroscopic imaging study. *J. Neurol.*, **248**, 403–409.
7. Leegwater, P.A., Yuan, B.Q., van der Steen, J., Mulders, J., Konst, A.A., Boor, P.K., Mejaski-Bosnjak, V., van der Maarel, S.M., Frants, R.R., Oudejans, C.B. *et al.* (2001) Mutations of MLC1 (KIAA0027), encoding a putative membrane protein, cause megalencephalic leukoencephalopathy with subcortical cysts. *Am. J. Hum. Genet.*, **68**, 831–838.
8. Boor, P.K., de Groot, K., Waisfisz, Q., Kamphorst, W., Oudejans, C.B., Powers, J.M., Pronk, J.C., Scheper, G.C. and van der Knaap, M.S. (2005) MLC1: a novel protein in distal astroglial processes. *J. Neuropathol. Exp. Neurol.*, **64**, 412–419.
9. Schmitt, A., Gofferje, V., Weber, M., Meyer, J., Mossner, R. and Lesch, K.P. (2003) The brain-specific protein MLC1 implicated in megalencephalic leukoencephalopathy with subcortical cysts is expressed in glial cells in the murine brain. *Glia*, **44**, 283–295.
10. Teijido, O., Martinez, A., Pusch, M., Zorzano, A., Soriano, E., Del Rio, J.A., Palacin, M. and Estevez, R. (2004) Localization and functional analyses of the MLC1 protein involved in megalencephalic leukoencephalopathy with subcortical cysts. *Hum. Mol. Genet.*, **13**, 2581–2594.
11. Teijido, O., Casaroli-Marano, R., Kharkovets, T., Aguado, F., Zorzano, A., Palacin, M., Soriano, E., Martinez, A. and Estevez, R. (2007) Expression patterns of MLC1 protein in the central and peripheral nervous systems. *Neurobiol. Dis.*, **26**, 532–545.
12. Gorospe, J.R. and Maletkovic, J. (2006) Alexander disease and megalencephalic leukoencephalopathy with subcortical cysts: leukodystrophies arising from astrocyte dysfunction. *Ment. Retard. Dev. Disabil. Res. Rev.*, **12**, 113–122.
13. Duarri, A., Lopez de Heredia, M., Capdevila-Nortes, X., Ridder, M.C., Montolio, M., Lopez-Hernandez, T., Boor, I., Lien, C.F., Hagemann, T., Messing, A. *et al.* (2011) Knockdown of MLC1 in primary astrocytes causes cell vacuolation: a MLC disease cell model. *Neurobiol. Dis.*, **43**, 228–238.
14. Ridder, M.C., Boor, I., Lodder, J.C., Postma, N.L., Capdevila-Nortes, X., Duarri, A., Brussaard, A.B., Estevez, R., Scheper, G.C., Mansvelder, H.D. *et al.* (2011) Megalencephalic leucoencephalopathy with cysts: Defect in chloride currents and cell volume regulation. *Brain*, **134**, 3342–3354.
15. Brignone, M.S., Lanciotti, A., Macioce, P., Macchia, G., Gaetani, M., Aloisi, F., Petrucci, T.C. and Ambrosini, E. (2011) The beta1 subunit of the na,K-ATPase pump interacts with megalencephalic leucoencephalopathy with subcortical cysts protein 1 (MLC1) in brain astrocytes: New insights into MLC pathogenesis. *Hum. Mol. Genet.*, **20**, 90–103.
16. Lanciotti, A., Brignone, M.S., Molinari, P., Visentin, S., De Nuccio, C., Macchia, G., Aiello, C., Bertini, E., Aloisi, F., Petrucci, T.C. *et al.* (2012) Megalencephalic leukoencephalopathy with subcortical cysts protein 1 functionally cooperates with the TRPV4 cation channel to activate the response of astrocytes to osmotic stress: dysregulation by pathological mutations. *Hum. Mol. Genet.*, **21**, 2166–2180.
17. Lopez-Hernandez, T., Ridder, M.C., Montolio, M., Capdevila-Nortes, X., Polder, E., Sirisi, S., Duarri, A., Schulte, U., Fakler, B., Nunes, V. *et al.* (2011) Mutant GlialCAM causes megalencephalic leukoencephalopathy with subcortical cysts, benign familial macrocephaly, and macrocephaly with retardation and autism. *Am. J. Hum. Genet.*, **88**, 422–432.
18. Lopez-Hernandez, T., Sirisi, S., Capdevila-Nortes, X., Montolio, M., Fernandez-Duenas, V., Scheper, G.C., van der Knaap, M.S., Casquero, P., Ciruela, F., Ferrer, I. *et al.* (2011) Molecular mechanisms of MLC1 and GLIALCAM mutations in megalencephalic leukoencephalopathy with subcortical cysts. *Hum. Mol. Genet.*, **20**, 3266–3277.
19. Favre-Kontula, L., Rolland, A., Bernasconi, L., Karmirantzou, M., Power, C., Antonsson, B. and Boschert, U. (2008) GlialCAM, an immunoglobulin-like cell adhesion molecule is expressed in glial cells of the central nervous system. *Glia*, **56**, 633–645.
20. Jeworutzki, E., Lopez-Hernandez, T., Capdevila-Nortes, X., Sirisi, S., Bengtsson, L., Montolio, M., Zifarelli, G., Arnedo, T., Muller, C.S., Schulte, U. *et al.* (2012) GlialCAM, a protein defective in a leukodystrophy, serves as a ClC-2 cl(-) channel auxiliary subunit. *Neuron*, **73**, 951–961.
21. Blanz, J., Schweizer, M., Auberson, M., Maier, H., Muenscher, A., Hubner, C.A. and Jentsch, T.J. (2007) Leukoencephalopathy upon disruption of the chloride channel ClC-2. *J. Neurosci.*, **27**, 6581–6589.
22. Scheper, G.C., van Berkel, C.G., Leisle, L., de Groot, K.E., Errami, A., Jentsch, T.J. and Van der Knaap, M.S. (2010) Analysis of CLCN2 as candidate gene for megalencephalic leukoencephalopathy with subcortical cysts. *Genet. Test. Mol. Biomarkers*, **14**, 255–257.
23. Depienne, C., Bugiani, M., Dupuits, C., Galanaud, D., Touitou, V., Postma, N., van Berkel, C., Polder, E., Tollard, E., Darios, F. *et al.* (2013) Brain white matter oedema due to ClC-2 chloride channel deficiency: An observational analytical study. *Lancet Neurol.*, **12**, 659–668.
24. van der Knaap, M.S., Lai, V., Kohler, W., Salih, M.A., Fonseca, M.J., Benke, T.A., Wilson, C., Jayakar, P., Aine, M.R., Dom, L. *et al.* (2010)

Megalencephalic leukoencephalopathy with cysts without MLC1 defect. *Ann. Neurol.*, **67**, 834–837.
25. Duarri, A., Teijido, O., Lopez-Hernandez, T., Scheper, G.C., Barriere, H., Boor, I., Aguado, F., Zorzano, A., Palacin, M., Martinez, A. *et al.* (2008) Molecular pathogenesis of megalencephalic leukoencephalopathy with subcortical cysts: mutations in MLC1 cause folding defects. *Hum. Mol. Genet.*, **17**, 3728–3739.
26. Leisle, L., Ludwig, C.F., Wagner, F.A., Jentsch, T.J. and Stauber, T. (2011) ClC-7 is a slowly voltage-gated 2Cl(-)/1H(+)-exchanger and requires Ostm1 for transport activity. *EMBO J.*, **30**, 2140–2152.
27. Jentsch, T.J., Stein, V., Weinreich, F. and Zdebik, A.A. (2002) Molecular structure and physiological function of chloride channels. *Physiol. Rev.*, **82**, 503–568.
28. Parkerson, K.A. and Sontheimer, H. (2004) Biophysical and pharmacological characterization of hypotonically activated chloride currents in cortical astrocytes. *Glia*, **46**, 419–436.
29. Ferroni, S., Marchini, C., Nobile, M. and Rapisarda, C. (1997) Characterization of an inwardly rectifying chloride conductance expressed by cultured rat cortical astrocytes. *Glia*, **21**, 217–227.
30. Benesova, J., Rusnakova, V., Honsa, P., Pivonkova, H., Dzamba, D., Kubista, M. and Anderova, M. (2012) Distinct expression/function of potassium and chloride channels contributes to the diverse volume regulation in cortical astrocytes of GFAP/EGFP mice. *PLoS ONE*, **7**, e29725.
31. Gagnon, K.B., Adragna, N.C., Fyffe, R.E. and Lauf, P.K. (2007) Characterization of glial cell K-cl cotransport. *Cell. Physiol. Biochem.*, **20**, 121–130.
32. Jayakumar, A.R., Panickar, K.S., Curtis, K.M., Tong, X.Y., Moriyama, M. and Norenberg, M.D. (2011) Na-K-cl cotransporter-1 in the mechanism of cell swelling in cultured astrocytes after fluid percussion injury. *J. Neurochem.*, **117**, 437–448.
33. Su, G., Kintner, D.B., Flagella, M., Shull, G.E. and Sun, D. (2002) Astrocytes from na(+)-K(+)-cl(-) cotransporter-null mice exhibit absence of swelling and decrease in EAA release. *Am. J. Physiol. Cell. Physiol.*, **282**, C1147–C1160.
34. Su, G., Kintner, D.B. and Sun, D. (2002) Contribution of na(+)-K(+)-cl(-) cotransporter to high-[K(+)](o)- induced swelling and EAA release in astrocytes. *Am. J. Physiol. Cell. Physiol.*, **282**, C1136–C1146.
35. Zhang, Y., Zhang, H., Feustel, P.J. and Kimelberg, H.K. (2008) DCPIB, a specific inhibitor of volume regulated anion channels (VRACs), reduces infarct size in MCAo and the release of glutamate in the ischemic cortical penumbra. *Exp. Neurol.*, **210**, 514–520.
36. Nilius, B. and Droogmans, G. (2003) Amazing chloride channels: An overview. *Acta Physiol. Scand.*, **177**, 119–147.
37. Komsic-Buchmann, K., Stephan, L.M. and Becker, B. (2012) The SEC6 protein is required for contractile vacuole function in chlamydomonas reinhardtii. *J. Cell. Sci.*, **125**, 2885–2895.
38. Schonemann, B., Bledowski, A., Sehring, I.M. and Plattner, H. (2012) A set of SNARE proteins in the contractile vacuole complex of paramecium regulates cellular calcium tolerance and also contributes to organelle biogenesis. *Cell Calcium*, **53**, 204–216.
39. Sivaramakrishnan, V. and Fountain, S.J. (2012) Intracellular P2X receptors as novel calcium release channels and modulators of osmoregulation in dictyostelium: a comparison of two common laboratory strains. *Channels (Austin)*, **7**, 43–46.
40. Ulrich, P.N., Jimenez, V., Park, M., Martins, V.P., Atwood, J. 3rd, Moles, K., Collins, D., Rohloff, P., Tarleton, R., Moreno, S.N. *et al.* (2011) Identification of contractile vacuole proteins in trypanosoma cruzi. *PLoS ONE*, **6**, e18013.
41. Essid, M., Gopaldass, N., Yoshida, K., Merrifield, C. and Soldati, T. (2012) Rab8a regulates the exocyst-mediated kiss-and-run discharge of the dictyostelium contractile vacuole. *Mol. Biol. Cell*, **23**, 1267–1282.
42. Benfenati, V., Nicchia, G.P., Svelto, M., Rapisarda, C., Frigeri, A. and Ferroni, S. (2007) Functional down-regulation of volume-regulated anion channels in AQP4 knockdown cultured rat cortical astrocytes. *J. Neurochem.*, **100**, 87–104.
43. Okiyoneda, T., Veit, G., Dekkers, J.F., Bagdany, M., Soya, N., Xu, H., Roldan, A., Verkman, A.S., Kurth, M., Simon, A. *et al.* (2013) Mechanism-based corrector combination restores DeltaF508-CFTR folding and function. *Nat. Chem. Biol.*, **9**, 444–454.
44. Verkman, A.S. and Galietta, L.J. (2009) Chloride channels as drug targets. *Nat. Rev. Drug Discov.*, **8**, 153–171.
45. Cleries, R., Galvez, J., Espino, M., Ribes, J., Nunes, V. and de Heredia, M.L. (2012) BootstRatio: a web-based statistical analysis of fold-change in qPCR and RT-qPCR data using resampling methods. *Comput. Biol. Med.*, **42**, 438–445.
46. Apaja, P.M., Xu, H. and Lukacs, G.L. (2010) Quality control for unfolded proteins at the plasma membrane. *J. Cell Biol.*, **191**, 553–570.

Expanding the spectrum of megalencephalic leukoencephalopathy with subcortical cysts in two patients with GLIALCAM mutations.

Article publicat el març del 2014 a la revista Neurogenetics.

Neurogenetics (2014) 15:41–48
DOI 10.1007/s10048-013-0381-x

ORIGINAL ARTICLE

Expanding the spectrum of megalencephalic leukoencephalopathy with subcortical cysts in two patients with *GLIALCAM* mutations

Tanit Arnedo · Chiara Aiello · Elena Jeworutzki · Maria Lisa Dentici · Graziella Uziel · Alessandro Simonati · Michael Pusch · Enrico Bertini · Raúl Estévez

Received: 9 August 2013 / Accepted: 9 October 2013 / Published online: 8 November 2013

Abstract Megalencephalic leukoencephalopathy with subcortical cysts (MLC) is a heterogeneous neurodegenerative leukodystrophy caused by recessive mutations in *MLC1* or *GLIALCAM* (types MLC1 and MLC2A) of by dominant mutations in *GLIALCAM* (MLC2B). GlialCAM functions as an auxiliary subunit of both MLC1 and ClC-2 chloride channel, increasing and modifying the function of the latter. Dominant mutations in *GLIALCAM* cause transient features of MLC but lacks clinical deterioration. Most recessive and dominant mutations in *GLIALCAM* studied so far affect the targeting of GlialCAM and its associated subunits. Here, we have investigated two patients with MLC2. The first patient has MLC2B disease, as shown by the improvement in MRI and clinical parameters. In this case, we identified a novel *GLIALCAM* mutation (p.Q56P) which affected the localization of GlialCAM and its associated subunits, however activating ClC-2 function as the wild-type protein. The second patient has MLC2A disease, as indicated by the lack of clinical improvement, even though, interestingly, the MRI of this patient shows a partial improvement. In this case, we found a recessive mode of inheritance, as the patient harbors two compound heterozygous mutations in *GLIALCAM*. One of them introduces a stop codon (p.Q56X), whereas the second mutation is a missense mutation (p.R73W), for which we could not identify any trafficking defect or an altered functional effect on ClC-2 in vitro.

Keywords Leukodystrophy · MLC · *MLC1* · *GLIALCAM* · ClC-2 · Remitting phenotype

Tanit Arnedo and Chiara Aiello contributed equally in this work, and Enrico Bertini and Raúl Estévez share the last authorship.

Electronic supplementary material The online version of this article (doi:10.1007/s10048-013-0381-x) contains supplementary material, which is available to authorized users.

T. Arnedo · R. Estévez
Sección de Fisiología, Departamento de Ciencias Fisiológicas II, Universidad de Barcelona, Barcelona, Spain

T. Arnedo · R. Estévez (✉)
U-750, Centro de Investigación en Red de Enfermedades Raras (CIBERER), ISCIII, Barcelona, Spain
e-mail: restevez@ub.edu

C. Aiello · M. L. Dentici · E. Bertini
Unit for Neuromuscular and Neurodegenerative Diseases and Scientific Direction, Bambino Gesù Children's Hospital, IRCCS, Rome, Italy

E. Jeworutzki · M. Pusch
Istituto di Biofisica, CNR, Genoa, Italy

G. Uziel
Department of Child Neurology, The Foundation "Carlo Besta" Neurological Institute, IRCCS, Milan, Italy

A. Simonati
Department of Neurological, Neuropsychological, Morphological, Motor Sciences-Neurology (Child Neurology) and Neuropathology, University of Verona, Verona, Italy

Introduction

Megalencephalic leukoencephalopathy with subcortical cysts (MLC) (MIM #604004) is a neurodegenerative spongiform leukodystrophy characterized by early onset macrocephaly that develops within the first year of life. Subsequently, slow deterioration of motor function with progressive ataxia and spasticity and moderate cognitive decline become evident. MRI criteria are clues for diagnosis [16]. About 75 % of MLC patients have an autosomal recessive inheritance with

mutations in the *MLC1* gene [3, 7] that encodes a putative membrane protein, expressed mainly in the brain at distal astrocyte junctions, near by the cerebrospinal fluid–brain barrier and the glial limiting membrane [3, 12, 13]. Genetic heterogeneity has been debated for long with linkage evidence for at least one other gene for MLC [2, 10]. Only, recently, a second gene, *HEPACAM* (*GLIALCAM*, hepatic and glial cell adhesion molecule, MIM 611642), was discovered through a combination of proteomics and genetics approaches and found to be responsible for the disease, confirming genetic heterogeneity, not only in terms of an additional gene but also in terms of inheritance [8, 15]. Patients with recessive mutations in *GLIALCAM* presented a classical MLC phenotype, overlapping with the clinical presentation of *MLC1* gene-mutated patients. Patients with dominant mutations in the *GLIALCAM* gene are always preceded by signs of MLC and, thereafter, are associated with various degrees of phenotypic expression, ranging from benign familial macrocephaly to macrocephaly–mental retardation with or without autism (MIM 613926) [8].

As GlialCAM but not MLC1 expression is detected in oligodendrocytes, it was suggested that GlialCAM could have additional protein partners. Proteomic studies revealed that GlialCAM is also an auxiliary subunit of the ClC-2 chloride channel [6]. Although the myelin vacuolation phenotype of *Clcn2* KO mice suggested its involvement in MLC [1], no *CLCN2* mutations were detected in MLC patients [11], and no changes of GlialCAM and MLC1 were observed in *Clcn2* KO mice [6], raising doubts about its functional implication in MLC. However, some *GLIALCAM* MLC-related mutations impair the trafficking of ClC-2 to the cell junctions [6], and very recently, *CLCN2* mutations have been found in a certain form of a human leukodystrophy characterized by white matter edema and visual impairment [4].

In this study, we screened two patients with clinical and radiological features of MLC, in which mutations in *MLC1* were previously excluded, and we identified *GLIALCAM* mutations in both subjects. In one patient who was affected by MLC2B, a novel dominant mutation was detected. Interestingly, the other patient shows no clinical improvement, indicating that she was affected by MLC2A, even though she showed improvement of MRI parameters. This phenomenon has also been observed in some patients with *MLC1* mutations [14], but it is the first time that this is found in a MLC2A patient. This patient presented two recessive compound heterozygous mutations in the *GLIALCAM* gene. We analyzed biochemically in vitro the effects of these mutations in protein expression, targeting of GlialCAM protein, interaction with MLC1 and ClC-2, and functional modification of ion channel properties of ClC-2.

Materials and methods

Molecular studies

Genomic DNA was isolated from peripheral blood leukocytes according to standard procedures. *MLC1* mutations were excluded by direct sequencing in both subjects. The entire *GLIALCAM* coding sequence as well as the exon/intron boundaries and flanking intronic portions were scanned for mutations by direct sequencing using BigDye 3.1 Chemistry (Applied Biosystems, Foster City, CA, USA) with the ABI Prism 3130 xl automatic sequencer (Applied Biosystems).

Primer pair sequences as well as PCR conditions are available upon request. Nucleotide numbering of the mutations and exonic disease-unrelated variants reflects cDNA numbering with 1 corresponding to the A of the ATG translation initiation codon in the reference sequence.

Transfection and immunofluorescence in transfected cells

Human embryonic kidney (HEK) 293A and HeLa cells were grown on DMEM containing 10 % (*v*/*v*) fetal bovine serum (Sigma) and 1 % penicillin at 37 °C in a humidity-controlled incubator with 10 % CO_2. Cells were cultured as described in (http://tools.invitrogen.com/content/sfs/manuals/293acells_man.pdf) and transfected with the Effectene Transfection Reagent (Qiagen, Germany). Twenty-four hours after transfection, the cells were splitted and transferred into glass-covered Petri dishes in which experiments were performed after further 24–48 h. For localization studies for ClC-2, green fluorescent protein (GFP) fluorescence was excited at 480 nm, and the emitted light was passed through a 520-nm-long pass filter, and pictures were taken with a CCD camera (Olympus C-5050 Zoom, Japan). For MLC1 and GlialCAM, we performed immunofluorescence staining of cells. They were fixed with phosphate-buffered saline (PBS) containing 3 % paraformaldehyde for 15 min and then blocked and permeabilized with 10 % FBS and 0.1 % Triton X-100 in PBS for 2 h at room temperature (RT). Primary antibodies were diluted in the same solution and incubated overnight at 4 °C. Cells were washed and incubated for 2 h at RT with secondary antibodies. Coverslips were mounted in the Vectashield medium (Vector Laboratories) with 1.5 μg/ml DAPI (Sigma) and visualized using the Olympus DSU spinning disk confocal.

Images were analyzed using ImageJ. To quantify the fluorescence at cell contacts versus the fluorescence at the cell membrane in contact-free zones, the free analysis program Image J (http://rsbweb.nih.gov/ij) was used. For this purpose, a shallow rectangle was drawn across a couple of cells, and the fluorescence profile across the rectangle was calculated with image J. The position of the cell membranes was identified by the peaks of the profile, and the intensity was averaged in a region of plus or minus three pixels around the peaks,

resulting in F_1, the fluorescence at the contact-free membrane of cell 1; F_2, the fluorescence at the contact- free membrane of cell 2; and F_C, the fluorescence at the cell contact. The relative fluorescence at the contact versus the contact-free zones, F_R, was defined as $F_R=F_C/(F_1+F_2)$.

Molecular biology

Plasmids used here were constructed using standard molecular biology techniques employing recombinant PCR and the Multisite Gateway system (Invitrogen). The integrity of all cloned constructs was confirmed by DNA sequencing. For localization studies in HEK or HeLa cells and patch clamp studies in HEK, rat ClC-2 was C-terminally fused to GFP, human MLC1 was HA tagged at the N-terminus, and human GlialCAM and mutants were Flag tagged at their C-terminus and cloned into the pCDNA3 vector (Invitrogen).

Patch clamp experiments

ClC-2::GFP ± human GlialCAM, were transferred into the measuring solution (in mM): 140 NaCl, 2 $MgSO_4$, 2 $CaCl_2$, and 10 hydroxyethyl piperazineethanesulfonic 4-(2-Hydroxyethyl)piperazine-1-ethanesulfonic acid (HEPES)/NaOH, pH 7.3. Patch pipettes were pulled from thin-walled borosilicate glass capillaries (Hilgenberg, Malsfeld, Germany) and filled with (in mM) 130 NaCl, 2 $MgSO_4$, 2 EGTA, and 10 HEPES/NaOH, pH 7.3. Patch pipettes had a resistance of 3–5 MΩ. Currents were measured in the whole-cell configuration with an EPC-7 amplifier (List Medical, Darmstadt, Germany) and recorded with GePulse. For ClC-2 currents, which exhibit slow hyperpolarization activation, an initial 1-s voltage pulse at 60 mV was applied, followed by 5-s voltage steps from −140 to 60 mV in 20-mV increments and a tail pulse of 1 s to 60 mV. Steady state currents were taken at the end of the 5-s voltage steps. To quantify the expression levels of the different constructs, the initial tail current (at 60 mV) after the −140-mV test pulse was estimated by back extrapolation of a single exponential fit to the decaying tail current. To estimate the number of constitutively activated channels, instantaneous currents were measured during a short test pulse to +60 mV without prior activation by hyperpolarization. Only cells for which currents were reversibly blocked by iodide were used for analysis.

Results

Clinical data

Case report 1 of family 1 with patients 1a and 1b

Patient 1a is the first child of healthy non-consanguineous parents, now aged 7 years. There is no history of neurological disease in the extended family. She was born as a normal baby after an uneventful pregnancy at 41 weeks of gestation. Head circumference (HC) was 33 cm (25th centile). Her psychomotor development was reported to be normal. At 4 months of age, she was referred to a pediatric neurologist because of an increasing growth rate of the HC with normal cerebral ultrasound. MRI performed at 6 months of age revealed diffuse cerebral white matter abnormalities with a reduced signal on T1 and enhanced signal on T2, involving also the subcortical U fibers (Fig. 1a–c). Subcortical cysts were detected in the temporal poles and, with a lesser extent, in the frontal–insular regions; the brain was overall increased in volume; lateral ventricles and subarachnoid spaces were normal. The abnormal white matter was swollen.

At the age of 14 months, her HC was 49 cm (above 97° centile), and she was extremely irritable, with brisk tendon reflexes at the lower limbs, and was unable to stand unsupported. Otherwise, neurological examination was normal without pyramidal or cerebellar signs. Aggregate general quotient (GQ) measured using the Griffiths scale was 78 at that age and 71 at 17 months of age. Unsupported walking was achieved at 21 months of age. Since then, the course of the disease was benign, and at the last follow-up visit at the age of 5, she had a normal neurological examination with no cognitive impairment, in spite of minimal behavioral problems. A second MRI performed at 17 months showed a clear improvement of swelling from the first exam, although there was persistence of hyperintensity in the posterior areas of the white matter (Fig. 1d–f) and subcortical cysts in both temporal poles. MR spectroscopy was normal.

The younger sister, patient 1b, now aged 5 years, also developed macrocephaly (98° centile) in the first year of life, and the MRI performed at 6 months of age showed the same radiological features of her sister. Her psychomotor development was referred as normal and neurological examination performed at 3 years of age was normal.

Case report 2 of family 2 with patient 2

Patient 2 is the second child of healthy non-consanguineous parents now aged 17 years. There is no family history for an infantile onset neurological disorder. The baby was born at 37 weeks of gestation by cesarean section due to maternal gestosis. At birth, HC was 33 cm (50th centile). Early developmental milestones were within normal range. Then, accelerated head growth occurred (HC, 51.5 cm; >2 SD, at 18 months); by 2 years of age, motor developmental delay and limb ataxia were recorded. At 9 years of age, clumsiness and difficulties for fine motor abilities were present; HC was 56 cm (>2 SD). She had developed mild learning difficulties as well as behavioral abnormalities; however, cognitive evaluation was within normal ranges (intelligence quotient (IQ), 95). At 14.5 years, she was attending secondary school,

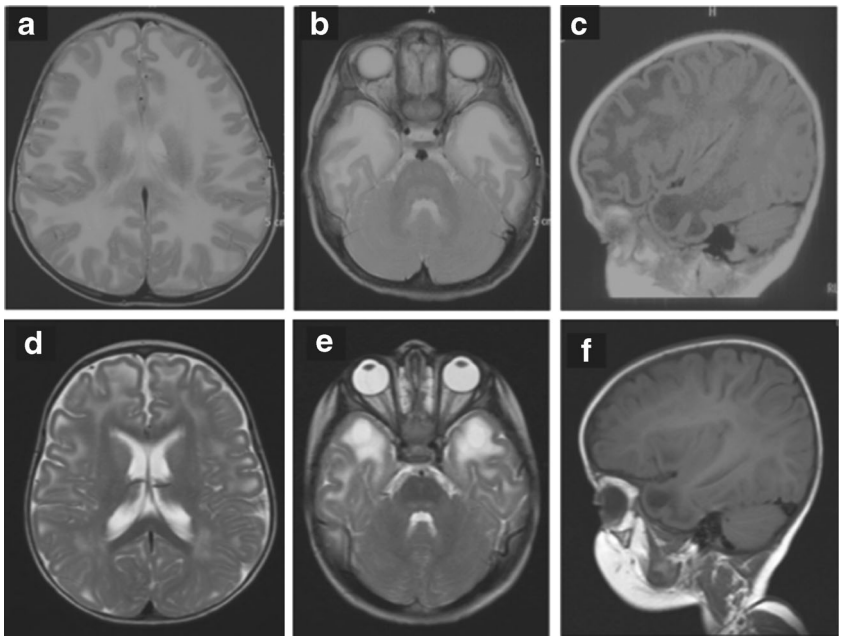

Fig. 1 Brain MRI of patient 1a at age 6 months (**a**–**c**) and at age 17 months (**d**–**f**). **a**, **b**, **d**, **e** T2-weighted axial; **c**, **f** T1-weighted parasagittal. Diffuse T2 hyperintensity of the white matter including the U fibers (**a**, **b**) and cystic formation at the level of both temporal horns (**c**). At 17 months, a control serial MRI showed a reduction of the abnormal T2 hyperintensity, particularly at the level of the internal capsule (**d**, **e**). Cystic formation of the temporal horns was persistent (**f**)

and mild attentive deficiency disorder was present. Neurological examination revealed mild spasticity in her legs with bilateral extensor plantar response, increased muscle tones, dystonic movements of the upper left limb, and mild cerebellar signs; HC was 58 cm (>2 SD).

Three head MRI scans were performed at different ages. At 2 years, the white matter of the cerebral hemispheres was severely affected, sparing the corpus callosum and internal capsules. Subcortical cysts were present in frontal and temporal regions. Subsequent MRI investigations (at 9 and 15 years of age) showed a progressive reduction of the signal abnormalities of the hemispheric white matter, whereas the volumes of the temporal cysts remained stable. Figure 2 shows axial MRI serial sections, respectively, at ages 2 (a), 9 (b), and 15 (c).

Supplementary Table 1 summarizes comparative clinical aspects of the two affected sisters from family 1 with patient 2 of family 2.

Genetic and biochemical studies

We analyzed the exons and surrounding intronic regions of *GLIALCAM* by Sanger sequencing. As a result of the sequencing, we identified that patient 1a (MA) was heterozygous for the mutation c.167 A>C, resulting in the amino acid change p.Q56P. The same mutation was found to be heterozygous in the younger sister (patient 1b) with macrocephaly and in the mother, who was healthy and had an occipital–frontal circumference in the mean range. Interestingly, the second case was compound heterozygous for mutations c.166 C>T, resulting in a premature stop codon in the protein (Q56X), and c.217 C>T, resulting in the amino acid change p.R73W. The p.Q56X mutation is predicted to produce no functional protein and is thus likely equivalent to a null mutation. Sequence analysis of *GLIALCAM* in the parents confirmed the genetic inheritance of the mutations.

Both missense mutations are located in the first immunoglobulin-like variable domain (IgV) of GlialCAM (Fig. 3a). Molecular modeling of the extracellular domain of GlialCAM (Fig. 3b) showed that these new mutations (in red), as previously identified dominant MLC2 mutations (in yellow), are located in a putative interface of the first immunoglobulin domain (Fig. 3b).

As previously found in all missense mutations identified in *GLIALCAM* in MLC2A or MLC2B patients, expression levels of all mutant GlialCAMs were not different from those of wild-type GlialCAM (Fig. 3c).

Trafficking studies of GlialCAM mutants

Most previously identified *GLIALCAM* mutations cause an impaired localization of the protein in cell–cell junctions. We expressed the novel mutants found in the patients in HeLa cells and determined their subcellular localization by immunofluorescence experiments. Typical examples for wild-type GlialCAM, GlialCAM Q56P, and GlialCAM R73W are shown in Fig. 4a–c, respectively. Multiple pictures from different experiments were taken, and the percentage of cells in which GlialCAM was located in junctions was quantified. As shown in Fig. 3b, d, mutant Q56P was not preferentially located in cell junctions. However, no defect was observed for the mutant R73W (Fig. 3c, d).

Next, we investigated whether the localization of the associated subunits MLC1 and ClC-2 was altered by the

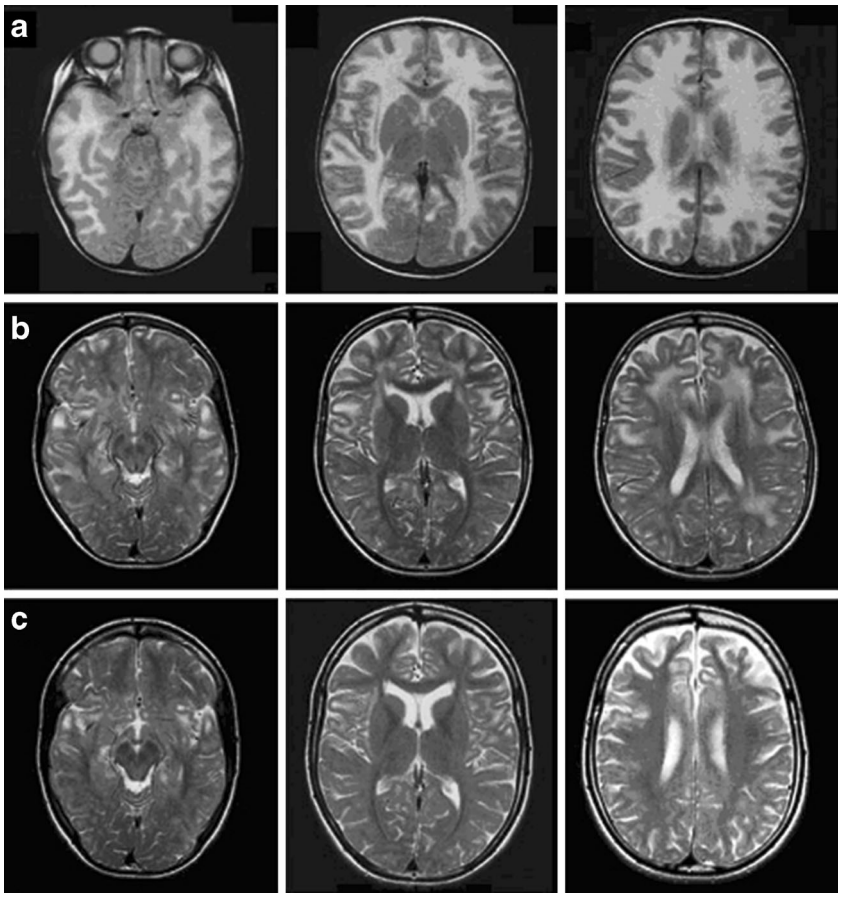

Fig. 2 Brain T2-weighted MRI axial of patient 2. **a** Two years of age. Signs of marked diffuse hyperintense and swelling abnormalities of the cerebral white matter; T2 hyperintensity partially involving the internal capsule, while the corpus callosum is spared. **b** Nine years of age. Overall reduction of the white matter abnormal T2 hyperintense signals and swelling. **c** Fifteen years of age. Clear reduction of T2 white matter abnormal signal that seems to persist at the insular and rolandic areas; subcortical cysts of frontal and temporal regions are reduced in size

mutations of GlialCAM. Typical pictures for coexpression experiments of MLC1 and GlialCAM in HeLa cells are shown in Supplementary Fig. 1a–c. Quantifications from different experiments are shown in Fig. 4e for MLC1 and Fig. 4f for ClC-2 coexpression experiments. Similar to what was found for GlialCAM expressed alone, MLC1 and ClC-2 were mislocalized when coexpressed with the mutant Q56P, but not with the mutant R73W.

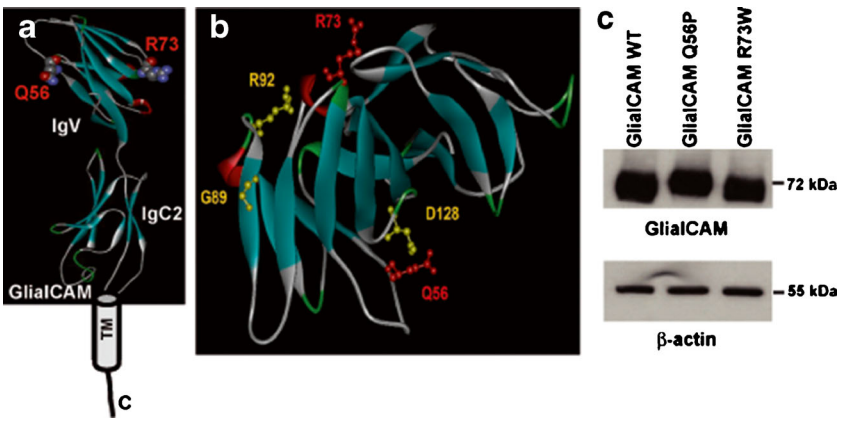

Fig. 3 Biochemical studies of the newly identified MLC2 *GLIALCAM* mutations Q56P and R73W. **a** Schematic representation of the GlialCAM molecule and position of the new residues which are mutated in MLC2A and MLC2B. The structural model of the extracellular domain was obtained by the automated homology-modeling server of the ExPASy server. **b** Ribbon representation viewed from the top of a structural model of the extracellular domain of GlialCAM. Previously identified dominantly mutated residues are highlighted in *yellow*, and new residues are highlighted in *red*. **c** HeLa cells were transfected with wild-type GlialCAM or with GlialCAM containing the MLC2B-identified mutation Q56P and the MLC2A-identified mutation R73W, harboring three Flag epitopes. Cells were harvested, solubilized, and processed by SDS-PAGE and Western blot analysis using an antibody that recognizes the Flag epitopes. β-Actin detection was used as a loading control. The result is a representative experiment of three with similar results

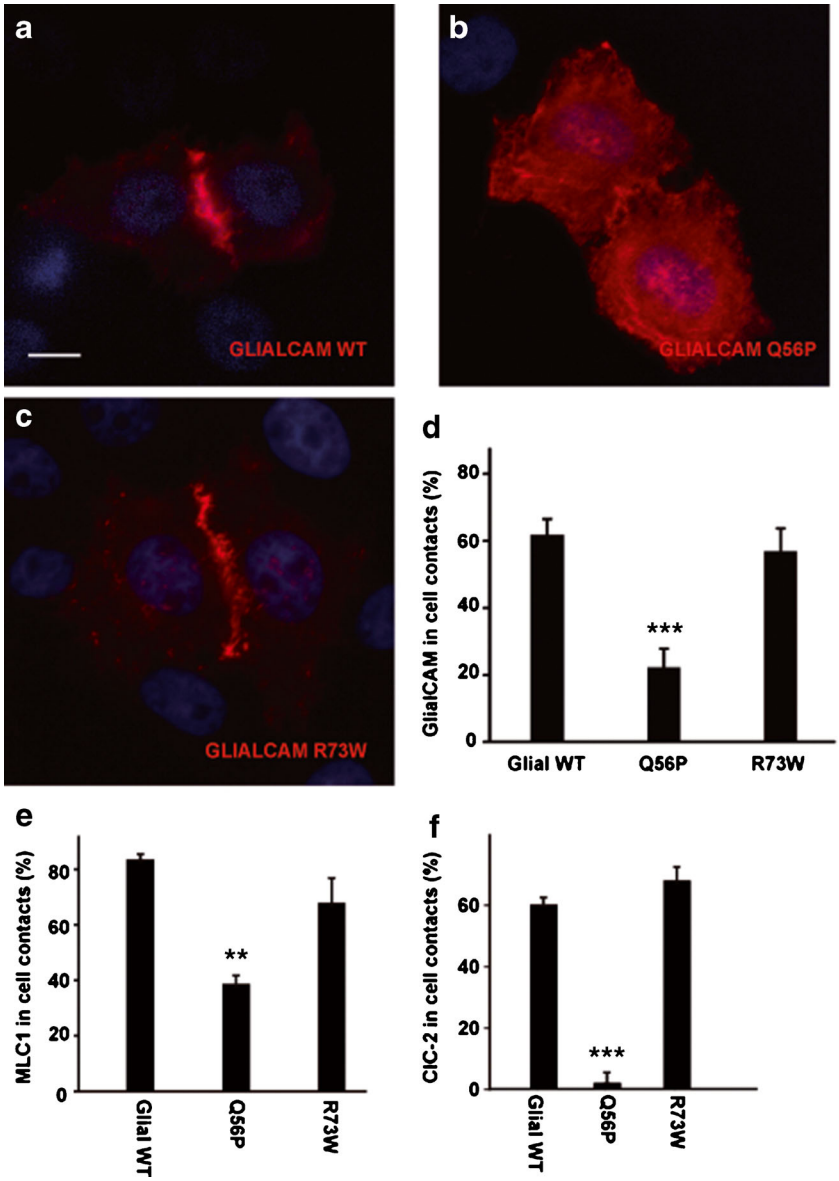

Fig. 4 Trafficking studies of GlialCAM proteins expressed in HeLa cells alone or together with MLC1 or ClC-2. HeLa cells were transfected with plasmids encoding Flag-tagged wild-type GlialCAM (**a**) or containing the mutations Q56P (**b**) or R73W (**c**). Cells were fixed and permeabilized, and then, immunofluorescence was performed using Flag monoclonal antibody detecting GlialCAM protein. *Scale bar* = 20 μm. **d** Pairs of cells were analyzed manually and quantified as being in junctions. Intensity profile analysis was used to discern between junctional and plasma membrane localizations. Data represent the mean of several independent experiments, corresponding to 843 cells (GlialCAM, $n=15$), 299 cells (Q56P, $n=7$), and 337 cells (R73W, $n=9$). Student's t test was used to estimate significance. ***$P<0.001$. **e**, **f** HeLa cells were transfected with plasmids expressing wild-type MLC1 or GFP-tagged ClC-2, together with flag-tagged wild-type GlialCAM or containing the mutations Q56P or R73W. Cells were fixed and permeabilized, and then, immunofluorescence was performed using rabbit polyclonal antibodies against human MLC1 (*green*) and flag monoclonal antibodies detecting GlialCAM protein (*red*). ClC-2 was monitored taking advantage of the fused fluorescent GFP. Colocalization is shown in *yellow* (merge). Using different images from at least seven independent experiments, the localization of MLC1 (**e**) and ClC-2 (**f**) in cell contacts was quantified, as described in "Materials and methods" Student's t test was used to estimate significance ** $P<0.005$, *** $P<0.001$

Electrophysiological analyses of the effect of GlialCAM mutations on ClC-2

We also analyzed the effect of the MLC-causing mutations in GlialCAM on the ability to modify the functional properties of ClC-2 by performing whole-cell patch clamp experiments in transfected cells. GlialCAM increases ClC-2-mediated currents and changes its rectification (currents are nearly ohmic, being opened at positive voltages) and activation/inactivation properties (are instantaneously active). To study the effect of GlialCAM mutants on the activation/inactivation properties, we performed an analysis of the deactivation kinetics at +60 mV after a hyperpolarization pulse of −120 mV for 2 s. Typical current traces are shown in Fig. 5a, and the quantification of

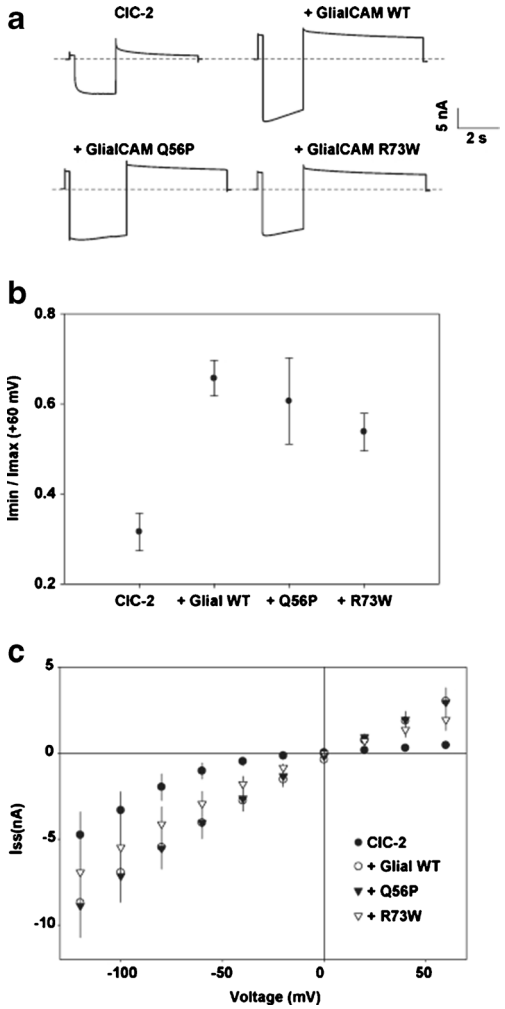

Fig. 5 Functional consequences of *GLIALCAM* mutations on ClC-2 activity. **a** Example of current traces of ClC-2 alone or coexpressed with wild-type GlialCAM or containing the mutations Q56P and R73W in HEK cells. **b** Average values of the ratio of I_{min} (5 s) and I_{max} of the tail pulse at +60 mV after the long hyperpolarizing pulse at −140 mV ($n \geq 6\pm$ SEM experiments per construct). **c** Normalized average steady state current–voltage relationship of HEK cells transfected with ClC-2 (*filled circles*), ClC-2 + wild-type GlialCAM (*circles*), ClC-2 + Q56P GlialCAM (*filled triangles*), and ClC-2 + R73W GlialCAM (*triangles*). Results correspond to six to eight measurements. No statistical differences were found between cells coexpressing GlialCAM

several experiments is shown in Fig. 5b. No differences were found on the inactivation properties between the GlialCAM mutants and the wild type. Changes in conductance and rectification properties were addressed by analyzing current–voltage relationships (Fig. 5c). No differences were also found compared to wild-type GlialCAM. These results indicate that the mutants do not show a reduced tendency to hetero-oligomerize with ClC-2.

Discussion

We report on two patients, negative for *MLC1* screening, with a clinical diagnosis of MLC based on the onset of macrocephaly during the first 6 months of life and the radiological images, as they showed abnormal hemispheric white matter and presence of subcortical cysts in the temporal region. Subsequently, serial MRI showed a striking improvement over the years in both patients 1a and 2. However, in patient 2, no clinical improvement was observed. Thus, the combination of MRI and clinical studies suggested that patient 1a was affected with MLC2B (remitting MLC), whereas the second patient was affected with MLC2A. This suggestion was verified by genetic analyses. Similar to both patients 1a and 1b, who are affected with MLC2B, their mother is now clearly asymptomatic. We speculate that the mother could have had an abnormal MRI at early stages, although evidence is lacking.

It should be remarked, as already mentioned [14], that some MLC1 patients may have a partial recovery of MRI parameters with time and do clinically very well. Here, we show that this may also occur in MLC2A patients. Thus, in order to distinguish between MLC1/MLC2A and MLC2B patients, it is important to follow MRI and clinical parameters during time. However, the final confirmation of MLC1, MLC2A, and MLC2B comes from genetic analysis and not from clinical and MRI observations.

Similar to what has been described in the earlier reports for MLC2B and MLC2A patients [8], patients 1a and 1b displayed a single *GLIALCAM* mutation (c.167 A>C; p.Q56P) while patient 2 displayed two *GLIALCAM* mutations with an autosomal recessive inheritance (c.166 C>T, p.Q56X, and c.217 C>T, p.R73W). All mutations found in MLC2B are clustered on the V set Ig-like extracellular domain of the GlialCAM protein [8], including the new mutation identified in this work. The majority of MLC mutations identified so far in *GLIALCAM* ([6, 8, 9] and data not shown) impair the correct trafficking of GlialCAM, MLC1, and ClC-2 to cell–cell junctions, without affecting the hetero-interaction and the change of ClC-2 functional properties. However, for some mutations, including one identified presently (R73W), no pathogenic mechanism has been found, indicating that the in vitro studies do not fully recapitulate the in vivo physiological situation, regarding biochemical or functional data or both. However, it has to be kept in mind that the function of the MLC1 protein is unknown, rendering impossible to evaluate a hypothetical effect of a GlialCAM mutation on MLC1 function. Furthermore, it can be speculated that additional functions of GlialCAM may need to be discovered.

In this sense, it is also unclear why MLC2B mutations are associated with different clinical phenotypes compared to MLC2A mutations and why the phenotype remits during postnatal development. One possibility is that GlialCAM may have additional roles at early stages of development [5]. Alternatively, it is possible that the GlialCAM distribution defect caused in vivo by dominant mutations is not as strong as the one caused by two recessive mutations. Therefore, the

function of GlialCAM/MLC1 and GlialCAM/ClC-2 complexes may be required mostly at early stages of development in humans, at the time of most active myelination, and this fact may explain the reversibility of the phenotype as development progresses on. Following this hypothesis, we speculate also that the MRI parameters in some MLC1 patients and the MLC2A patient described here reverse because the mutations in these patients lead to a minor reduction of the function of GlialCAM/MLC1 in vivo, explaining the partial reversibility of the MRI phenotype.

In summary, our work reinforces the concept that MLC2B is caused by one mutation in the first immunoglobulin domain of *GLIALCAM* and indicates that some MLC2A patients may also have a partial MRI remitting phenotype although without showing clinical improvement.

Acknowledgments This study was supported in part by SAF 2009-07014 (RE) and SAF 2012-31486 (RE), PS09/02672-ERARE (RE), ELA Foundation 2012-014C2 (RE), 2009 SGR 719 (RE). RE is a recipient of an ICREA Academia prize. MP and EJ were supported by Telethon Italy (grant GGP12008), the Italian Ministry of Education (progetto PRIN), and the Compagnia San Paolo. EB and CA acknowledge funds from the Italian Ministry of Health and ELA Foundation project 2009-045C3B.

References

1. Blanz J, Schweizer M, Auberson M, Maier H, Muenscher A, Hubner CA, Jentsch TJ (2007) Leukoencephalopathy upon disruption of the chloride channel ClC-2. J Neurosci 27:6581–6589
2. Blattner R, Von Moers A, Leegwater PA, Hanefeld FA, Van Der Knaap MS, Kohler W (2003) Clinical and genetic heterogeneity in megalencephalic leukoencephalopathy with subcortical cysts (MLC). Neuropediatrics 34:215–218
3. Boor PK, de Groot K, Waisfisz Q, Kamphorst W, Oudejans CB, Powers JM, Pronk JC, Scheper GC, van der Knaap MS (2005) MLC1: a novel protein in distal astroglial processes. J Neuropathol Exp Neurol 64:412–419
4. Depienne C, Bugiani M, Dupuits C, Galanaud D, Touitou V, Postma N, van Berkel C, Polder E, Tollard E, Darios F, Brice A, de Die-Smulders CE, Vles JS, Vanderver A, Uziel G, Yalcinkaya C, Frints SG, Kalscheuer VM, Klooster J, Kamermans M, Abbink TE, Wolf NI, Sedel F, van der Knaap MS (2013) Brain white matter oedema due to ClC-2 chloride channel deficiency: an observational analytical study. Lancet Neurol 12:659–668
5. Favre-Kontula L, Rolland A, Bernasconi L, Karmirantzou M, Power C, Antonsson B, Boschert U (2008) GlialCAM, an immunoglobulin-like cell adhesion molecule is expressed in glial cells of the central nervous system. Glia 56:633–645
6. Jeworutzki E, Lopez-Hernandez T, Capdevila-Nortes X, Sirisi S, Bengtsson L, Montolio M, Zifarelli G, Arnedo T, Muller CS, Schulte U, Nunes V, Martinez A, Jentsch TJ, Gasull X, Pusch M, Estevez R (2012) GlialCAM, a protein defective in a leukodystrophy, serves as a ClC-2 cl(−) channel auxiliary subunit. Neuron 73: 951–961
7. Leegwater PA, Yuan BQ, van der Steen J, Mulders J, Konst AA, Boor PK, Mejaski-Bosnjak V, van der Maarel SM, Frants RR, Oudejans CB, Schutgens RB, Pronk JC, van der Knaap MS (2001) Mutations of MLC1 (KIAA0027), encoding a putative membrane protein, cause megalencephalic leukoencephalopathy with subcortical cysts. Am J Hum Genet 68:831–838
8. Lopez-Hernandez T, Ridder MC, Montolio M, Capdevila-Nortes X, Polder E, Sirisi S, Duarri A, Schulte U, Fakler B, Nunes V, Scheper GC, Martinez A, Estevez R, van der Knaap MS (2011) Mutant GlialCAM causes megalencephalic leukoencephalopathy with subcortical cysts, benign familial macrocephaly, and macrocephaly with retardation and autism. Am J Hum Genet 88:422–432
9. Lopez-Hernandez T, Sirisi S, Capdevila-Nortes X, Montolio M, Fernandez-Duenas V, Scheper GC, van der Knaap MS, Casquero P, Ciruela F, Ferrer I, Nunes V, Estevez R (2011) Molecular mechanisms of MLC1 and GLIALCAM mutations in megalencephalic leukoencephalopathy with subcortical cysts. Hum Mol Genet 20: 3266–3277
10. Patrono C, Di Giacinto G, Eymard-Pierre E, Santorelli FM, Rodriguez D, De Stefano N, Federico A, Gatti R, Benigno V, Megarbane A, Tabarki B, Boespflug-Tanguy O, Bertini E (2003) Genetic heterogeneity of megalencephalic leukoencephalopathy and subcortical cysts. Neurology 61:534–537
11. Scheper GC, van Berkel CG, Leisle L, de Groot KE, Errami A, Jentsch TJ, Van der Knaap MS (2010) Analysis of CLCN2 as candidate gene for megalencephalic leukoencephalopathy with subcortical cysts. Genet Test Mol Biomarkers 14:255–257
12. Teijido O, Casaroli-Marano R, Kharkovets T, Aguado F, Zorzano A, Palacin M, Soriano E, Martinez A, Estevez R (2007) Expression patterns of MLC1 protein in the central and peripheral nervous systems. Neurobiol Dis 26:532–545
13. Teijido O, Martinez A, Pusch M, Zorzano A, Soriano E, Del Rio JA, Palacin M, Estevez R (2004) Localization and functional analyses of the MLC1 protein involved in megalencephalic leukoencephalopathy with subcortical cysts. Hum Mol Genet 13:2581–2594
14. van der Knaap MS, Boor I, Estevez R (2012) Megalencephalic leukoencephalopathy with subcortical cysts: chronic white matter oedema due to a defect in brain ion and water homoeostasis. Lancet Neurol 11:973–985
15. van der Knaap MS, Lai V, Kohler W, Salih MA, Fonseca MJ, Benke TA, Wilson C, Jayakar P, Aine MR, Dom L, Lynch B, Kalmanchey R, Pietsch P, Errami A, Scheper GC (2010) Megalencephalic leukoencephalopathy with cysts without MLC1 defect. Ann Neurol 67:834–837
16. van der Knaap MS, Valk J, Barth PG, Smit LM, van Engelen BG, Tortori DP (1995) Leukoencephalopathy with swelling in children and adolescents: MRI patterns and differential diagnosis. Neuroradiology 37:679–686

Functional analyses of mutations in HEPACAM causing megalencephalic leukoencephalopathy.

Article publicat l'agost del 2014 a la revista Human Mutation.

BRIEF REPORT

Human Mutation

OFFICIAL JOURNAL HGVS HUMAN GENOME VARIATION SOCIETY www.hgvs.org

Functional Analyses of Mutations in *HEPACAM* Causing Megalencephalic Leukoencephalopathy

Tanit Arnedo,[1,2†] Tania López-Hernández,[1†] Elena Jeworutzki,[3] Xavier Capdevila-Nortes,[1] Sònia Sirisi,[1] Michael Pusch,[3] and Raúl Estévez[1,2*]

[1] *Sección de Fisiología, Departamento de Ciencias Fisiológicas II, University of Barcelona, Barcelona, Spain;* [2] *U-750, Centro de Investigación en red de enfermedades raras (CIBERER), ISCIII, Barcelona, Spain;* [3] *Istituto di Biofisica, Consiglio Nazionale delle Ricerche, Genoa 16149, Italy*

Communicated by Christine Van Broeckhoven

Received 20 December 2013; accepted revised manuscript 3 July 2014.
Published online 18 July 2014 in Wiley Online Library (www.wiley.com/humanmutation). DOI: 10.1002/humu.22622

ABSTRACT: Megalencephalic leukoencephalopathy with subcortical cysts (MLC) is a rare type of leukodystrophy characterized by white matter edema. Autosomal-recessive mutations in *MLC1* cause MLC type 1, and autosomal-recessive or dominant mutations in *HEPACAM* (also called *GLIALCAM*) cause MLC type 2A and type 2B, respectively. The role of MLC1 and HEPACAM is unknown, although they have been related with the processes of cell–volume regulation and potassium siphoning by astrocytes. Previous studies with some of the mutations identified in *HEPACAM* showed that most of them are associated with a trafficking defect. Here, we analyzed biochemically and functionally most mutations identified up-to-date in *HEPACAM*. Our results allow classifying the effect of mutations in different subtypes and we indicate different cellular mechanisms that lead to MLC pathogenesis.

Hum Mutat 00:1–4, 2014. © 2014 Wiley Periodicals, Inc.

KEY WORDS: leukodystrophy; astrocyte; chloride channels; HEPACAM; GLIALCAM

Megalencephalic leukoencephalopathy with subcortical cysts (MLC) is a rare type of leukodystrophy that affects brain chloride and fluid homeostasis [van der Knaap et al., 2012]. Studies from an MLC patient brain biopsy and from *Mlc1* and *GlialCAM*$^{-/-}$ mice revealed that the major phenotype of the disease is myelin and astrocyte vacuolation [van der Knaap et al., 1996; Duarri et al., 2011; Hoegg-Beiler et al., 2014].

MLC is caused by mutations in either *MLC1* (MIM #605908) or *HEPACAM* (also called GLIALCAM due to the fact that its expression in normal tissues is mainly restricted to glial cells) (MIM #611642) genes. Although the HUGO-approved gene symbol is *HEPACAM*, we prefer the name GlialCAM for the related protein.

Additional Supporting Information may be found in the online version of this article.

†These authors contributed equally to this study.

*Correspondence to: Raúl Estévez, University of Barcelona, Department of Physiological Sciences II, C/Feixa llarga s/n L'Hospitalet de Llobregat, Barcelona 08907, Spain. E-mail: restevez@ub.edu

Contract grant sponsors: SAF 2009-0714; SAF 2012-31486; PS09/02672-ERARE; ELA Foundation (ELA2009-017C4 and ELA 2012-014C2B); Catalonian Government (2009 SGR 719); ERA-NET E-RARE-2 framework by ISCIII through CIBERER and Icrea Academia Prize; Telethon Italy (grant GGP12008); Compagnia San Paolo.

Detailed characterization of MLC patients with *HEPACAM* mutations revealed two different phenotypes [van der Knaap et al., 2012]: a MLC2A type (MIM #613925) that is indistinguishable from the MLC1 type (MIM #604004), and a MLC2B type (MIM #613926) that shows a remitting MLC phenotype.

Data obtained from both in vitro and from *Mlc1* and *GlialCAM*$^{-/-}$ mice, *mlc1*$^{-/-}$ zebrafish and from a human biopsy from an MLC1 patient have indicated that there is a macromolecular complex between MLC1, GlialCAM, and ClC-2 proteins, involving interactions among different types of glial cells [Lopez-Hernandez et al., 2011a; Lopez-Hernandez et al., 2011b; Jeworutzki et al., 2012; Capdevila-Nortes et al., 2013; Hoegg-Beiler et al., 2014; Sirisi et al., 2014].

Some recessive *HEPACAM* mutations identified in MLC2A patients do not affect their own protein expression, but interfere with the formation of homocomplexes and with their localization at cell–cell contact areas [Lopez-Hernandez et al., 2011b]. However, for some mutations, the cellular defect is unknown.

In the present work, we have analyzed biochemically and functionally the consequences of most missense mutations identified up-to-date in MLC2A and MLC2B patients [van der Knaap et al., 2012]. Our work extends previous analyses of *HEPACAM* mutations and identifies differences compared with the wild-type protein for all mutations.

All methods used in the present work have been previously described [Lopez-Hernandez et al., 2011b]. Detailed methods can be found in the Supp. Materials and Methods in the Supporting Information section. Accession numbers of the reference sequences are NM_152722.4 (mRNA) and NT_033899.8 (gDNA).

All known MLC-causing *HEPACAM* mutations have been found in the sequence coding for the extracellular region of GlialCAM [van der Knaap et al., 2012]. First, we investigated the biochemical impact of two presumably deleterious recessive mutations, the signal peptide mutation p.L23H and the truncation p.W263X. Mutation p.L23H completely abolished protein expression. The truncation mutation p.W263X reduced GlialCAM protein expression and was detected scattered in the cytoplasm (Supp. Fig. S1). Coexpression of GlialCAM p.W263X with MLC1 also causes intracellular retention of the latter (Supp. Fig. S1), suggesting that the mutant has not lost the ability to interact with MLC1.

As previously described [Lopez-Hernandez et al., 2011a, 2011b], none of the new studied *HEPACAM* missense mutations affected GlialCAM protein expression levels (data not shown). Next, we aimed to analyze the molecular consequences of these MLC-causing *HEPACAM* mutations on the ability to homooligomerize and heterooligomerize. For comparison, we also introduced data from previous studies [Lopez-Hernandez et al., 2011b; Jeworutzki et al.,

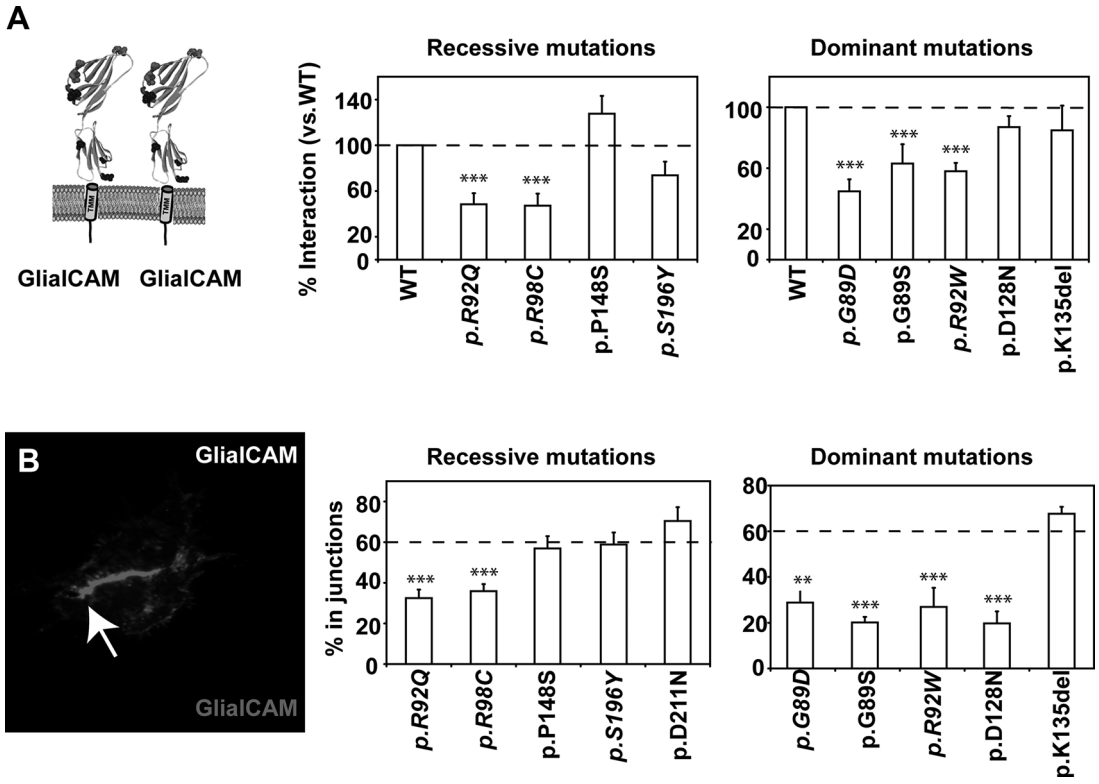

Figure 1. Analysis of homophilic interactions and trafficking to cell junctions of GlialCAM variants. **A:** Schematic representation of two GlialCAM molecules. Interaction in HeLa cells between GlialCAM molecules was monitored by the split-TEV assay. The signal that was obtained for homooligomerization of wild-type GlialCAM was set to 100%. Bars indicate the percentage of interaction compared with the interaction between the corresponding wild-type proteins ± SEM. The result is a summary of at least five independent experiments. In cursive, we indicated mutants that were described in previous work, as a comparison. Student's *t*-test was used for statistical analyses. *, $P < 0.05$; ***, $P < 0.001$. **B**: HeLa cells were transfected with plasmids expressing flag-tagged GlialCAM variants and then immunofluorescence was performed. An intensity profile analysis was used to discern between junctional and plasma membrane localization. Arrows point to junctions. Data represent the mean of four to 10 independent experiments, corresponding to 121–144 cells. The dotted line corresponds to the mean of wild-type GlialCAM. Student's *t*-test was used for statistical analyses. **, $P < 0.01$; ***, $P < 0.001$.

2012]. Only some recessive (p.R92Q and p.R98C) and dominant (p.G89D, p.G89S, and p.R92W) mutants showed a highly significant reduced ability to homooligomerize (Fig. 1A). In contrast, all mutations showed similar ability to heterooligomerize with MLC1 and ClC-2 (Supp. Fig. S2A and S2B).

We next analyzed whether the studied mutations affect the localization in junctions of GlialCAM alone (Fig. 1B), or, in coexpression experiments, whether the mutants affect the ability of GlialCAM to direct MLC1 or ClC-2 to cell junctions (Supp. Fig. S2C and S2D). All GlialCAM mutants with a reduced ability to homooligomerize displayed a significant trafficking defect (Fig. 1B). An exception to this rule was the dominant mutant p.D128N, which, despite having a normal ability to homooligomerize (Fig. 1A), exhibited a defect in junction localization (Fig. 1B). Some mutations such as p.S196Y, p.P148S, p.D211N, and p.K135del did not display any trafficking defect. Similar results were found in primary cultures of rat astrocytes (Supp. Fig. S3A) or in astrocytes first depleted of endogenous GlialCAM in astrocytes by adenovirus-mediated RNA interference, and then complemented with GlialCAM variants (Supp. Fig. S3B).

We then analyzed the effect of the MLC-causing mutations in GlialCAM on its ability to modify the functional properties of ClC-2. No differences in conductance and rectification properties for all studied GlialCAM mutants were found compared with wild type (Supp. Fig. S4). These mutants did not show any defect in the ability to rescue the vacuolation defect caused by the lack of GlialCAM (data not shown), which is indicative of normal VRAC function.

As previously described [Sirisi et al., 2014], wild-type GlialCAM was mislocalized in *Mlc1*$^{-/-}$ astrocytes in the presence of high potassium (Fig. 2A–D). In contrast, the dominant mutant p.K135del (Fig. 2E–H), the recessive mutants p.S196Y (Fig. 2M–P), and p.D211N (Fig. 2Q–T) were always localized in cell junctions, irrespective of the condition studied. Interestingly, the recessive mutant p.P148S showed a different phenotype, being mislocalized in *Mlc1*$^{-/-}$ astrocytes in physiological and high-potassium conditions (Fig. 2I–L).

In the present study, we extend our knowledge of the functional consequence of recessive and dominant *HEPACAM* mutations. We suggest that the *HEPACAM* mutations described up to now can be classified in several groups. Some mutations can affect GlialCAM protein expression. Lack of GlialCAM expression implies the lack of functional MLC1 [Capdevila-Nortes et al., 2013; Hoegg-Beiler et al., 2014], as MLC1 appears not to be able to arrive at the plasma membrane without GlialCAM.

The remaining missense mutations neither affect GlialCAM protein expression nor its trafficking to the plasma membrane. However, most mutations affect its ability to *cis*-homooligomerize and consequently reduce their localization in cell–cell junctions. We have identified here a dominant mutation (p.D128N) that does not affect the *cis*-homooligomerization of GlialCAM but compromises its cell

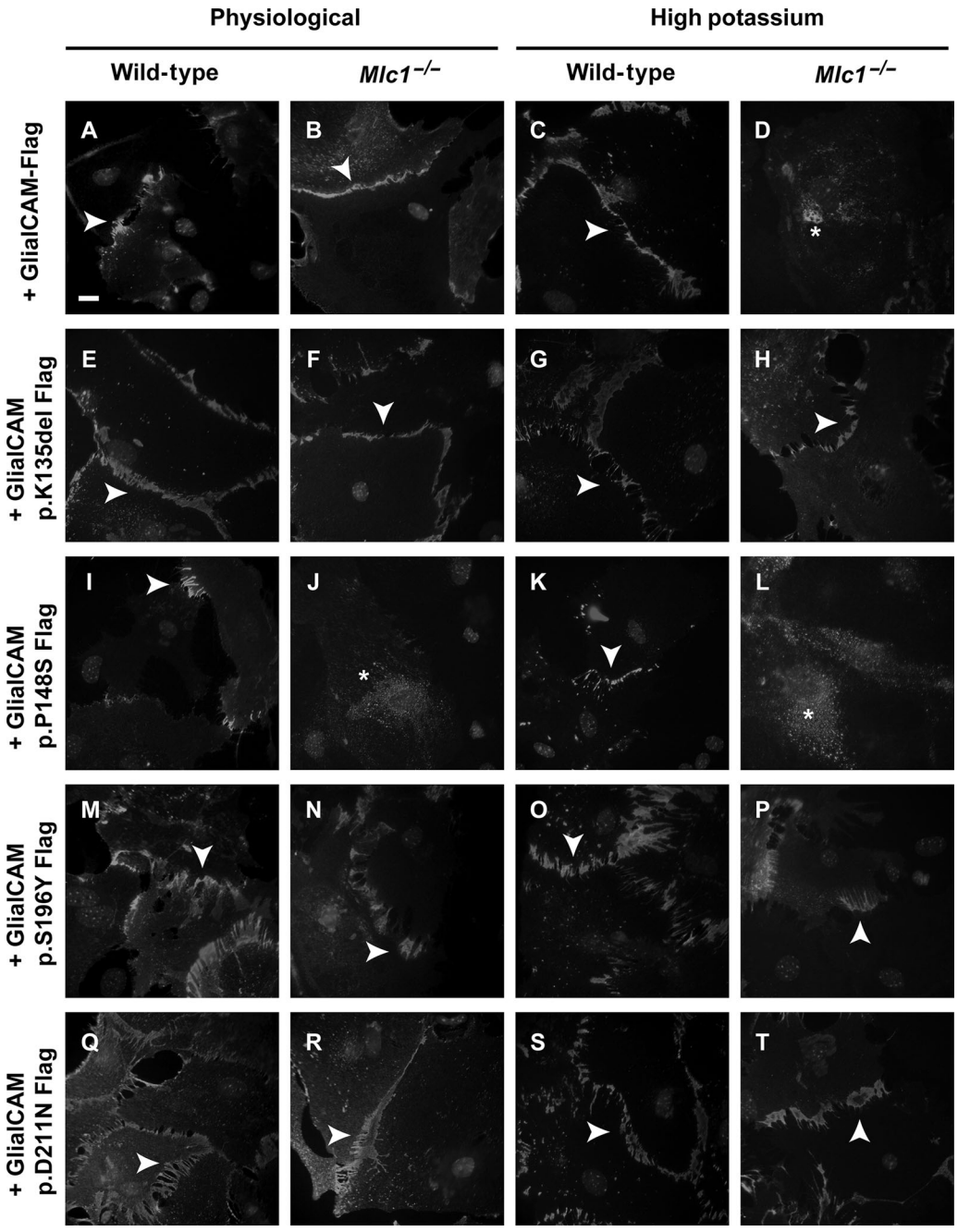

Figure 2. GlialCAM mutants localization studied in wild-type or Mlc1$^{-/-}$ cultured mouse astrocytes in physiological and high-extracellular potassium. Adenoviral-mediated expression of flag-tagged GlialCAM variants in wild-type and *Mlc1*$^{-/-}$ cultured mouse astrocytes. They were subjected to 6-h treatment with physiological solution or with high-extracellular potassium. **A–D:** Wild type, (**E–H**) p.K135del, (**I–L**) p.P148S, (**M–P**) p.S196Y, and (**Q–T**) p.D211N. Four independent experiments gave similar results. Arrows point to junctions between different astrocytes and asterisks point to the cytoplasm. Scale bar: 10 μm.

junction targeting. As GlialCAM targeting in junctions depends on homophilic transinteractions [Hoegg-Beiler et al., 2014], we speculate that this mutation may affect specifically only transinteractions between GlialCAM molecules.

Other recessive mutations (p.S196Y, p. D211N) and dominant mutations (p.K135del) do not compromise GlialCAM localization in junctions. Expression studies in *Mlc1*$^{-/-}$ astrocytes suggest that some mutations act as gain-of-function mutations, and that they are not mislocalized as wild-type GlialCAM in high-potassium conditions. We still do not understand how such gain of function mutants may lead to MLC. We suggest that the localization of the protein complex GlialCAM/MLC1 may be regulated by endocytosis, as previously suggested [Lanciotti et al., 2010], and that this process may be important to fulfill its physiological role. Endocytosis-defective mutants will then have an altered physiological function.

Finally, we identified a recessive mutation (p.P148S) that is mislocalized only in astrocytes derived from *Mlc1*$^{-/-}$ mice. We suggest that this mutant may be unstable without MLC1. Thus, we can speculate

that not only GlialCAM is needed to stabilize MLC1, but also MLC1 might stabilize GlialCAM, an effect that could not be observed previously in cell lines or in primary astrocytes expressing endogenous MLC1.

In summary, this work provides a detailed analysis of the effects of most *HEPACAM/GLIALCAM* mutations identified, extending previous results. We believe that these new results will be important to understand the physiological role of GlialCAM/MLC1 in glial cells.

Acknowledgment

We thank Herbert Schwartz for previous experiments and revising the manuscript. We thank all members of the group for revising the manuscript, and Virginia Nunes group for providing pups of Mlc1 KO mice.

Disclosure statement: The authors have no conflict of interest to declare.

References

Capdevila-Nortes X, López-Hernández T, Apaja PM, López de Heredia M, Sirisi S, Callejo G, Arnedo T, Nunes V, Lukacs GL, Gasull X, Estévez R. 2013. Insights into MLC pathogenesis: GlialCAM is an MLC1 chaperone required for proper activation of volume-regulated anion currents. Hum Mol Genet 22:4405–4416.

Duarri A, Lopez de Heredia M, Capdevila-Nortes X, Ridder MC, Montolio M, Lopez-Hernandez T, Boor I, Lien CF, Hagemann T, Messing A, Gorecki DC, Scheper GC, et al. 2011. Knockdown of MLC1 in primary astrocytes causes cell vacuolation: a MLC disease cell model. Neurobiol Dis 43:228–238.

Hoegg-Beiler MB, Sirisi S, Orozco IJ, Ferrer I, Hohensee S, Auberson M, Gödde K, Vilches C, Heredia ML de, Nunes V, Estévez R, Jentsch TJ. 2014. Disrupting MLC1 and GlialCAM and ClC-2 interactions in leukodystrophy entails glial chloride channel dysfunction. Nat Commun 5:3475.

Jeworutzki E, Lopez-Hernandez T, Capdevila-Nortes X, Sirisi S, Bengtsson L, Montolio M, Zifarelli G, Arnedo T, Muller CS, Schulte U, Nunes V, Martinez A, et al. 2012. GlialCAM, a protein defective in a leukodystrophy, serves as a ClC-2 Cl(-) channel auxiliary subunit. Neuron 73:951–961.

Lanciotti A, Brignone MS, Camerini S, Serafini B, Macchia G, Raggi C, Molinari P, Crescenzi M, Musumeci M, Sargiacomo M, Aloisi F, Petrucci TC, et al. 2010. MLC1 trafficking and membrane expression in astrocytes: role of caveolin-1 and phosphorylation. Neurobiol Dis 37:581–595.

Lopez-Hernandez T, Ridder MC, Montolio M, Capdevila-Nortes X, Polder E, Sirisi S, Duarri A, Schulte U, Fakler B, Nunes V, Scheper GC, Martinez A, et al. 2011a. Mutant GlialCAM causes megalencephalic leukoencephalopathy with subcortical cysts, benign familial macrocephaly, and macrocephaly with retardation and autism. Am J Hum Genet 88:422–432.

Lopez-Hernandez T, Sirisi S, Capdevila-Nortes X, Montolio M, Fernandez-Duenas V, Scheper GC, Knaap MS van der, Casquero P, Ciruela F, Ferrer I, Nunes V, Estevez R. 2011b. Molecular mechanisms of MLC1 and GLIALCAM mutations in megalencephalic leukoencephalopathy with subcortical cysts. Hum Mol Genet 20:3266–3277.

Sirisi S, Folgueira M, López-Hernández T, Minieri L, Pérez-Rius C, Gaitán-Peñas H, Zang J, Martínez A, Capdevila-Nortes X, la Villa P de, Roy U, Alia A, et al. 2014. Megalencephalic leukoencephalopathy with subcortical cysts protein 1 regulates glial surface localization of GLIALCAM from fish to humans. Hum Mol Genet pii:ddu231.

van der Knaap MS, Barth PG, Vrensen GF, Valk J. 1996. Histopathology of an infantile-onset spongiform leukoencephalopathy with a discrepantly mild clinical course. Acta Neuropathol 92:206–212.

van der Knaap MS, Boor I, Estevez R. 2012. Megalencephalic leukoencephalopathy with subcortical cysts: chronic white matter oedema due to a defect in brain ion and water homoeostasis. Lancet Neurol 11:973–985.